Electronic Supplementary Material (ESI) for Dalton Transactions.

Electronic Supporting Information

Predictable Electronic Tuning of Fe^{II} and Ru^{II} Complexes via Choice of Azine: Correlation of Ligand pKa with $E_{pa}(M^{III/II})$ of Complex

Matthew G. Robb,[a] Luca Bondì,[a] Santiago Rodríguez-Jiménez,[a] Anna L. Garden,[a] Paul Jerabek*[b] and Sally Brooker*[a]

[a] *Department of Chemistry and MacDiarmid Institute of Advanced Materials and Nanotechnology, University of Otago, P.O. Box 56, Dunedin 9054, New Zealand, E-mail: sbrooker@chemistry.otago.ac.nz*

[b] *Institute of Hydrogen Technology, Helmholtz Zentrum Hereon, Max Planck-Straße 1, 21502 Geesthacht, Germany*

Table of Contents

Single Crystal X-Ray Data

Table S1: Selected crystallographic data for complexes $[Ru(\mathbf{L}^{pyridine})_3](PF_6)_2$, $[Ru(\mathbf{L}^{4\text{-pyrimidine}})_3](PF_6)_2$ and $[Ru(\mathbf{L}^{pyrazine})_3](PF_6)_2$ (Cambridge Structural Database CCDC 2250256 – 2250258).

	$[Ru(L^{pyridine})_3](PF_6)_2$ ·2MeCN·Et_2O	**$[Ru(L^{4\text{-pyrimidine}})_3](PF_6)_2$ ·2MeCN·Et_2O**	**$[Ru(L^{pyrazine})_3](PF_6)$ ·2MeCN**
	1 · 2MeCN·Et_2O	**3** · 2MeCN·Et_2O	**4** · 2MeCN
CCDC #	2250556	2250257	2250257
Empirical formula	$C_{64}H_{54}F_{12}N_{14}P_2Ru$	$C_{57}H_{45}F_{12}N_{15}P_2Ru$	$C_{61}H_{51}F_{12}N_{17}P_2Ru$
Formula weight	1410.22	1331.09	1413.19
Temperature/K	100.15	100.01(10)	100.01(10)
Crystal system	triclinic	triclinic	monoclinic
Space group	P-1	P-1	$P2_1/c$
a/Å	14.3806(6)	14.4360(10)	18.2893(5)
b/Å	16.2266(5)	16.0577(10)	17.5489(6)
c/Å	17.3781(5)	17.3704(12)	18.9097(6)
α/°	102.239(3)	103.299(6)	90
β/°	112.933(3)	112.553(7)	95.352(3)
γ/°	105.195(3)	105.024(6)	90
Volume/Å³	3371.5(2)	3337.6(4)	6042.7(3)
Z	2	2	4
ρ_{calc}g/cm³	1.389	1.325	1.553
μ/mm⁻¹	3.052	3.055	3.422
F(000)	1436	1348	2872
Crystal size/mm³	0.679 × 0.125 × 0.045	0.189 × 0.1 × 0.029	0.09 × 0.05 × 0.009
Radiation	Cu Kα (λ = 1.54184)	Cu Kα (λ = 1.54184)	Cu Kα (λ = 1.54184)
2Θ range for data collection/°	7.226 to 145.624	7.19 to 153.366	8.17 to 152.594
Index ranges	-17 ≤ h ≤ 17, -18 ≤ k ≤ 19, -21 ≤ l ≤ 15	-17 ≤ h ≤ 18, -20 ≤ k ≤ 16, -21 ≤ l ≤ 19	-22 ≤ h ≤ 23, -20 ≤ k ≤ 21, -23 ≤ l ≤ 16
Reflections collected	24603	27976	35206
Independent reflections	12926 [R_{int} = 0.0376, R_{sigma} = 0.0392]	13638 [R_{int} = 0.0688, R_{sigma} = 0.0843]	12393 [R_{int} = 0.1303, R_{sigma} = 0.1339]
Data/restraints/parameter	12926/252/910	13638/0/787	12393/0/843
Goodness-of-fit on F²	1.064	1.112	0.973
Final R indexes [I>=2σ (I)]	R_1 = 0.0598, wR_2 = 0.1615	R_1 = 0.0967, wR_2 = 0.2727	R_1 = 0.0741, wR_2 = 0.1736
Final R indexes [all data]	R_1 = 0.0651, wR_2 = 0.1662	R_1 = 0.1240, wR_2 = 0.3036	R_1 = 0.1173, wR_2 = 0.1992
Largest diff. peak/hole / e Å⁻³	1.32/-0.91	2.00/-1.02	1.66/-1.27

Additional X-ray crystal structure determination details

Complex [Ru($\mathbf{L}^{\mathbf{pyridine}}$)$_3$](PF$_6$)$_2$·2MeCN·Et$_2$O (**1**·2MeCN·Et$_2$O) crystallises in the triclinic P-1 space group. A whole complex is found in the asymmetric unit along with two solvent acetonitrile molecules and a diethyl ether molecule. Due to disorder in the lattice the diethyl ether solvent molecule could not be satisfactorily modelled and as such a solvent mask was applied (SQUEEZE through Platon).[1, 2] The residual electron density removed from the unit cell unit was equivalent to 80 e$^-$ (V = 414 Å^3) which is consistent with the removal of two diethyl ether molecules from the unit cell unit (84 e$^-$).

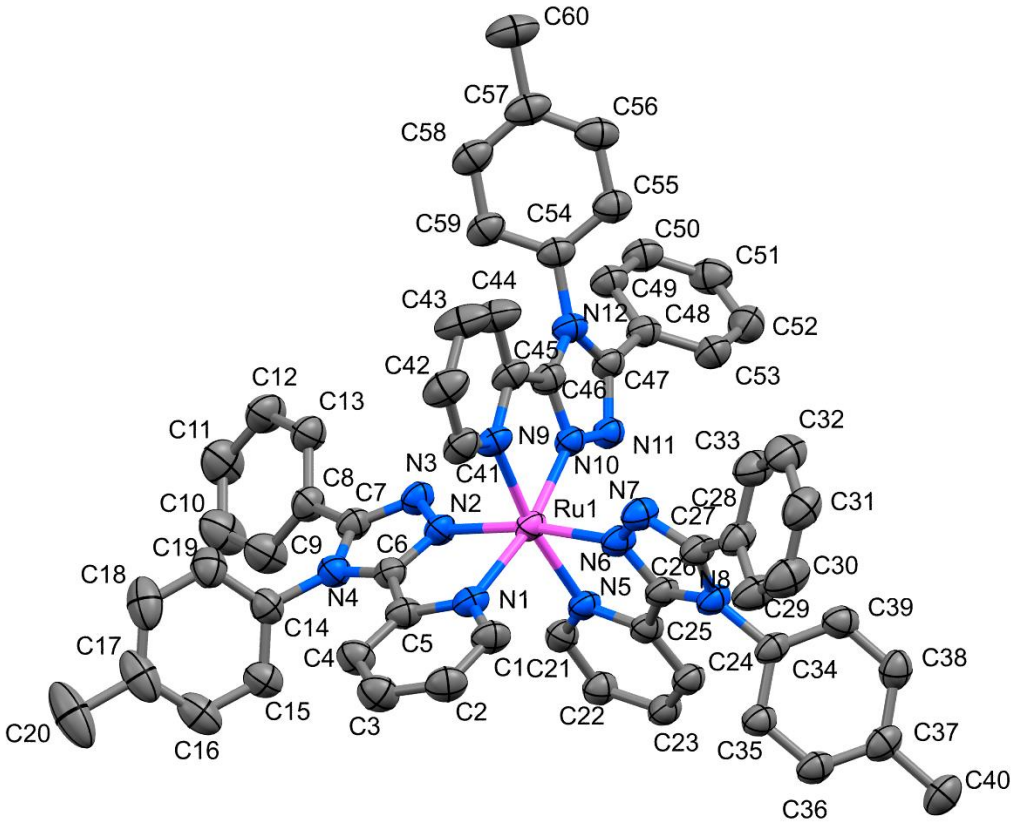

Figure S1: The cation of [Ru($\mathbf{L}^{\mathbf{pyridine}}$)$_3$](PF$_6$)$_2$·2MeCN·Et$_2$O (**1**·2MeCN·Et$_2$O), with anions, solvents and hydrogen atoms omitted for clarity.

Complex [Ru(**L**$^{4\text{-pyrimidine}}$)$_3$](PF$_6$)$_2$·2MeCN·Et$_2$O (**3**·2MeCN·Et$_2$O) crystallises in the triclinic P-1 space group. A whole complex is found in the asymmetric unit along with some disordered solvent molecules. Due to disorder in the lattice the solvent molecules could not be satisfactorily modelled and as such a solvent mask was applied (through SQUEEZE in PLATON). [1, 2] The residual electron density removed from the asymmetric unit was equivalent to 171 e$^-$ (V = 772 Å^3) which is consistent with the removal of four acetonitrile molecules and two diethyl ether molecules from the unit cell (172 e$^-$).

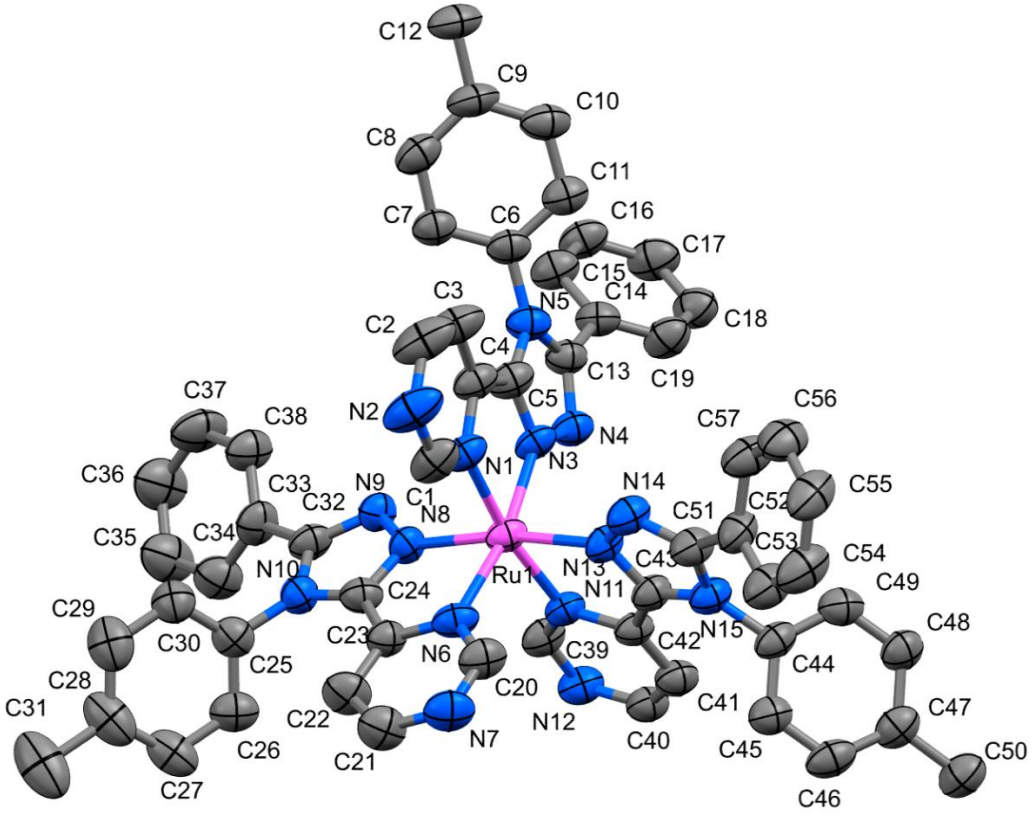

Figure S2: The cation of [Ru(**L**$^{4\text{-pyrimidine}}$)$_3$](PF$_6$)$_2$·2MeCN·Et$_2$O (**3**·2MeCN·Et$_2$O) with solvents, counterions and hydrogen atoms omitted for clarity.

Complex [Ru($\mathbf{L}^{\mathbf{pyrazine}}$)$_3$](PF$_6$)$_2$·2MeCN (**4**·2MeCN) crystallises in P2$_1$/c with one complex and two acetonitrile molecules in the asymmetric unit.

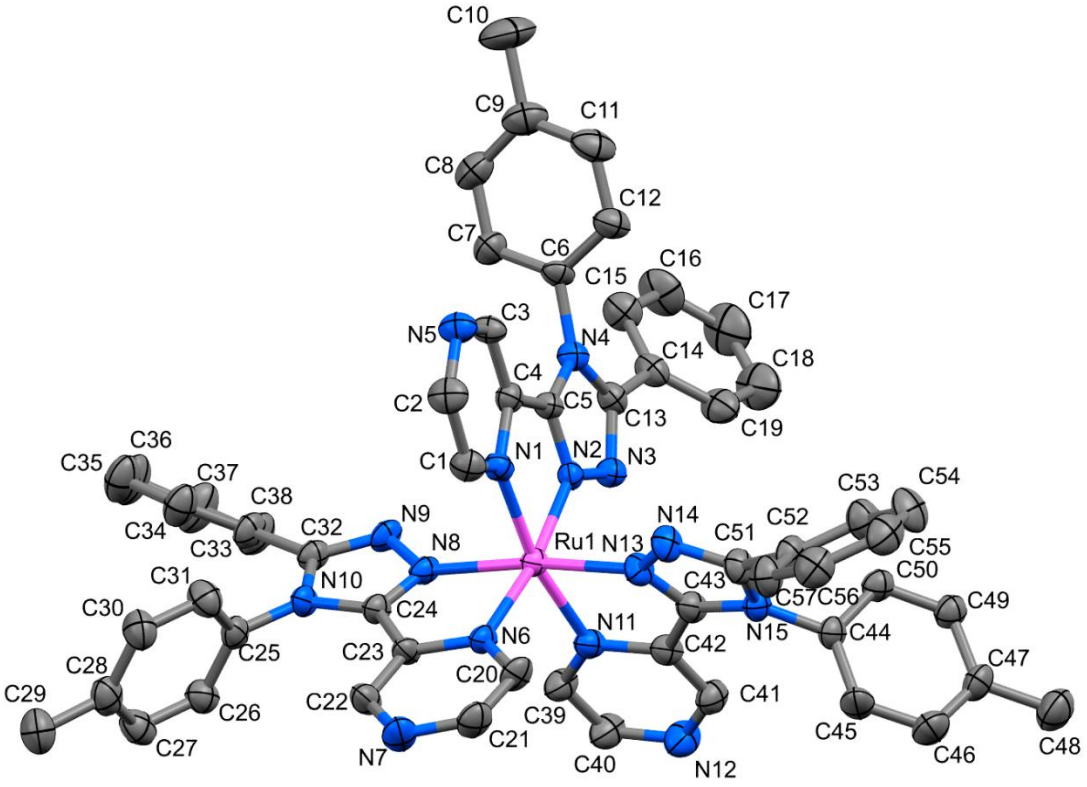

Figure S3: The cation of [Ru($\mathbf{L}^{\mathbf{pyrazine}}$)$_3$](PF$_6$)$_2$·2MeCN (**4**·2MeCN) with counterions, solvent of crystallisation and hydrogen atoms omitted for clarity.

In all three cases, the complex cations are isostructural (Figure S4), with the Ru^{II} centre bound in an octahedral N$_6$ coordination sphere composed of 3 $\mathbf{L}^{\mathbf{azine}}$ ligands bound in a bidentate manner. Notably the complexes crystallise as the meridonial isomer, with both Δ and Λ stereoisomers in the crystal structure. Some key parameters are shown in Table S2.

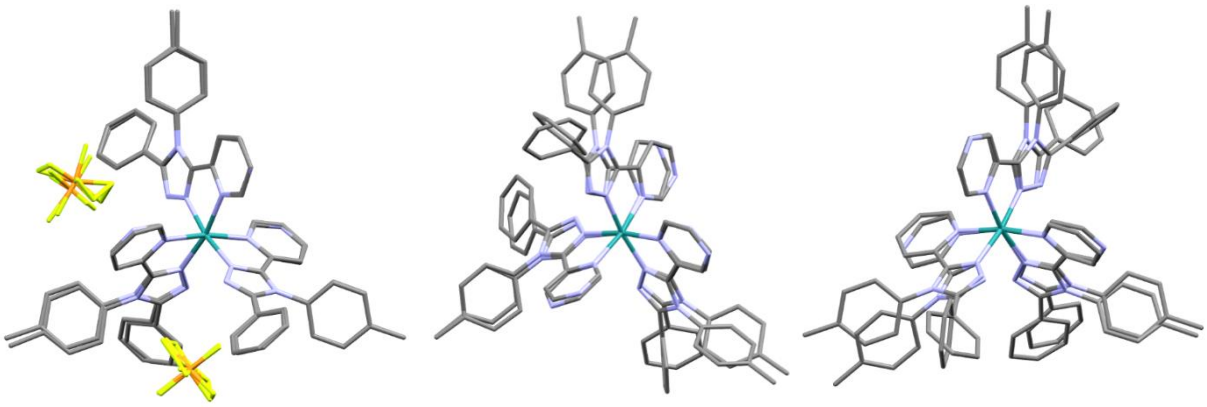

Figure S4: Overlay of crystal structures of **1** ·2MeCN·Et_2O and **3** ·2MeCN·Et_2O (left), **4** ·2MeCN and **3** ·2MeCN·Et_2O (centre) and **1**·2MeCN·Et_2O and **4** ·2MeCN (right). Solvent, counter ions and hydrogens omitted for clarity. Generated with Mercury.[3]

Table S2: Key structural data (averages in blue italics in brackets).

	$[Ru(L^{pyridine})_3](PF_6)_2$ ·2MeCN·Et_2O (4·2MeCN·Et_2O)	**$[Ru(L^{4\text{-}pyrimidine})_3](PF_6)_2$ ·2MeCN·Et_2O (4·2MeCN·Et_2O)**	**$[Ru(L^{pyrazine})_3](PF_6)_2$ ·2MeCN (4·2MeCN)**
Crystal system	Triclinic	Triclinic	Monoclinic
Space group	P-1	P-1	$P2_1/c$
Z	2	2	4
Ru-triazole / Å	2.035(3), 2.044(3), 2.034(3) *(2.037)*	2.015(5), 2.069(5), 2.048(5) *(2.044)*	2.048(5), 2.075(5), 2.036(4) *(2.052)*
Ru-azine / Å	2.077(3), 2.075(3), 2.083(3) *(2.0783)*	2.068(5), 2.070(6), 2.068(6) *(2.069)*	2.055(5), 2.067(5), 2.073(4) *(2.066)*
Σ / °	74.04	76.8	78.5
Azine twist / °	4.63, 6.21, 11.84 *(7.56)*	2.19, 9.82, 3.41 *(5.14)*	4.33, 8.26, 13.27 *(8.62)*
Phenyl twist / °	38.07, 49.26, 46.60 *(44.64)*	39.91, 46.35, 47.21 *(44.49)*	44.81, 37.90, 53.78 *(45.50)*
Tolyl twist / °	72.10, 7.79, 60.97 *(66.95)*	72.00, 59.29, 70.96 *(67.42)*	76.98, 85.60, 84.12 *(82.23)*

Mass Spectra of the complexes

$[Ru(L^{pyridine})_3](PF_6)_2$

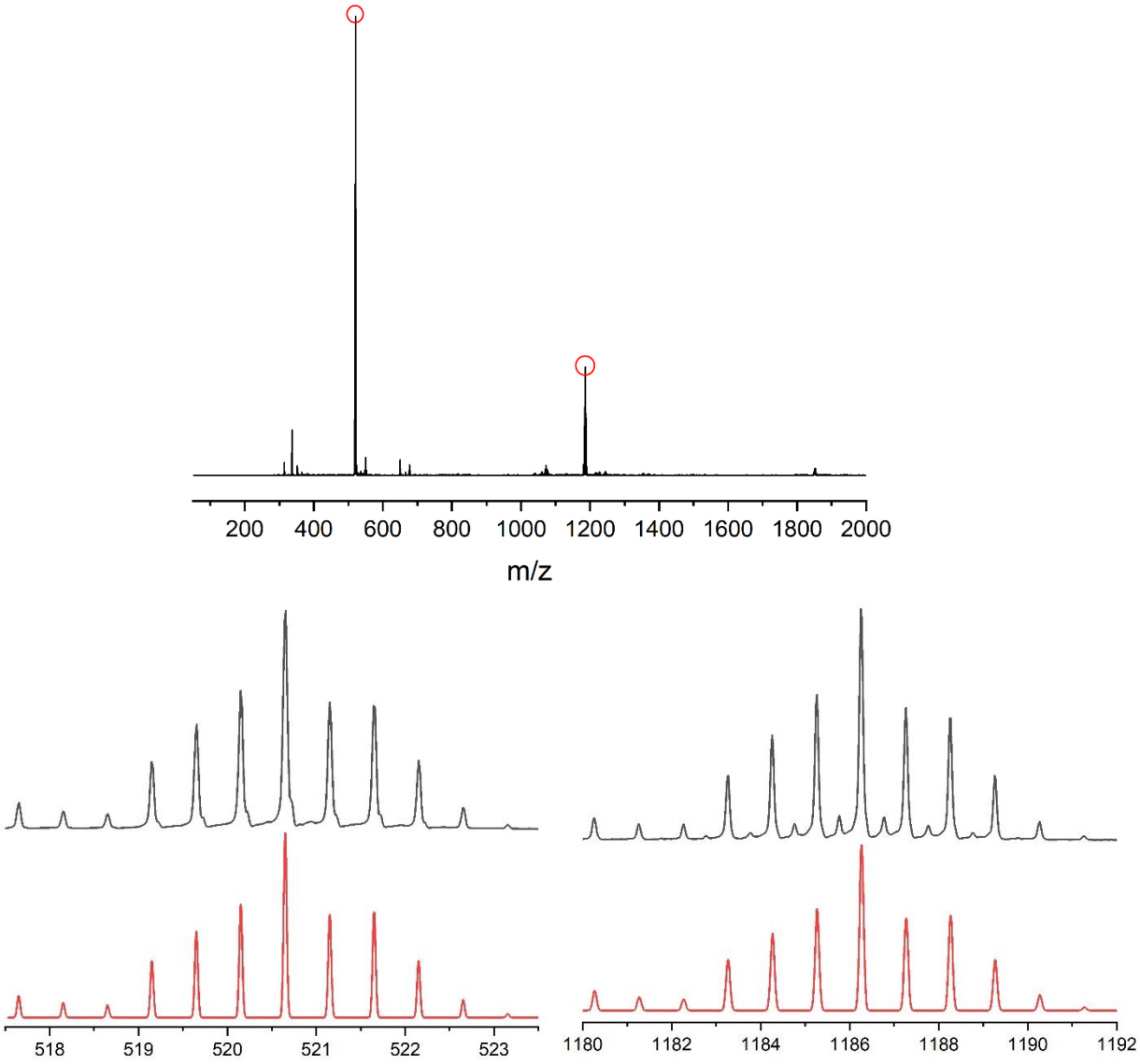

Figure S5: Mass spectrum of $[Ru(\mathbf{L}^{pyridine})_3](PF_6)_2$. Top shows full spectrum, bottom left shows $[Ru(\mathbf{L}^{pyridine})_3]^{2+}$ fit (calculated in red, found in black), bottom right shows $[Ru(\mathbf{L}^{pyridine})_3](PF_6)^{+}$ fit (calculated in red, found in black).

$[Ru(L^{pyrazine})_3](PF_6)_2$

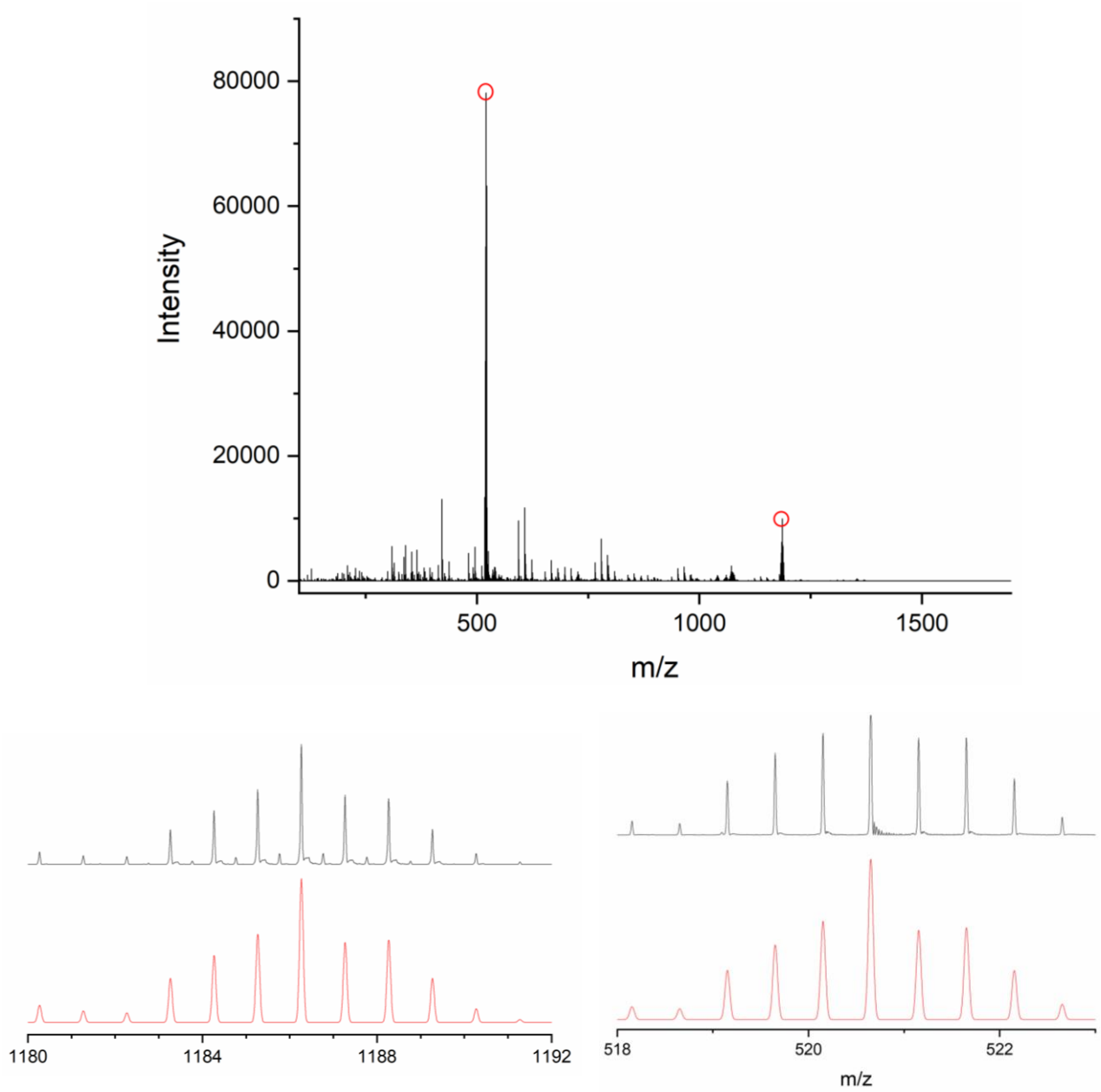

Figure S6: Mass spectrum of $[Ru(\mathbf{L}^{pyrazine})_3](PF_6)_2$. Top shows full spectrum, bottom left shows calculated fit of $[Ru(\mathbf{L}^{pyazine})_3]^{2+}$ in red, found in black, bottom right shows calculated fit of $[Ru(\mathbf{L}^{pyrazine})_3](PF_6)^{+}$ in red, found in black.

$[Ru(L^{4\text{-pyrimidine}})_3](PF_6)_2$

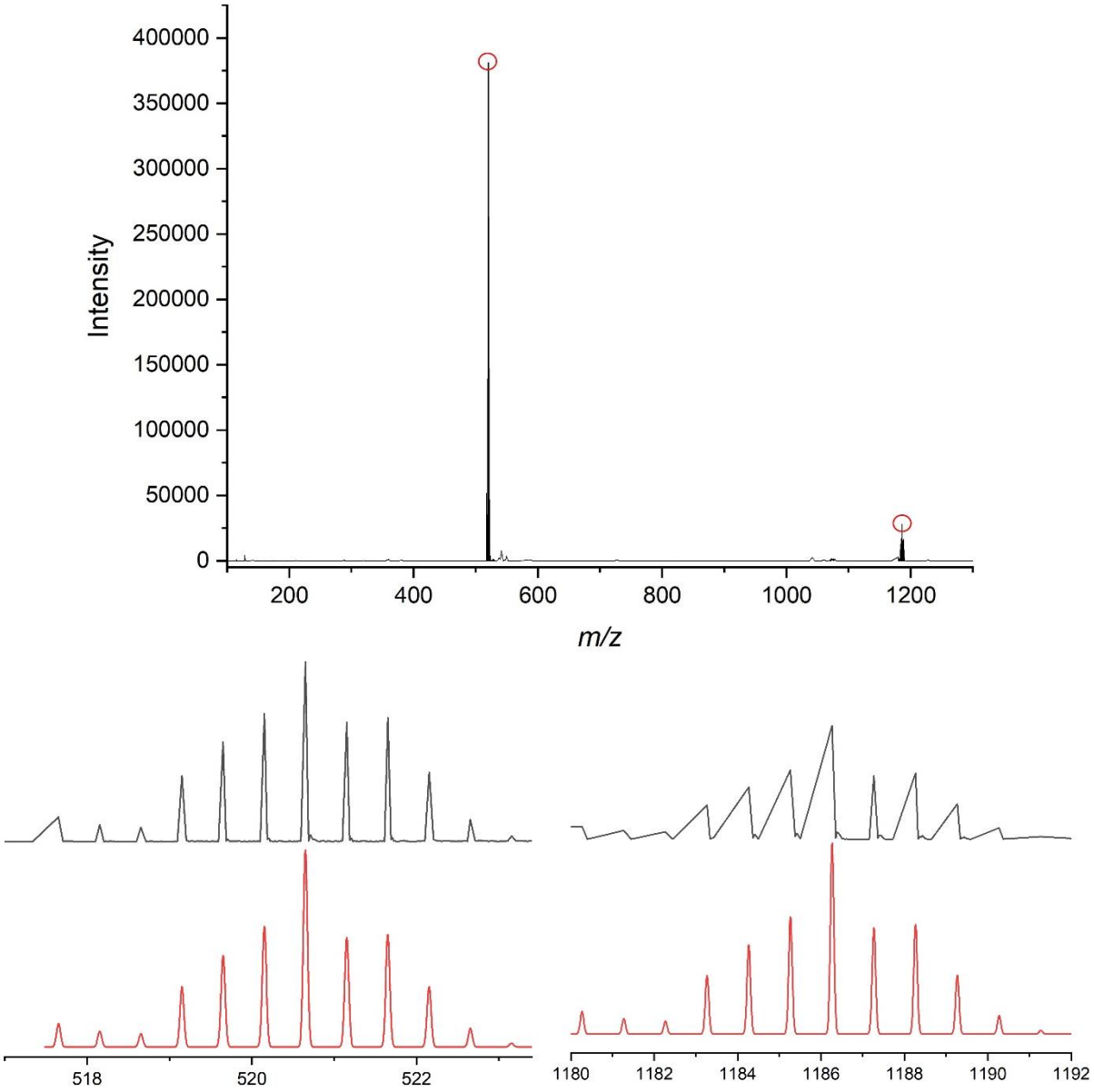

Figure S7: Mass spectrum of $[Ru(\mathbf{L}^{4\text{-pyrimidine}})_3](PF_6)_2$. Top shows full spectrum, bottom left shows calculated fit of $[Ru(\mathbf{L}^{4\text{-pyrimidine}})_3]^{2+}$ in red, found in black, bottom right shows calculated fit of $[Ru(\mathbf{L}^{4\text{-pyrimidine}})_3](PF_6)^{+}$ in red, found in black.

$[Ru(L^{2\text{-pyrimidine}})_3](PF_6)_2$

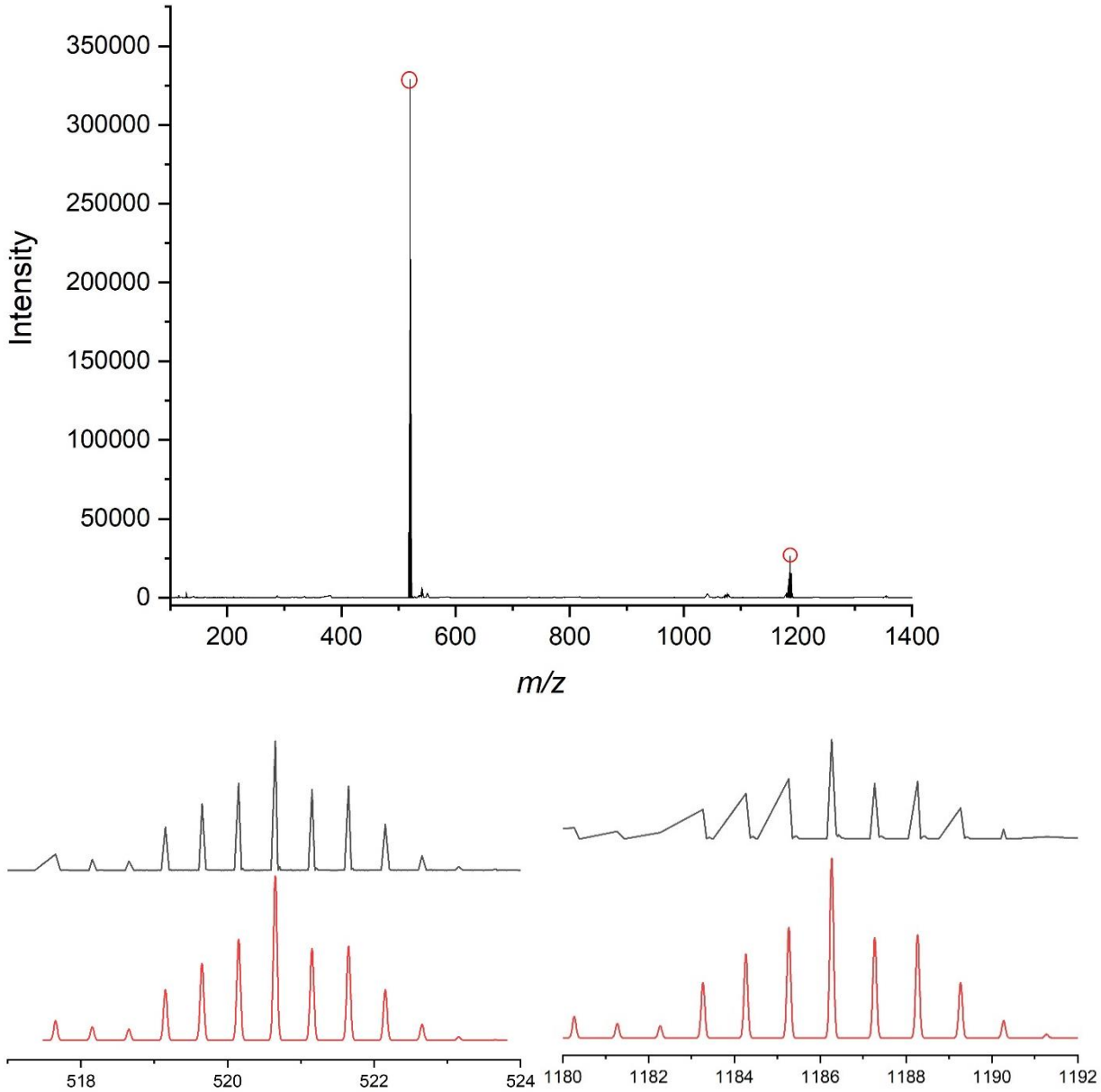

Figure S8: Mass spectrum of $[Ru(\mathbf{L}^{\mathbf{2\text{-pyrimidine}}})_3](PF_6)_2$. Top shows full spectrum, bottom left shows calculated fit of $[Ru(\mathbf{L}^{\mathbf{2\text{-pyrimidine}}})_3]^{2+}$ in red, found in black, bottom right shows calculated fit of $[Ru(\mathbf{L}^{\mathbf{2\text{-pyrimidine}}})_3](PF_6)^{+}$ in red, found in black.

$[Ru(L^{pyridazine})_3](PF_6)_2$

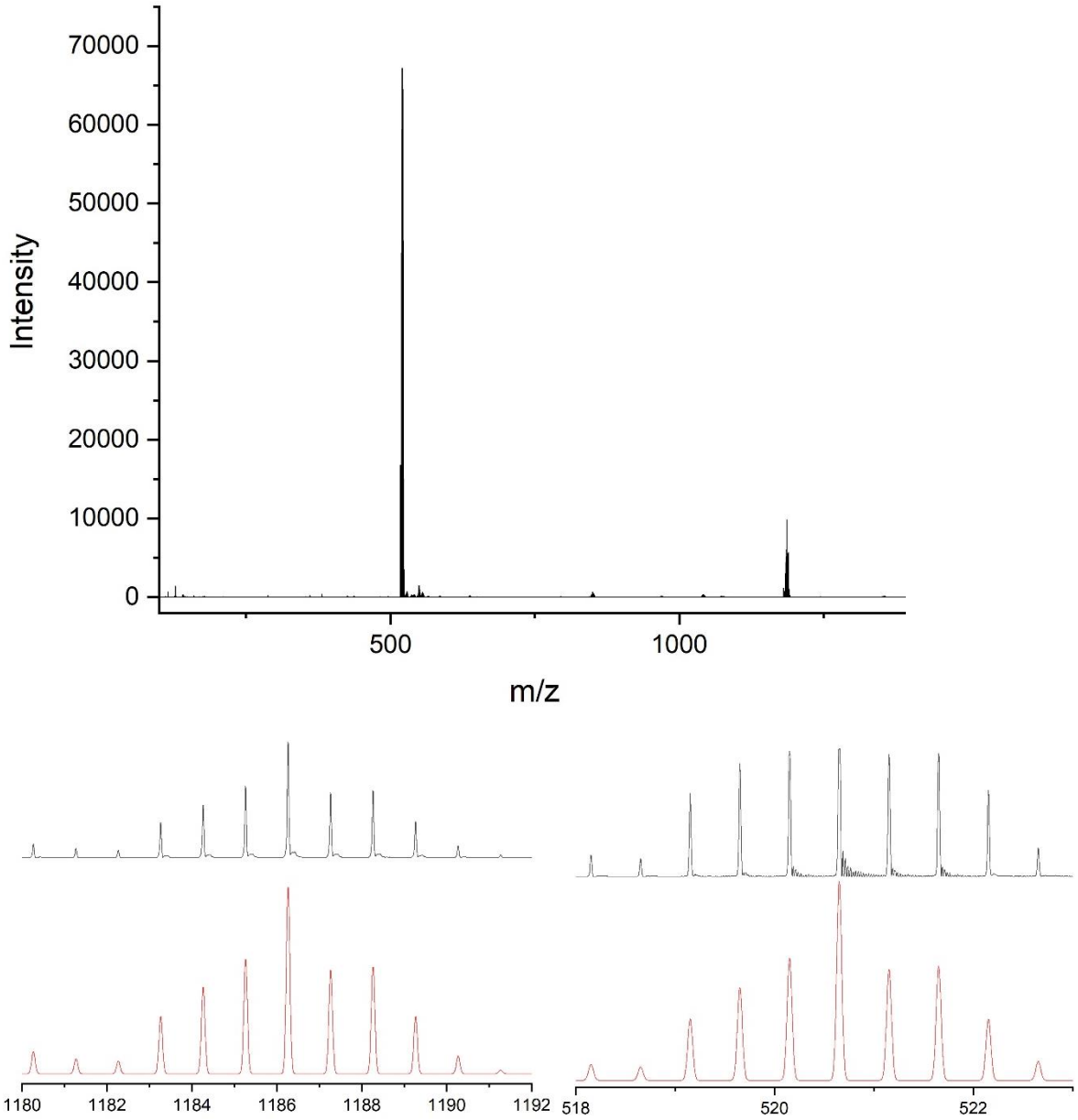

Figure S9: Mass spectrum of $[Ru(\mathbf{L}^{pyridazine})_3](PF_6)_2$. Top shows full spectrum, bottom left shows calculated fit of $[Ru(\mathbf{L}^{pyridazine})_3]^{2+}$ in red, found in black, bottom right shows calculated fit of $[Ru(\mathbf{L}^{pyridazine})_3](PF_6)^{+}$ in red, found in black.

Electrochemistry

In all cases freshly distilled (over CaH) acetonitrile was used, with the studied solutions containing 0.66 M of the appropriate $[Ru(\mathbf{L}^{azine})_3](PF_6)_2$ complex. The supporting electrolyte was 0.1 M $TBAPF_6$. The $Fc^{+/0}$ redox event was consistently observed at $E_m(\Delta E)$ 0.07(0.08) V, versus the 0.01 M $AgNO_3$/Ag reference electrode.

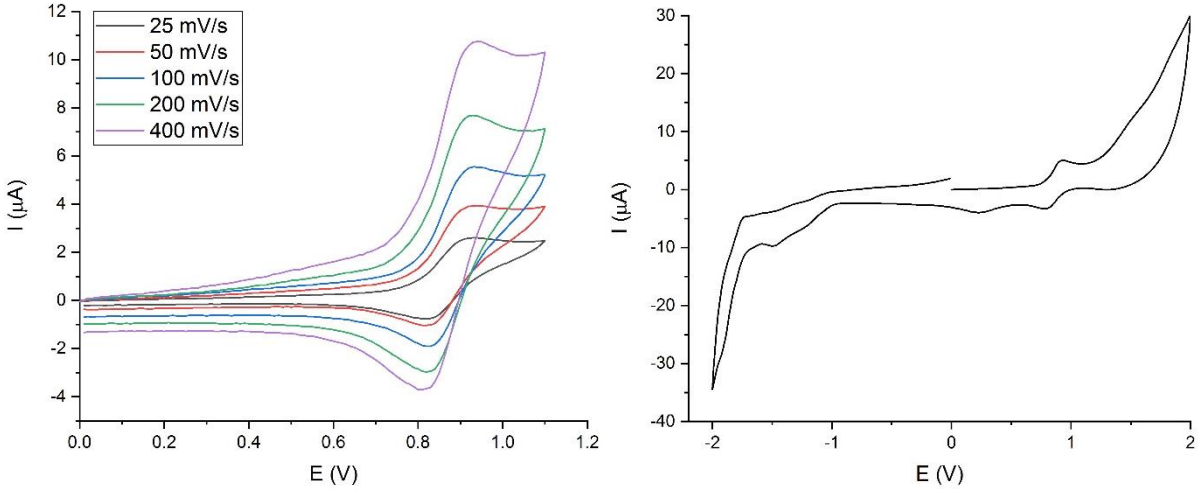

Figure S10: Cyclic voltammograms of 0.66 M $[Ru(\mathbf{L}^{pyridine})_3](PF_6)_2$ in MeCN with 0.1 M $TBAPF_6$ (left) scan rate study and (right) full range. Potentials are versus 0.01 M $AgNO_3$/Ag.

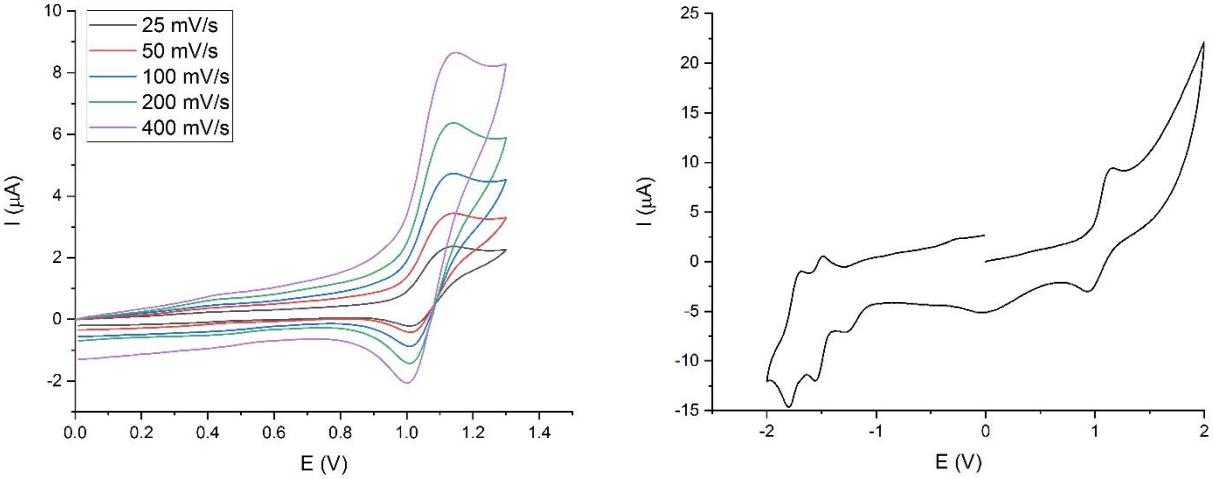

Figure S11: Cyclic voltammograms of 0.66 M $[Ru(\mathbf{L}^{pyridazine})_3](PF_6)_2$ in MeCN with 0.1 M $TBAPF_6$ (left) scan rate study and (right) full range at 400 mV/s. Potentials are versus 0.01 M $AgNO_3$/Ag.

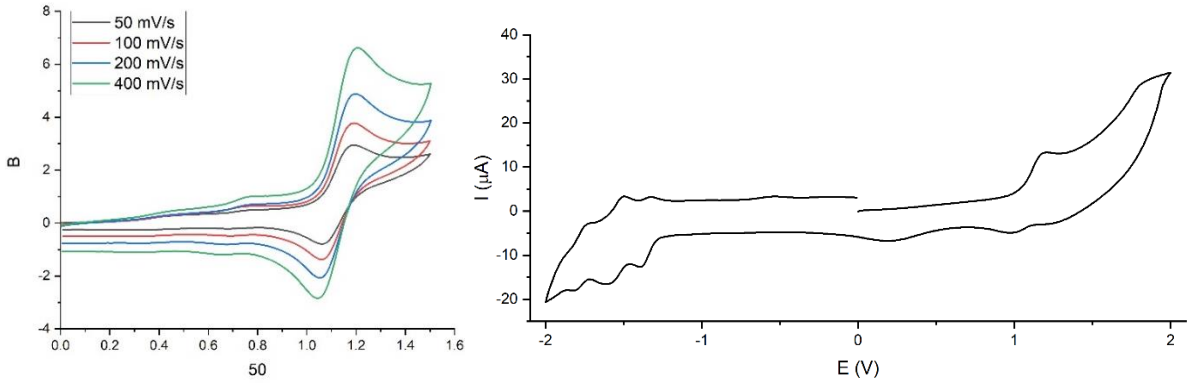

Figure S12: Cyclic voltammograms of 0.66 M [Ru($\mathbf{L^{4\text{-pyrimidine}}}$)$_3$](PF$_6$)$_2$ in MeCN with 0.1 M TBAPF$_6$; (left) scan rate study and (right) full range at 400 mV/s. Potential is versus 0.01 M AgNO$_3$/Ag.

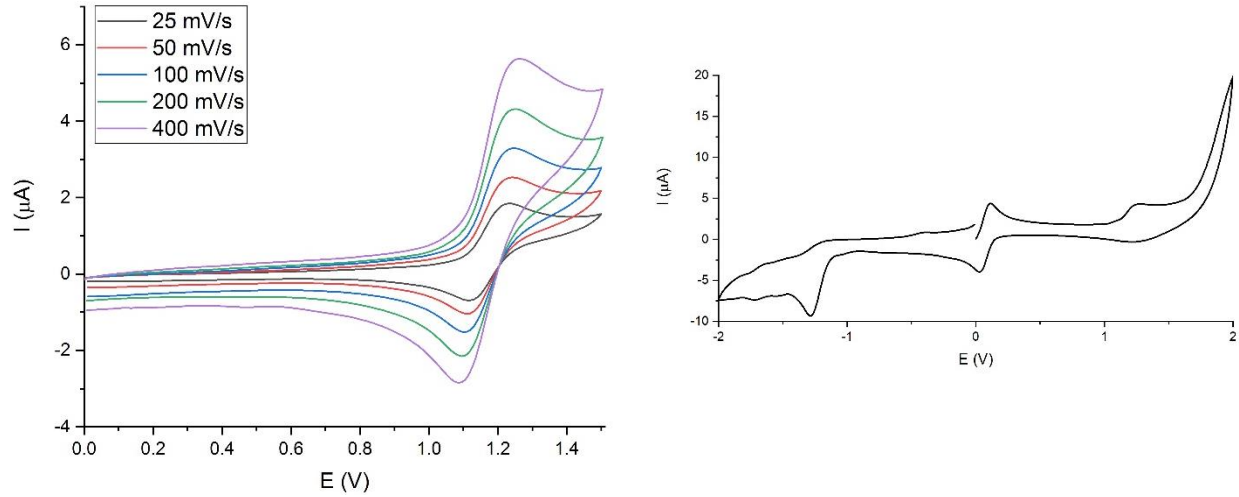

Figure S13: Cyclic voltammograms of 0.66 M [Ru($\mathbf{L^{pyrazine}}$)$_3$](PF$_6$)$_2$ in MeCN with 0.1 M TBAPF$_6$ (left) scan rate study and (right) full range at 100 mV/s with ferrocene internal reference. Potentials are versus 0.01 M AgNO$_3$/Ag.

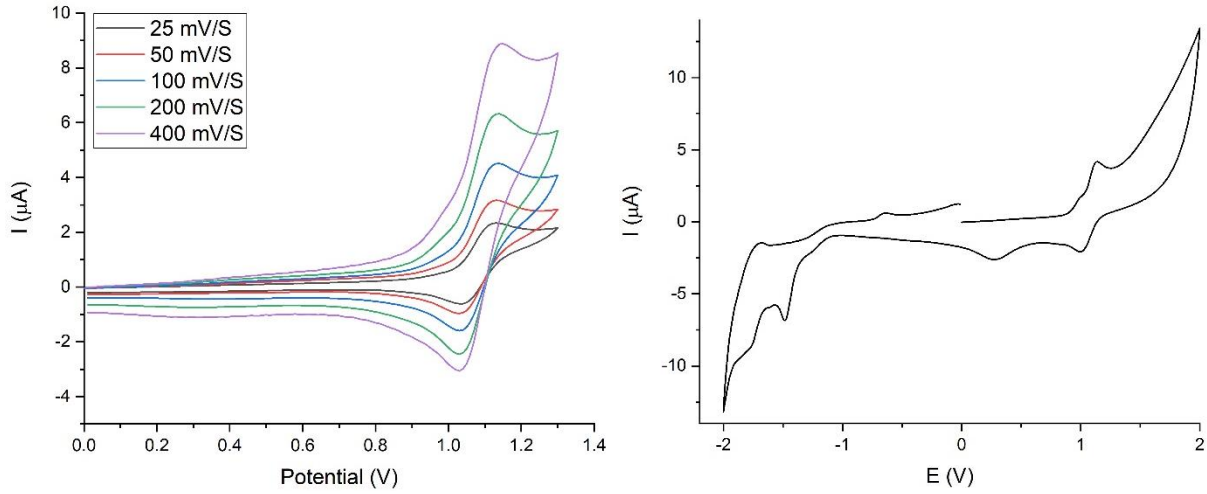

Figure S14: Cyclic voltammograms of 0.66 M [Ru($\mathbf{L^{2\text{-pyrimidine}}}$)$_3$](PF$_6$)$_2$ in MeCN with 0.1 M TBAPF$_6$ (left) scan rate study and (right) full range at 100 mV/s. Potentials are versus 0.01 M AgNO$_3$/Ag.

Tabulated values of redox potentials

Table S3: Oxidation, reduction and midpoint potentials for the $Ru^{III/II}$ process, at different scan rates for 0.66 M solutions of the ruthenium(II) tris-$\mathbf{L^{azine}}$ hexafluorophosphate complexes, carried out in 0.1 M $TBAPF_6$ in dry acetonitrile, against a 0.01 M $AgNO_3$/Ag reference.

$[RU(\mathbf{L^{PYRIDAZINE}})_3](PF_6)_2$						
V / MV/S	**E_{PA} (V)**	**I_A (µA)**	**E_{PC} (V)**	**I_C (µA)**	**ΔE (V)**	**E_M (V)**
400	1.14	6.36	0.94	-2.93	0.20	1.04
200	1.11	4.98	0.96	-2.41	0.15	1.04
100	1.12	3.87	0.97	-1.30	0.15	1.05
50	1.12	2.71	0.98	-0.78	0.14	1.05
25	1.12	2.09	0.99	-0.25	0.13	1.06
$[RU(\mathbf{L^{4\text{-}PYRIMIDINE}})_3](PF_6)_2$						
V / MV/S	**E_{PA} (V)**	**I_A (µA)**	**E_{PC} (V)**	**I_C (µA)**	**ΔE (V)**	**E_M (V)**
400	1.21	6.62	1.06	-2.85	0.15	1.13
200	1.20	4.88	1.06	-2.08	0.14	1.13
100	1.19	3.77	1.06	-1.38	0.13	1.13
50	1.19	2.95	1.06	-0.80	0.13	1.13
$[RU(\mathbf{L^{PYRAZINE}})_3](PF_6)_2$						
V / MV/S	**E_{PA} (V)**	**I_A (µA)**	**E_{PC} (V)**	**I_C (µA)**	**ΔE (V)**	**E_M (V)**
400	1.26	5.64	1.09	-2.85	0.18	1.18
200	1.25	4.32	1.10	-2.15	0.15	1.17
100	1.25	3.29	1.10	-1.52	0.15	1.18
50	1.24	2.53	1.11	-1.04	0.13	1.18
25	1.23	1.85	1.12	-0.69	0.11	1.18
$[RU(\mathbf{L^{2\text{-}PYRIMIDINE}})_3](PF_6)_2$						
V / MV/S	**E_{PA} (V)**	**I_A (µA)**	**E_{PC} (V)**	**I_C (µA)**	**ΔE (V)**	**E_M (V)**
400	1.15	8.89	1.03	-3.06	0.12	1.09
200	1.14	6.32	1.03	-2.45	0.11	1.09
100	1.14	4.51	1.03	-1.59	0.11	1.09
50	1.13	3.17	1.03	-0.96	0.1	1.08
25	1.13	2.34	1.03	-0.61	0.1	1.08
$[RU(\mathbf{L^{PYRIDINE}})_3](PF_6)_2$						
V / MV/S	**E_{PA} (V)**	**I_A (µA)**	**E_{PC} (V)**	**I_C (µA)**	**ΔE (V)**	**E_M (V)**
400	0.93	10.76	0.81	-3.71	0.13	0.87
200	0.93	7.68	0.82	-2.97	0.11	0.88
100	0.93	5.55	0.83	-1.90	0.10	0.88
50	0.94	3.94	0.82	-1.03	0.12	0.88
25	0.93	2.60	0.82	-0.76	0.11	0.88

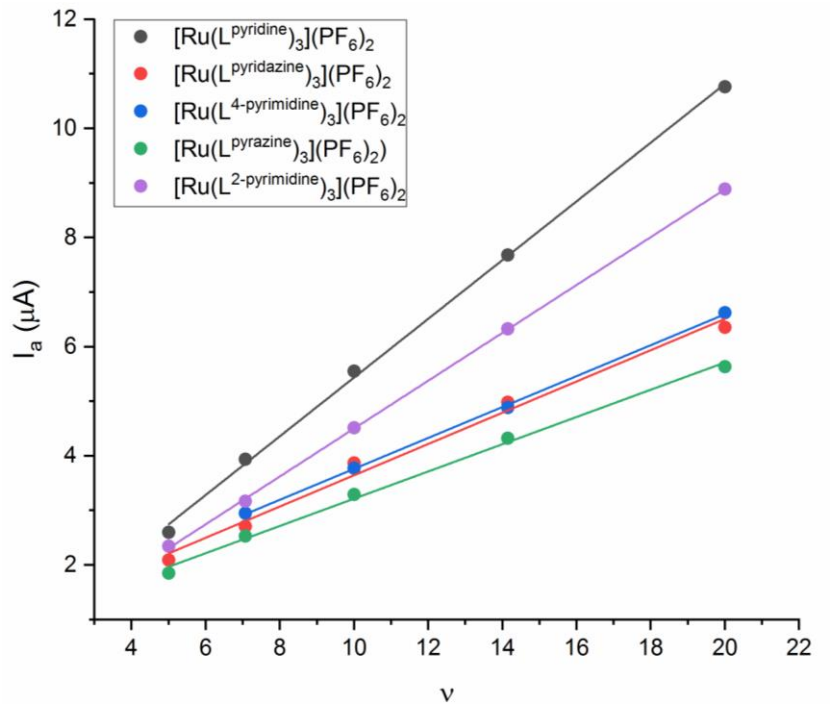

Figure S15: Plot of I_a against $\sqrt{\nu}$ shows linear correlations for the $Ru^{III/II}$ process for all five complexes.

UV-Vis Spectroscopy

For completeness, UV-vis spectra were recorded in acetonitrile (Figure S16-S21). All five complexes show a strong absorbance in the visible, with λ_{max} in the range 437-464 nm and extinction coefficients in the range 9600-18000 $M^{-1}cm^{-1}$. These are similar in energy and intensity to the simpler Ru^{II} tris-bipyridine and tris-diazine complexes,[4-6] and appear to show a similar trend in absorbance, although this is complicated by the overlapping bands in these spectra (Table S4).

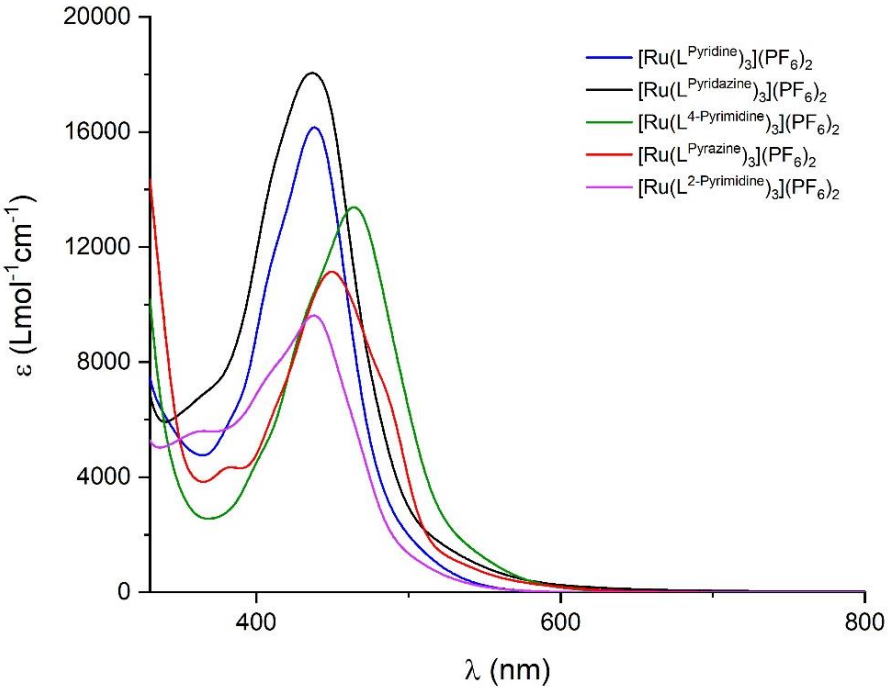

Figure S16: UV-Vis spectra of the five $[Ru^{II}(\mathbf{L^{azine}})_3](PF_6)_2$ complexes measured in acetonitrile.

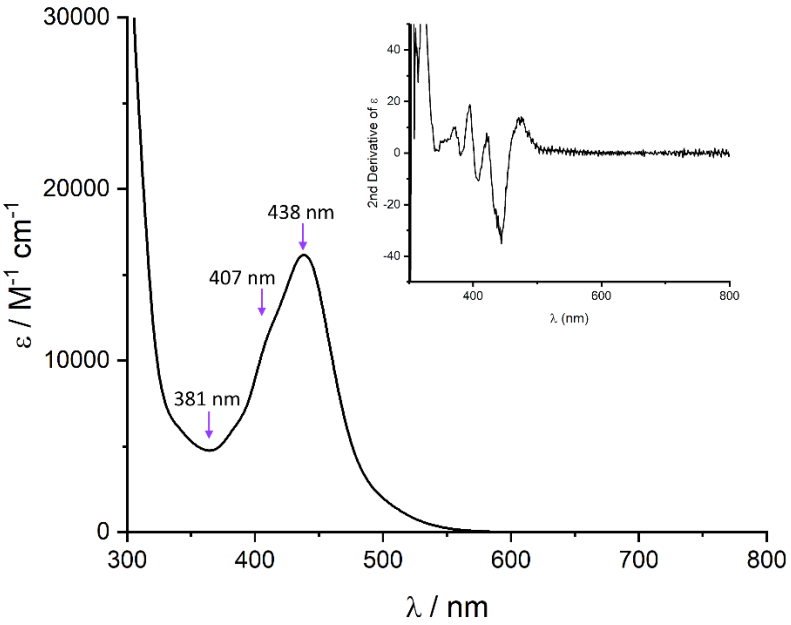

Figure S17: UV-Vis spectrum of $[Ru^{II}(\mathbf{L^{pyridine}})_3](PF_6)_2$ (**1**) measured in acetonitrile. Inset: 2nd Derivative of the extinction coefficient.

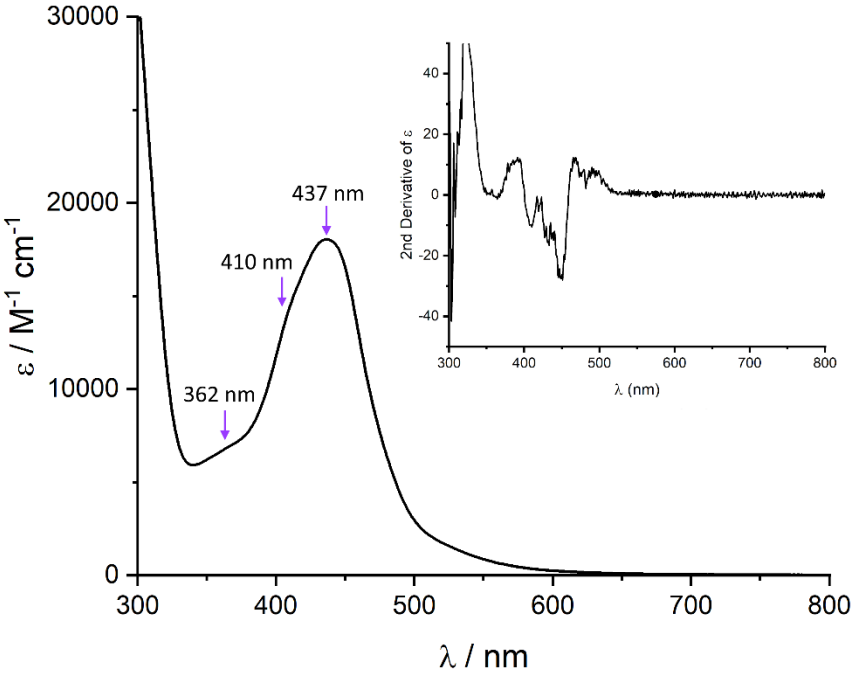

Figure S18: UV-Vis spectrum of $[Ru^{II}(\mathbf{L^{pyridazine}})_3](PF_6)_2$ (**2**) measured in acetonitrile. Inset: 2nd Derivative of the extinction coefficient.

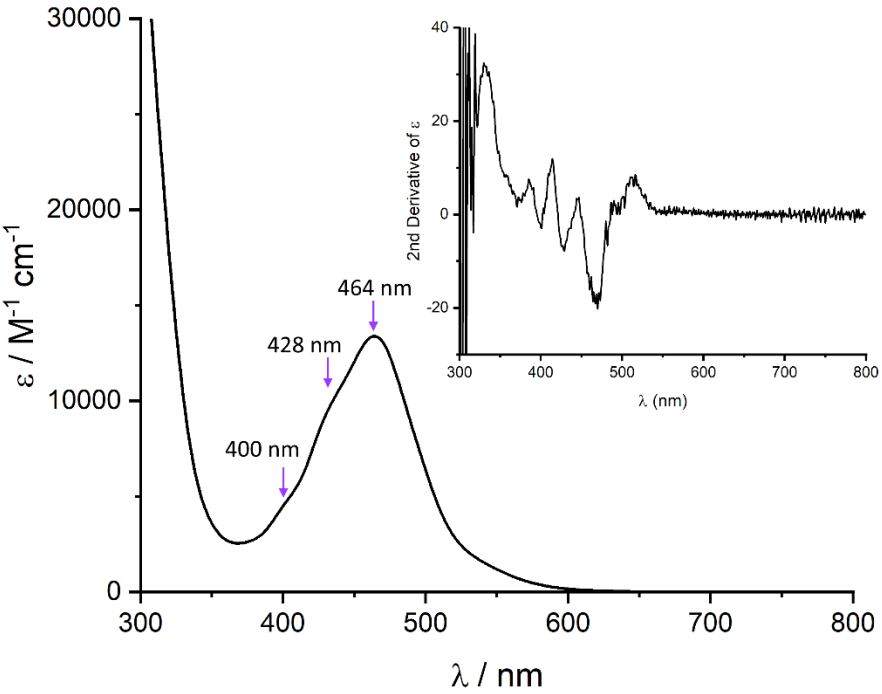

Figure S19: UV-Vis spectrum of $[Ru^{II}(\mathbf{L^{4\text{-}pyrimidine}})_3](PF_6)_2$ (**3**) measured in acetonitrile. Inset: 2nd Derivative of the extinction coefficient.

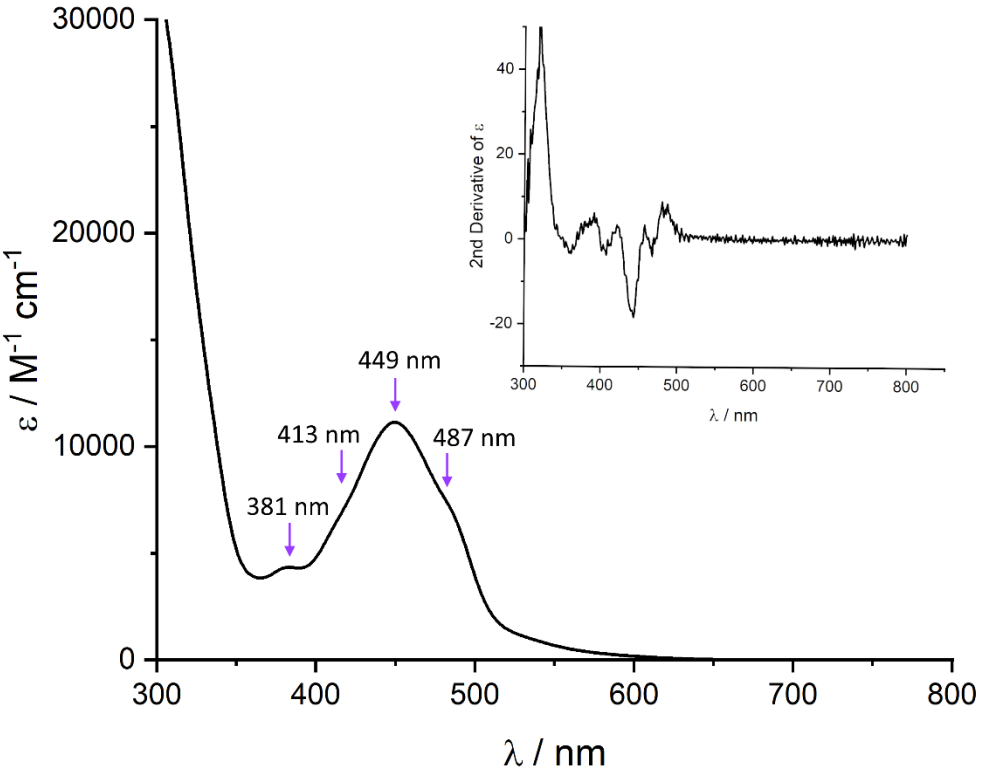

Figure S20: UV-Vis spectrum of $[Ru^{II}(\mathbf{L^{pyrazine}})_3](PF_6)_2$ (**4**) measured in acetonitrile. Inset: 2nd Derivative of the extinction coefficient.

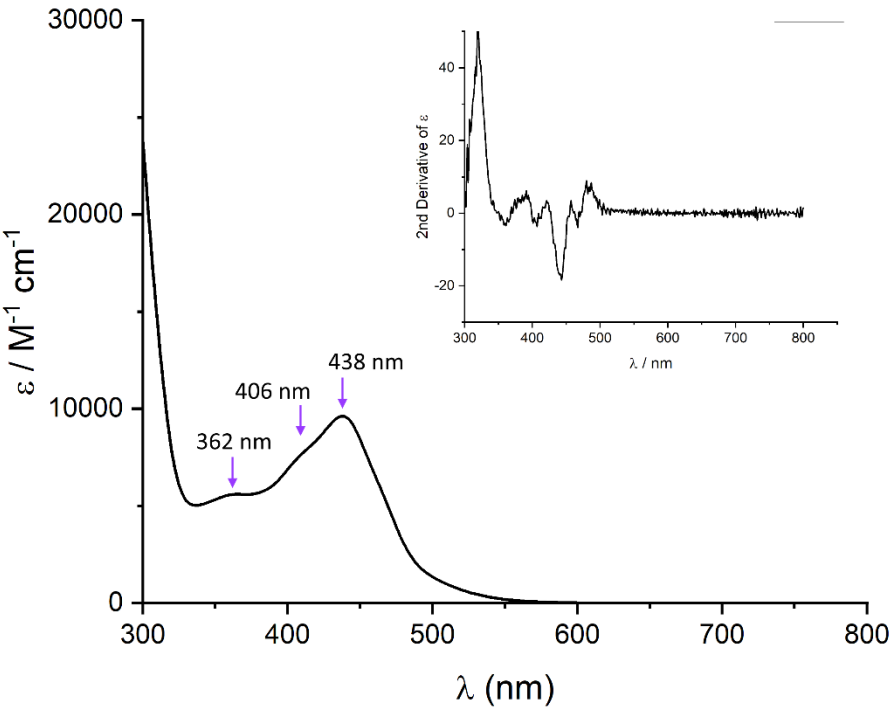

Figure S21: UV-Vis spectrum of $[Ru^{II}(\mathbf{L^{2\text{-}pyrimidine}})_3](PF_6)_2$ (**5**) measured in acetonitrile. Inset: 2nd Derivative of the extinction coefficient.

Table S4: Comparison of the UV-Vis spectra of the $[Ru(\mathbf{L}^{azine})_3]^{2+}$ complexes in acetonitrile with some literature $[Ru(biazine)_3]^{2+}$ complexes.[4, 5] [a]Note that the ligand used in the study by Kawanishi and co-workers was 6,6'-dimethyl-4,4'-bipyrimidine.

Azine	Ours		Kaim – $[Ru(biazine)_2]^{2+}$		Kawanishi– $[Ru(biazine)_2]^{2+}$	
	λ / nm	ε / L mol^{-1} cm^{-1}	λ / nm	ε / L mol^{-1} cm^{-1}	λ / nm	ε / L mol^{-1} cm^{-1}
pyridazine	362				360	11748
	410		410	12022	412	12022
	437	18053	444	11481	447	12022
pyridine	381					
	407					
	438	16163	451	14125	449	14791
2pyrimidine	362					
	406		418	8128	331	16982
	438	9620	454	8511	450	8709
pyrazine	381					
	413		415			
	449	11144	440	12882	439	13803
	487					
4pyrimidine [a]	428		462			
	464	13385	496	6456	497	10000

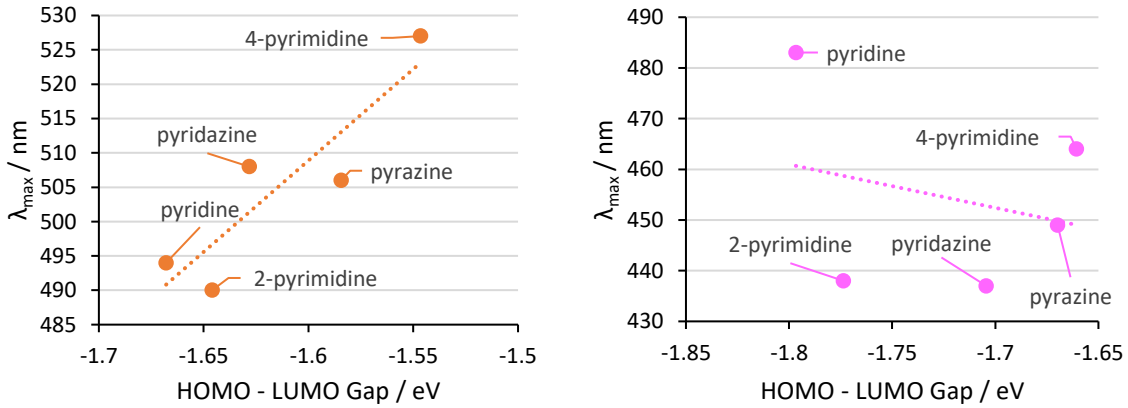

Figure S22: No correlations were found between the λ_{max} value observed experimentally for each of the complexes and the respective calculated HOMO-LUMO energy gap, for either $[Fe(\mathbf{L}^{azine})_3]^{2+}$ (left, orange) or $[Ru(\mathbf{L}^{azine})_3]^{2+}$ (right, pink).

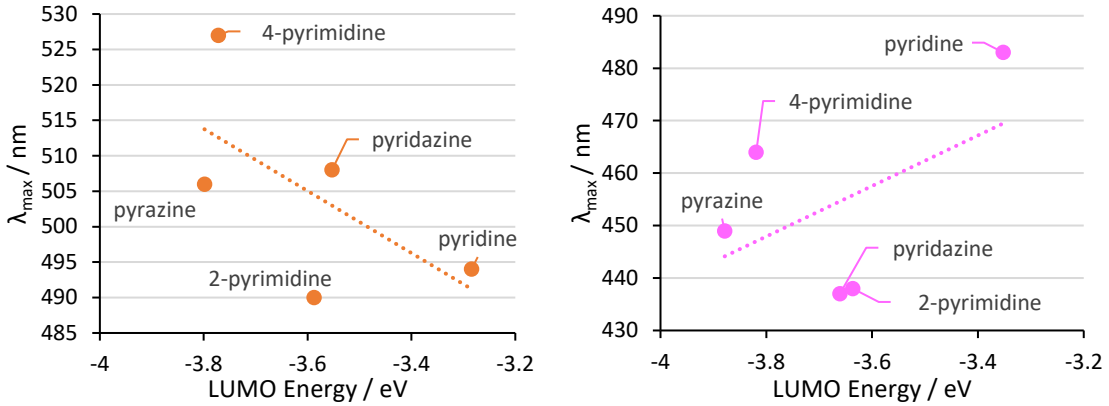

Figure S23: No correlations were found between the λ_{max} value observed experimentally for each of the complexes and the respective calculated LUMO energy, for either $[Fe(\mathbf{L}^{azine})_3]^{2+}$ (left, orange) or $[Ru(\mathbf{L}^{azine})_3]^{2+}$ (right, pink).

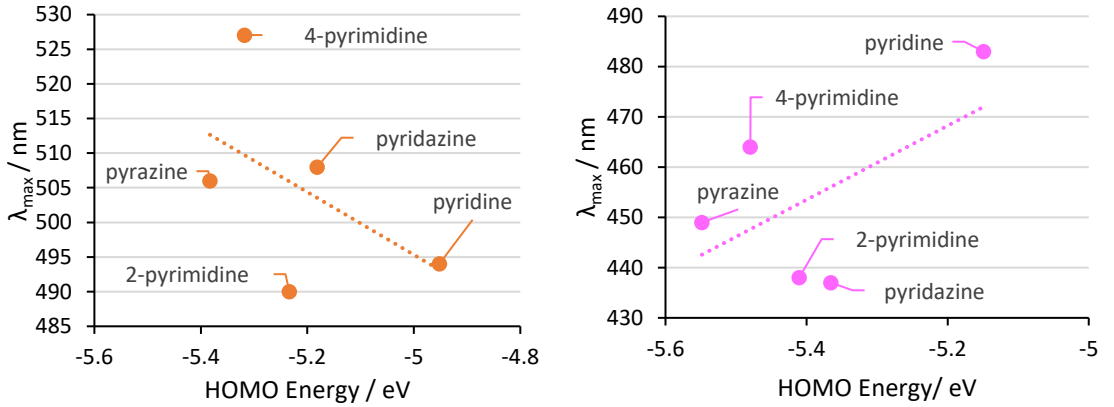

Figure S24: No correlations were found between the λ_{max} value observed experimentally for each of the complexes and the respective calculated HOMO energy, for either $[Fe(\mathbf{L}^{azine})_3]^{2+}$ (left, orange) or $[Ru(\mathbf{L}^{azine})_3]^{2+}$ (right, pink).

Density Functional Theory Calculations – Orca 4.0.1

Initial DFT testing of the ruthenium complexes was done using Orca 4.0.1 to look at the difference in energies of the isomers (*mer* and *fac*) on the Ru(II) complexes. Calculations of the HOMO energies of all the isomers of the ruthenium complexes were also carried out.

All calculations were performed within DFT theory with the BP86 functional set.[7, 8] In all cases dispersion corrections were added using D3 version of Grimmes dispersion with Becke-Johnson damping.[9] For Ru and the corresponding def2-ECP was used.[10] Where applicable the complexes were optimised from the crystal structure data obtained. For the complexes where no crystal structure was available the geometry was optimised from the $\mathbf{L^{pyridine}}$ complex with the appropriate CH replaced with N. Geometries were optimised first with the def2-SVP basis set with all atoms in the phase.[11] The minima were confirmed through the absence of imaginary frequencies. A second geometry optimisation was performed with the def2-TZVPP basis set.[11] Using the CPCM model with MeCN a final single point calculation was carried out.[12] The data from these calculations is listed below.

Tabulated electronic energy and molecular orbital energy values for $[Ru^{II}(L^{azine})_3](PF_6)_2$

Table S5: Summary of computed electronic energy values (E_{el}) of the *mer* and *fac* isomers of the ruthenium(II) complexes.

	E_{el} (Hartree)			
	Fac-Δ	**Fac-Λ**	**Mer-Δ**	**Mer-Λ**
$[Ru^{II}(\mathbf{L^{pyridine}})_3](PF_6)_2$	-3068.2526	-3068.2582	-3068.2589	-3068.2579
$[Ru^{II}(\mathbf{L^{pyridazine}})_3](PF_6)_2$	-3116.3105	-3116.3106	-3116.3093	-3116.3087
$[Ru^{II}(\mathbf{L^{2\text{-}pyrimdine}})_3](PF_6)_2$	-3116.3829	-3116.3831	-3116.3862	-3116.3852
$[Ru^{II}(\mathbf{L^{4\text{-}pyrimidine}})_3](PF_6)_2$	-3116.3874	-3116.3877	-3116.3878	-3116.3872
$[Ru^{II}(\mathbf{L^{pyrazine}})_3](PF_6)_2$	-3116.3688	-3116.3692	-3116.3673	-3116.3690

Table S6: Selected MO energies of the five $[Ru^{II}(\mathbf{L^{azine}})_3]^{2+}$ complexes, as calculated by DFT.

	Isomer	**HOMO / eV**	**LUMO / eV**	**HOMO-LUMO Gap / eV**
$[Ru^{II}(\mathbf{L^{4\text{-}pyrimidine}})_3](PF_6)_2$	**fac delta**	-5.527724	-3.867556	1.660168
	fac lambda	-5.526907	-3.867284	1.659623
	mer delta	-5.530989	-3.877625	1.653365
	mer lambda	-5.531533	-3.879801	1.651732
$[Ru^{II}(\mathbf{L^{2\text{-}pyrimdine}})_3](PF_6)_2$	**fac delta**	-5.436566	-3.654491	1.782075
	fac lambda	-5.421871	-3.645239	1.776632
	mer delta	-5.441736	-3.658845	1.782891
	mer lambda	-5.447450	-3.665920	1.781530
$[Ru^{II}(\mathbf{L^{pyridine}})_3](PF_6)_2$	**fac delta**	-5.161730	-3.385642	1.776088
	fac lambda	-5.168805	-3.370404	1.798401
	mer delta	-5.176425	-3.379928	1.796497
	mer lambda	-5.176969	-3.494488	1.682481
$[Ru^{II}(\mathbf{L^{pyrazine}})_3](PF_6)_2$	**fac delta**	-5.640379	-3.903747	1.736632
	fac lambda	-5.636842	-3.900210	1.736632
	mer delta	-5.603916	-3.938850	1.665066
	mer lambda	-5.597657	-3.930143	1.667515
$[Ru^{II}(\mathbf{L^{pyridazine}})_3](PF_6)_2$	**fac delta**	-5.425681	-3.621021	1.804660
	fac lambda	-5.426497	-3.621565	1.804932
	mer delta	-5.362300	-3.660600	1.701700
	mer lambda	-5.354115	-3.657756	1.696359

Plots of HOMO Energies versus E_m at Varying Scan Rates

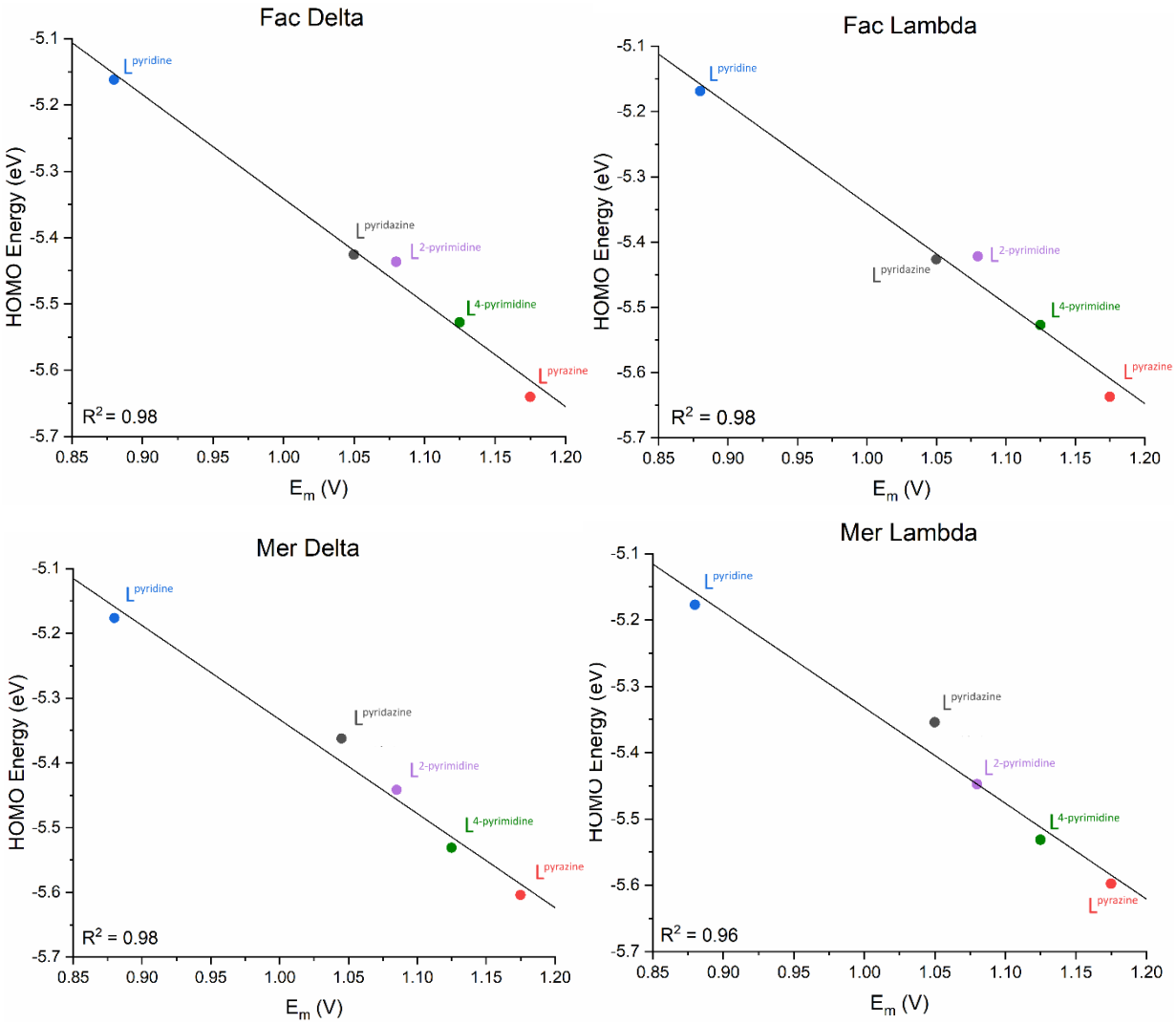

Figure S25: Plots showing the linear fit of experimental $E_m(Ru^{III/II})$ values for the $[Ru(\mathbf{L}^{azine})_3](PF_6)_2$ of the complexes as measured by CV (100 mV/s) in dry MeCN containing 0.1 M $TBAPF_6$ against 0.01 M $AgNO_3$/Ag reference electrode versus DFT calculated energies of the HOMOs.

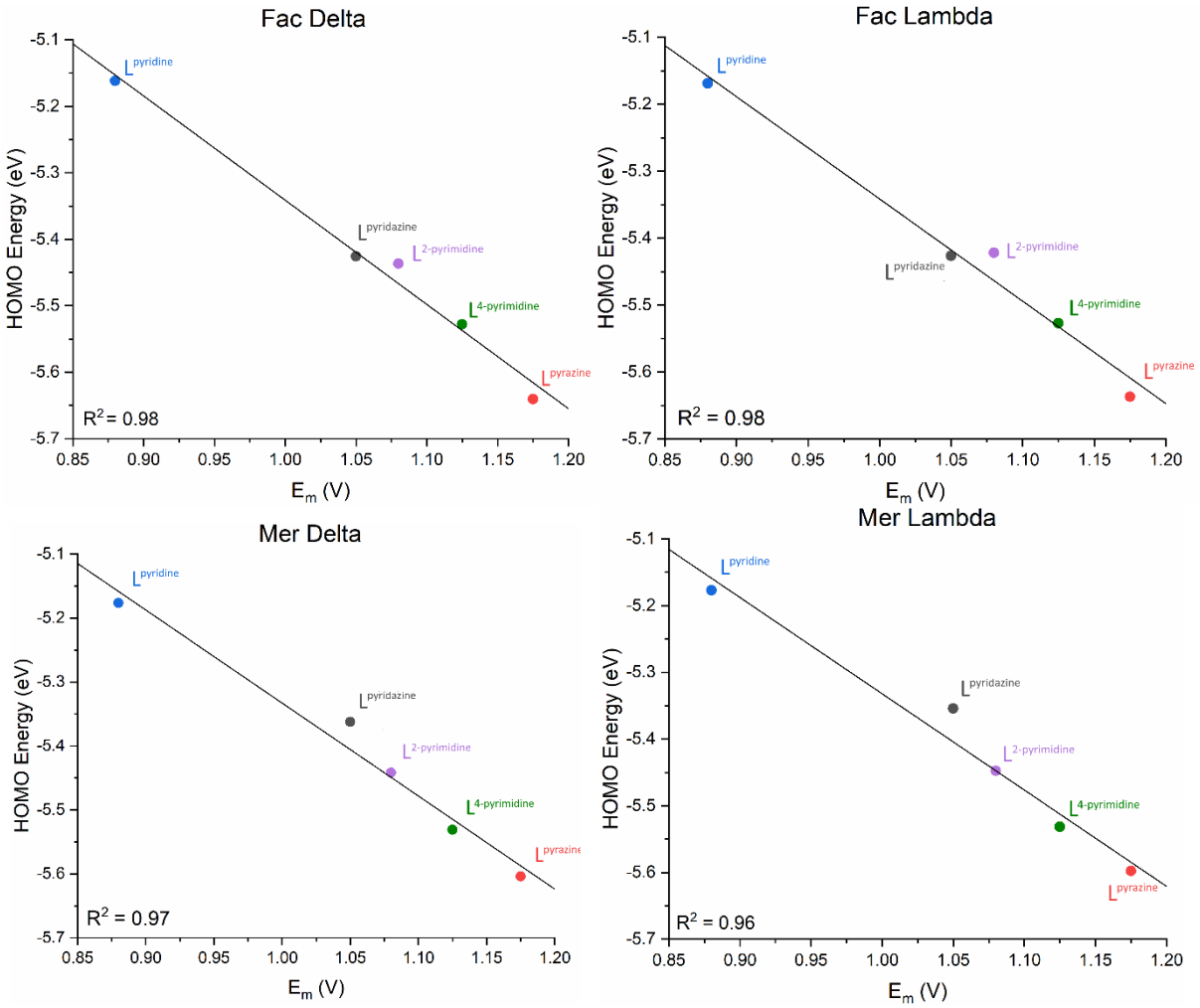

Figure 26: Plots showing the linear fit of experimental $E_m(Ru^{III/II})$ values for the $[Ru(\mathbf{L}^{azine})_3](PF_6)_2$ of the complexes as measured by CV (50 mV/s) in dry MeCN containing 0.1 M $TBAPF_6$ against 0.01 M $AgNO_3$/Ag reference electrode versus DFT calculated energies of the HOMOs.

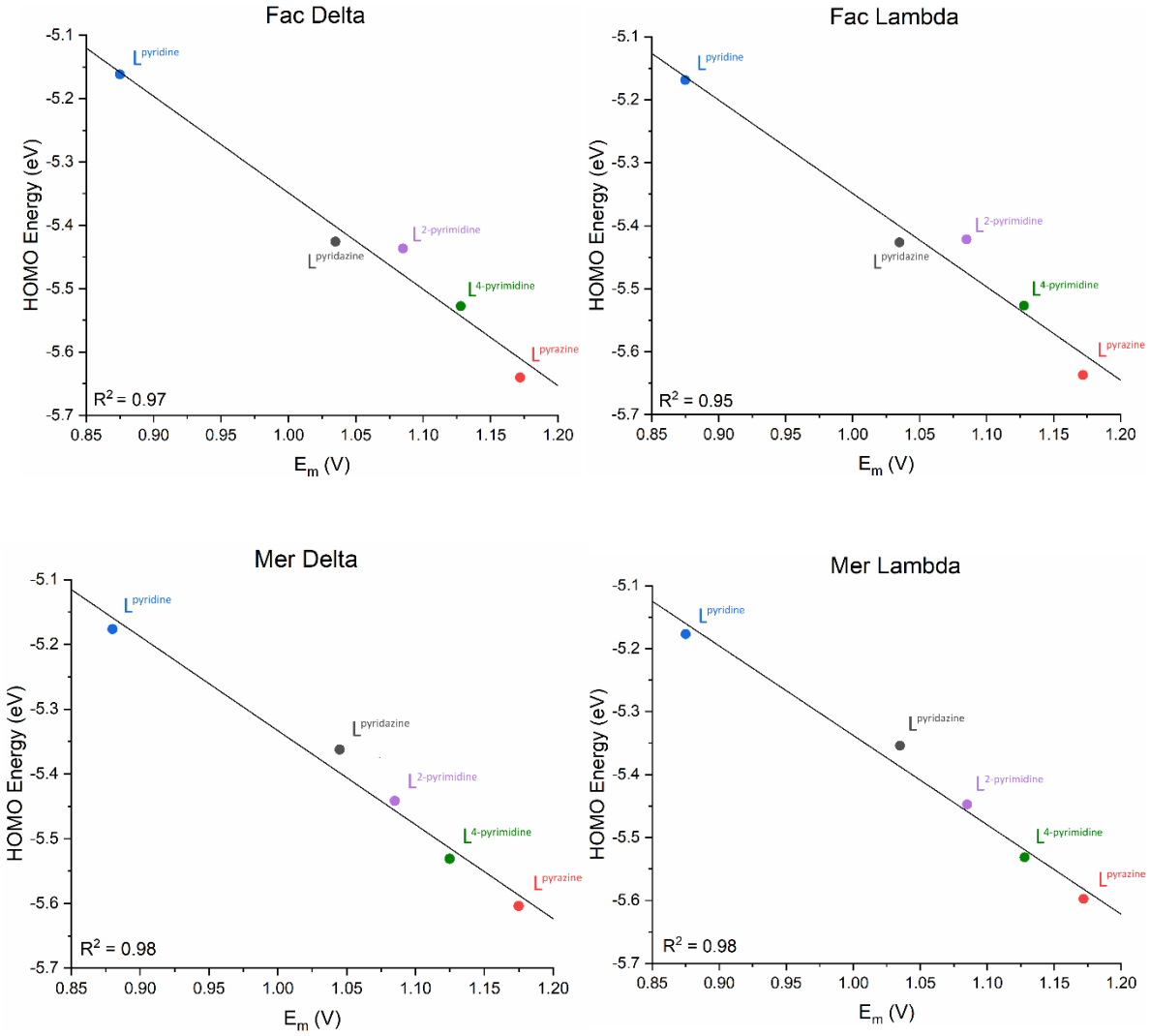

Figure S27: Plots showing the linear fit of experimental $E_m(Ru^{III/II})$ values for the $[Ru(\mathbf{L}^{azine})_3](PF_6)_2$ of the complexes as measured by CV (200 mV/s) in dry MeCN containing 0.1 M $TBAPF_6$ against 0.01 M $AgNO_3$/Ag reference electrode versus DFT calculated energies of the HOMOs.

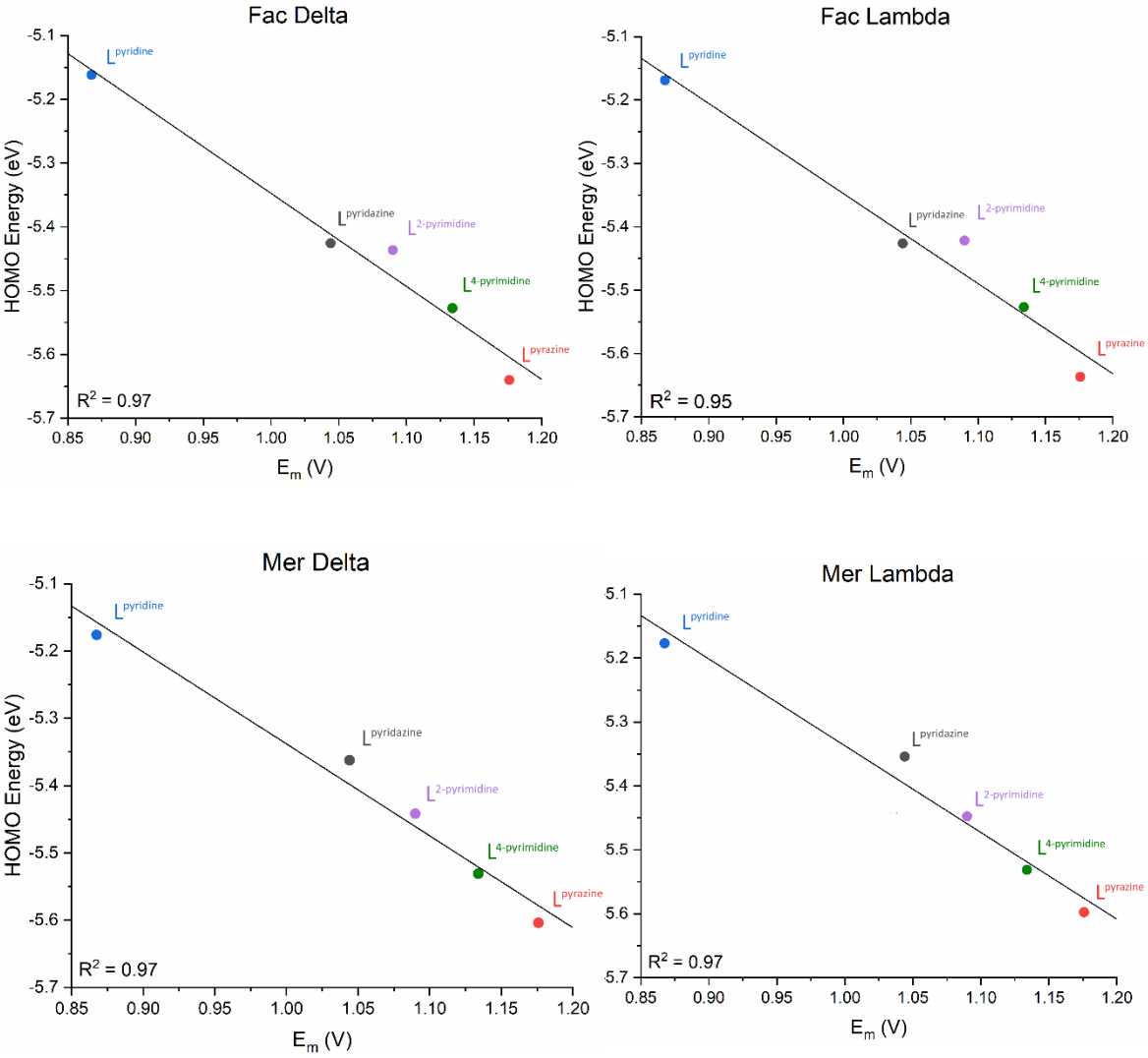

Figure S28: Plots showing the linear fit of experimental $E_m(Ru^{III/II})$ values for the $[Ru(\mathbf{L}^{azine})_3](PF_6)_2$ of the complexes as measured by CV (400 mV/s) in dry MeCN containing 0.1 M $TBAPF_6$ against 0.01 M $AgNO_3$/Ag reference electrode versus DFT calculated energies of the HOMOs.

Density Functional Theory Calculations – Orca 5.0.3

All further calculations were done using Orca 5.0.3 on the iron, ruthenium and osmium mer-Δ complexes.[13] All calculations were performed within DFT theory with the BP86 functional set.[7, 8] In all cases dispersion corrections were added using D3 version of Grimmes dispersion with Becke-Johnson damping.[9] For Ru and Os the corresponding def2-ECP was used.[10] Where applicable the complexes were optimised from the crystal structure data obtained. For the Fe and Ru complexes where no crystal structure was available the geometry was optimised from the $\mathbf{L^{pyridine}}$ complex with the appropriate CH replaced with N. The structures of the Os complexes were optimised starting from the Ru^{II} geometries. Geometries were optimised first with the def2-SVP basis set with all atoms in the phase.[11] The minima were confirmed through the absence of imaginary frequencies. A second geometry optimisation was performed with the def2-TZVPP basis set.[11] Using the CPCM model with MeCN a final single point calculation was carried out.[12] The data from these calculations is listed below.

Table S7: Selected structural parameters of the calculated structures of the $[M^{II}(\mathbf{L^{azine}})_3]^{2+}$ families of compounds.

		Average M-L bond length / Å			**Octahedral distortion /°**		
		R	**NR**	**Δ**	**R**	**NR**	**Δ**
Fe^{II}	pyridine	1.941	-	-	54.87	-	-
	pyridazine	1.927	-	-	53.01	-	-
	2pyrimidine	1.940	-	-	58.13	-	-
	4pyrimidine	1.941	-	-	63.66	-	-
	pyrazine	1.939	-	-	55.35	-	-
Ru^{II}	pyridine	2.044	2.061	0.017	73.93	76.32	2.39
	pyridazine	2.033	2.050	0.017	71.95	74.04	2.09
	2pyrimidine	2.044	2.061	0.017	73.21	74.48	1.27
	4pyrimidine	2.044	2.061	0.018	74.85	75.99	1.14
	pyrazine	2.041	2.058	0.017	73.26	74.54	1.28
Os^{II}	pyridine	2.055	2.105	0.050	78.49	84.24	5.75
	pyridazine	2.045	2.100	0.055	78.27	107.04	28.77
	2pyrimidine	2.055	2.106	0.051	78.42	82.05	3.63
	4pyrimidine	2.055	2.105	0.050	80.04	82.96	2.93
	pyrazine	2.052	2.102	0.050	78.39	81.49	3.10

Table S8: Selected MO energies for the M^{2+} complexes calculated with Orca5.0.3.

Metal	Ligand	HOMO / eV	LUMO / eV	HOMO-LUMO Gap / eV
Fe	pyridine	-4.9522	-3.2843	-1.6679
	pyridazine	-5.1813	-3.553	-1.6283
	4pyrimidine	-5.3183	-3.7718	-1.5465
	pyrazine	-5.383	-3.7986	-1.5844
	2pyrimidine	-5.2337	-3.5877	-1.646
Ru	pyridine	-5.149	-3.3523	-1.7967
	pyridazine	-5.3654	-3.661	-1.7044
	4pyrimidine	-5.4797	-3.8191	-1.6606
	pyrazine	-5.5484	-3.8786	-1.6698
	2pyrimidine	-5.4104	-3.6368	-1.7736
Os	pyridine	-5.0197	-3.4103	-1.6094
	pyridazine	-5.2379	-3.7284	-1.5095
	4pyrimidine	-5.3433	-3.8655	-1.4778
	pyrazine	-5.4314	-3.9433	-1.4881
	2pyrimidine	-5.2904	-3.6953	-1.5951

Table S9: Selected MO energies for the adiabatic M^{3+} complexes calculated with Orca5.0.3. Geometry optimised with M^{3+}

Metal	Ligand	SOMO / eV	LUMO / eV	HOMO-LUMO Gap / eV
Fe	pyridine	-6.4303	-3.8946	-2.5357
	pyridazine	-6.5111	-4.0979	-2.4132
	4pyrimidine	-6.5927	-4.2579	-2.3348
	pyrazine	-6.5445	-4.2977	-2.2468
	2pyrimidine	-6.4806	-4.1177	-2.3629
Ru	pyridine	-6.3363	-3.8036	-2.5327
	pyridazine	-6.457	-4.1036	-2.3534
	4pyrimidine	-6.5011	-4.2732	-2.2279
	pyrazine	-6.4775	-4.278	-2.1995
	2pyrimidine	-6.3979	-4.0817	-2.3162
Os	pyridine	-6.2373	-3.8564	-2.3809
	pyridazine	-6.3912	-4.1822	-2.209
	4pyrimidine	-6.4525	-4.3235	-2.129
	pyrazine	-6.4076	-4.352	-2.0556
	2pyrimidine	-6.354	-4.1469	-2.2071

Table S10: Selected MO energies for the vertical M^{3+} complexes calculated with Orca5.0.3. Structure optimised with M^{2+} geometry. Single point calculation carried out as M^{3+}.

Metal	Ligand	SOMO / eV	LUMO / eV	HOMO-LUMO Gap / eV
Fe	pyridine	-6.4601	-3.9021	-2.558
	pyridazine	-6.542	-4.1097	-2.4323
	4pyrimidine	-6.5977	-4.3414	-2.2563
	pyrazine	-6.5673	-4.3169	-2.2504
	2pyrimidine	-6.5281	-4.1633	-2.3648
Ru	pyridine	-6.3514	-3.833	-2.5184
	pyridazine	-6.4944	-4.1507	-2.3437
	4pyrimidine	-6.5049	-4.3027	-2.2022
	pyrazine	-6.4723	-4.3271	-2.1452
	2pyrimidine	-6.4606	-4.1068	-2.3538
Os	pyridine	-6.2604	-3.9017	-2.3587
	pyridazine	-6.4585	-4.2319	-2.2266
	4pyrimidine	-6.4605	-4.3615	-2.099
	pyrazine	-6.4437	-4.4103	-2.0334
	2pyrimidine	-6.4016	-4.1847	-2.2169

Table S11: Selected MO energies for the non-relativistic M^{2+} complexes calculated with Orca5.0.3.

Metal	Ligand	HOMO / eV	LUMO / eV	HOMO-LUMO Gap / eV	Difference in non-relativistic and relativistic HOMO ($HOMO_{nonrel} - HOMO_{rel}$)
Ru	pyridine	-5.2028	-3.3364	-1.8664	-0.0538
	pyridazine	-5.4125	-3.644	-1.7685	-0.0471
	4pyrimidine	-5.5169	-3.8076	-1.7093	-0.0372
	pyrazine	-5.5936	-3.8578	-1.7358	-0.0452
	2pyrimidine	-5.4607	-3.6195	-1.8412	-0.0503
Os	pyridine	-5.221	-3.3548	-1.8662	-0.2013
	pyridazine	-5.4521	-3.6974	-1.7547	-0.2142
	4pyrimidine	-5.5227	-3.8197	-1.703	-0.1794
	pyrazine	-5.6016	-3.8761	-1.7255	-0.1702
	2pyrimidine	-5.4682	-3.631	-1.8372	-0.1778

Perspective view of the HOMO of the mer complexes calculated with Orca 5.0.3

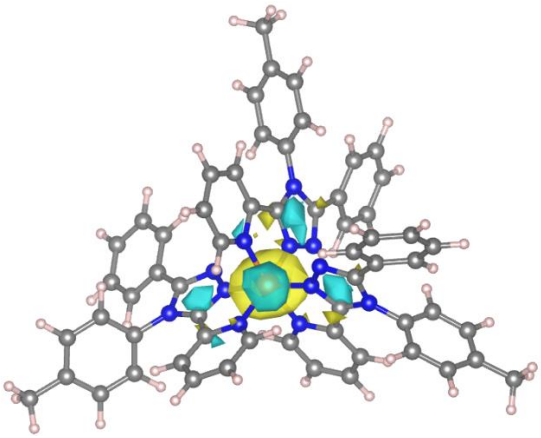

Figure S29: Perspective view of the HOMO of $[Fe^{II}(\mathbf{L^{pyridine}})_3]^{2+}$.

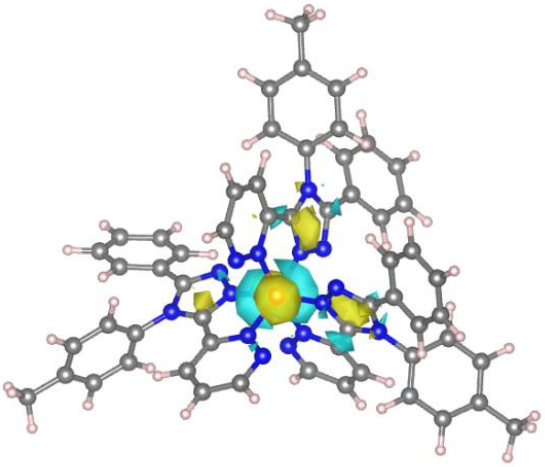

Figure S30: Perspective view of the HOMO of $[Fe^{II}(\mathbf{L^{pyridazine}})_3]^{2+}$.

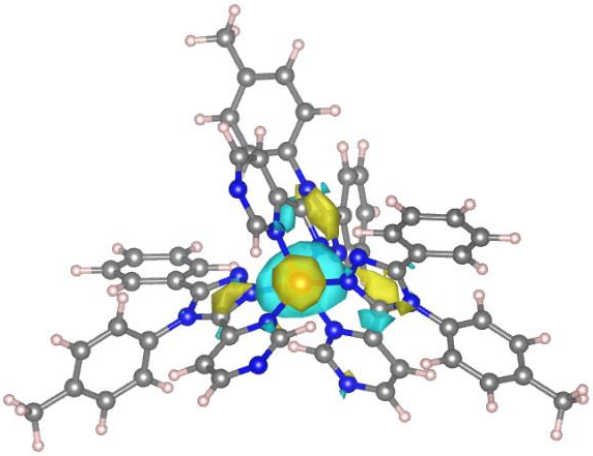

Figure S31: Perspective view of the HOMO of $[Fe^{II}(\mathbf{L^{4\text{-}pyrimidine}})_3]^{2+}$.

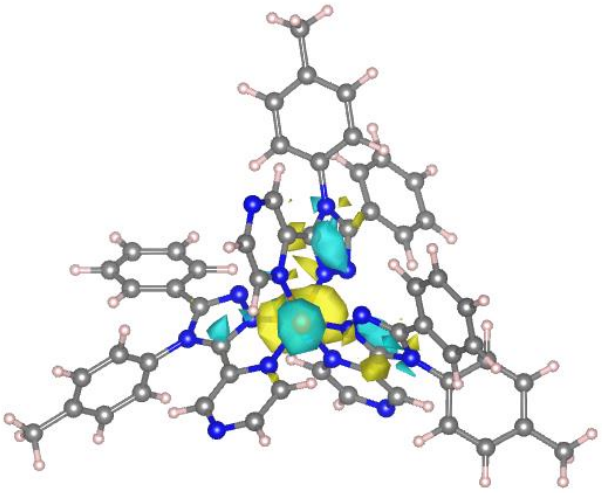

Figure S32: Perspective view of the HOMO of $[Fe^{II}(\mathbf{L}^{\mathbf{pyrazine}})_3]^{2+}$.

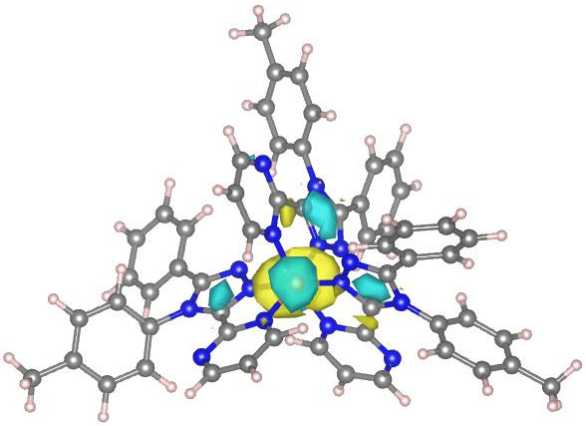

Figure S33: Perspective view of the HOMO of $[Fe^{II}(\mathbf{L}^{\mathbf{2\text{-}pyrimidine}})_3]^{2+}$.

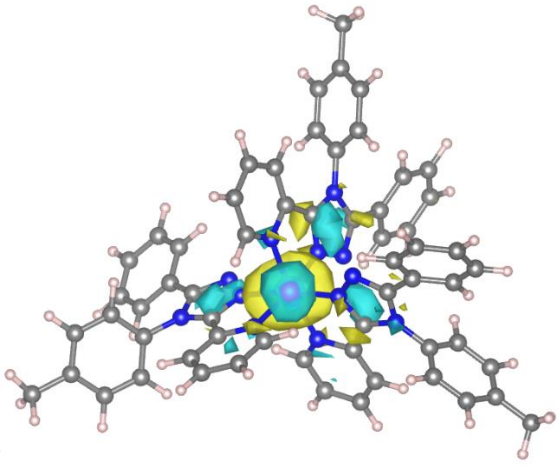

Figure S34: Perspective view of the HOMO of $[Ru^{II}(\mathbf{L}^{\mathbf{pyridine}})_3]^{2+}$.

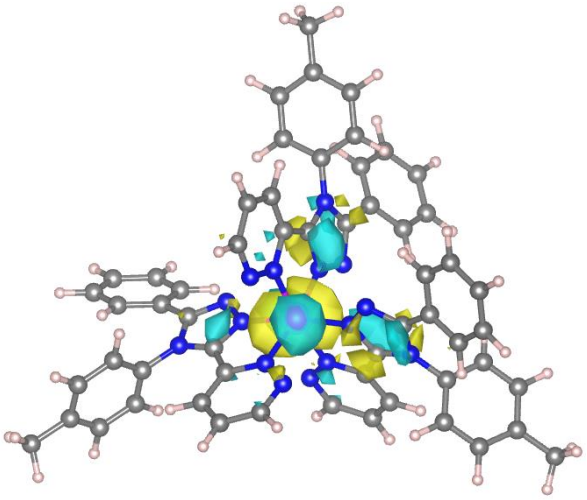

Figure S35: Perspective view of the HOMO of $[Ru^{II}(\mathbf{L}^{\mathbf{pyridazine}})_3]^{2+}$.

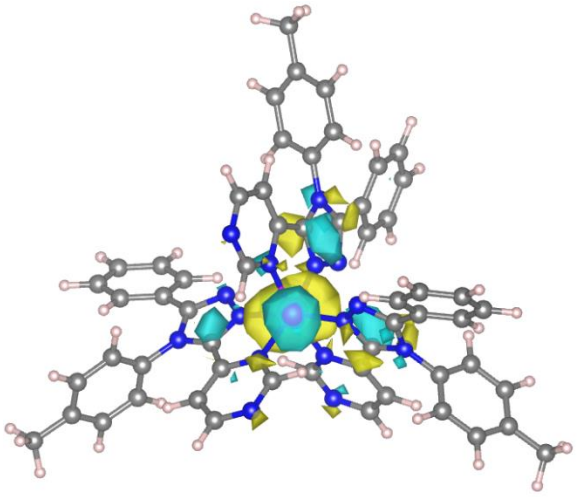

Figure S36: Perspective view of the HOMO of $[Ru^{II}(\mathbf{L}^{\mathbf{4\text{-}pyrimidine}})_3]^{2+}$.

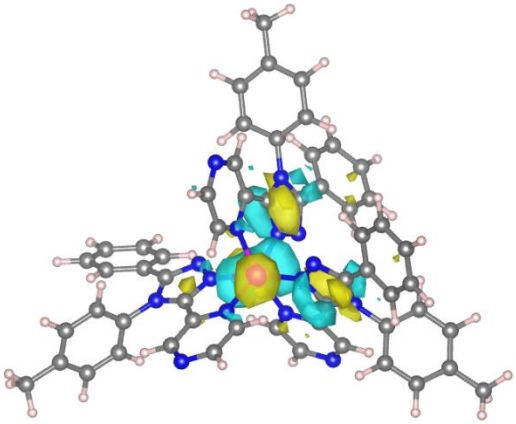

Figure S37: Perspective view of the HOMO of $[Ru^{II}(\mathbf{L}^{\mathbf{pyrazine}})_3]^{2+}$.

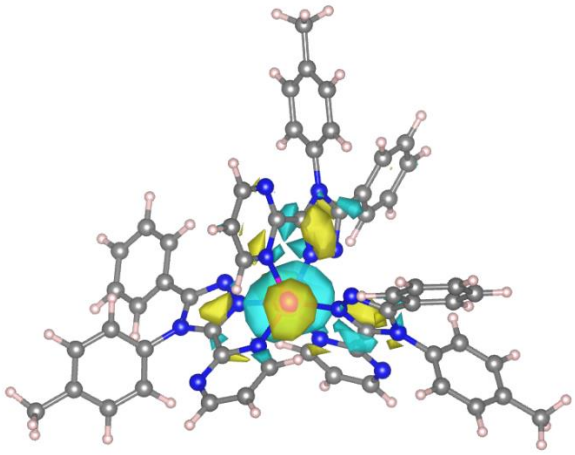

Figure S38: Perspective view of the HOMO of $[Ru^{II}(\mathbf{L}^{\mathbf{2\text{-}pyrimidine}})_3]^{2+}$.

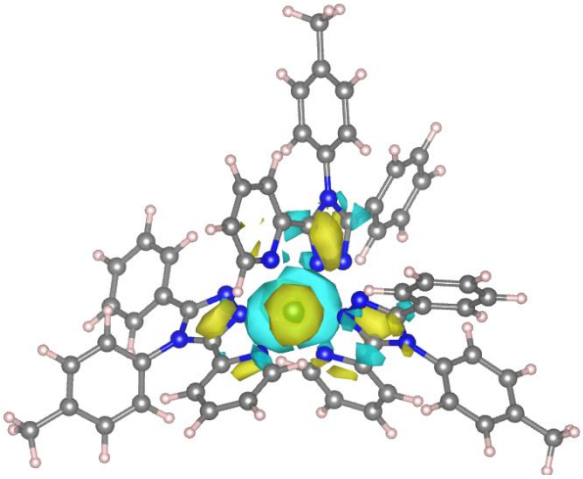

Figure S39: Perspective view of the HOMO of $[Os^{II}(\mathbf{L}^{\mathbf{pyridine}})_3]^{2+}$.

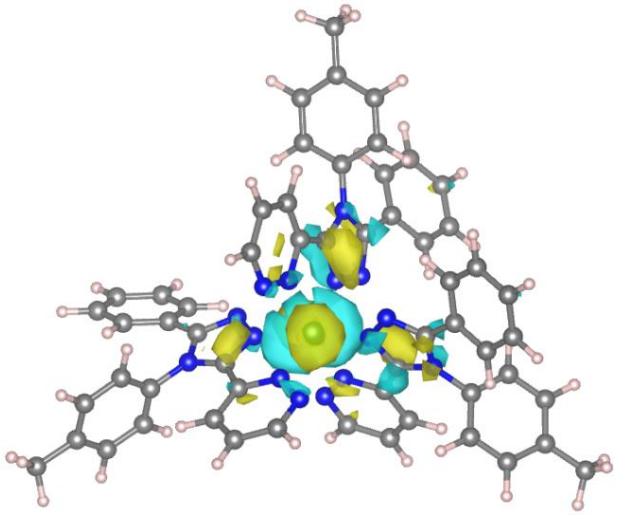

Figure S40: Perspective view of the HOMO of $[Os^{II}(\mathbf{L}^{\mathbf{pyridazine}})_3]^{2=}$.

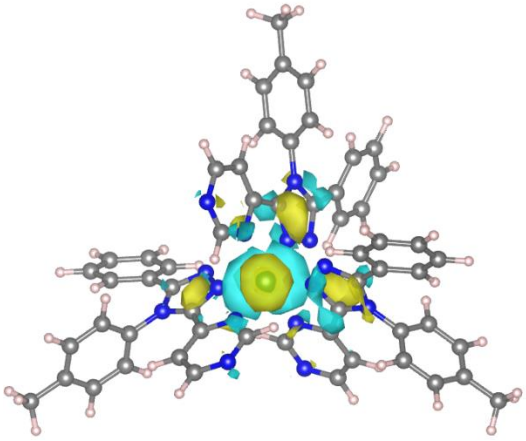

Figure S41: Perspective view of the HOMO of $[Os^{II}(\mathbf{L^{4\text{-}pyrimidine}})_3]^{2+}$.

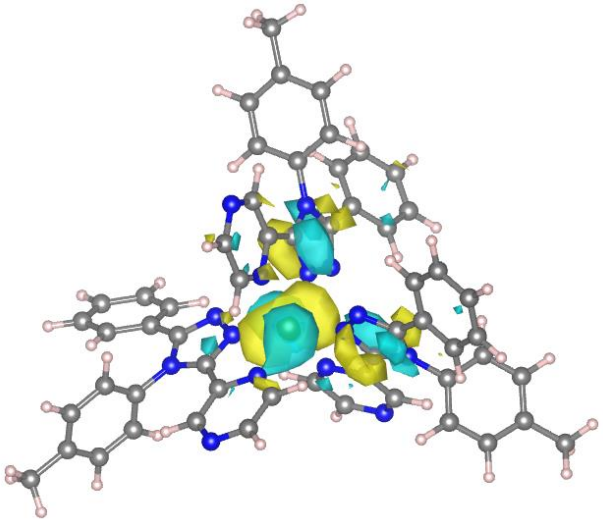

Figure S42: Perspective view of the HOMO of $[Os^{II}(\mathbf{L^{pyrazine}})_3]^{2+}$.

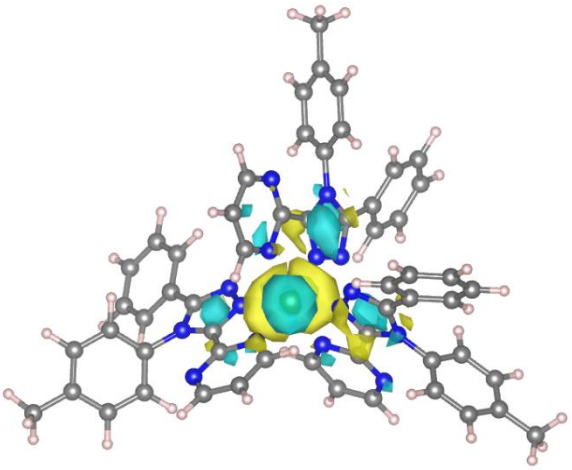

Figure S43: Perspective view of the HOMO of $[Os^{II}(\mathbf{L^{2\text{-}pyrimidine}})_3]^{2+}$.

Ionisation Potentials

Table S12: Tabulated values of final single point energy and calculated ionisation potentials. All values are calculated relativistically. All values given are in a.u unless specified otherwise

		Pyridine	Pyridazine	2-Pyrimidine	4-Pyrimidine	Pyrazine
Fe	**Fe(II)**	-3064.514286	-3112.572957	-3112.649016	-3112.651842	-3112.634407
	Fe(III)	-3064.31744602	-3112.36796609	-3112.44292503	-3112.44322959	-3112.42485560
	Fe(III) static	-3064.31428392	-3112.36619299	-3112.43985752	-3112.44046122	-3112.42138793
	Adiabatic	0.19683969	0.20499132	0.20609057	0.20861269	0.20955130
	Vertical	0.20000179	0.20676442	0.20915808	0.21138106	0.21301896
	Adiabatic/ kcal mol^{-1}	123.5	129.7	131.2	132.6	133.7
	Vertical / kcal mol^{-1}	125.5	129.7	131.2	132.6	133.7
Ru	**Ru(II)**	-3068.70637442	-3116.76295389	-3116.84109348	-3116.84344100	-3116.82497359
	Ru(III)	ls	-3116.55267553	-3116.62958281	-3116.62960812	-3116.61014611
	Ru(III) static	-3068.50059703	-3116.55075778	-3116.62696499	-3116.62676550	-3116.60746333
	Adiabatic	#VALUE!	0.21027836	0.21151067	0.21383288	0.21482749
	Vertical	0.20577739	0.21219611	0.21412849	0.21667550	0.21751027
	Adiabatic/ kcal mol^{-1}	#VALUE!	132.0	132.7	134.2	134.8
	Vertical/ kcal mol^{-1}	129.1	133.2	134.4	136.0	136.5
Os	**Os(II)**	-3064.514286	-3112.572957	-3112.649016	-3112.651842	-3112.634407
	Os(III)	-3064.31744602	-3112.36796609	-3112.44292503	-3112.44322959	-3112.42485560
	Os(III) static	-3064.31428392	-3112.36619299	-3112.43985752	-3112.44046122	-3112.42138793
	Adiabatic	0.19683969	0.20499132	0.20609057	0.20861269	0.20955130
	Vertical	0.20000179	0.20676442	0.20915808	0.21138106	0.21301896
	Adiabatic / kcal mol^{-1}	123.5	128.6	129.3	130.9	131.5
	Vertical/ kcal mol^{-1}	125.5	129.7	131.2	132.6	133.7

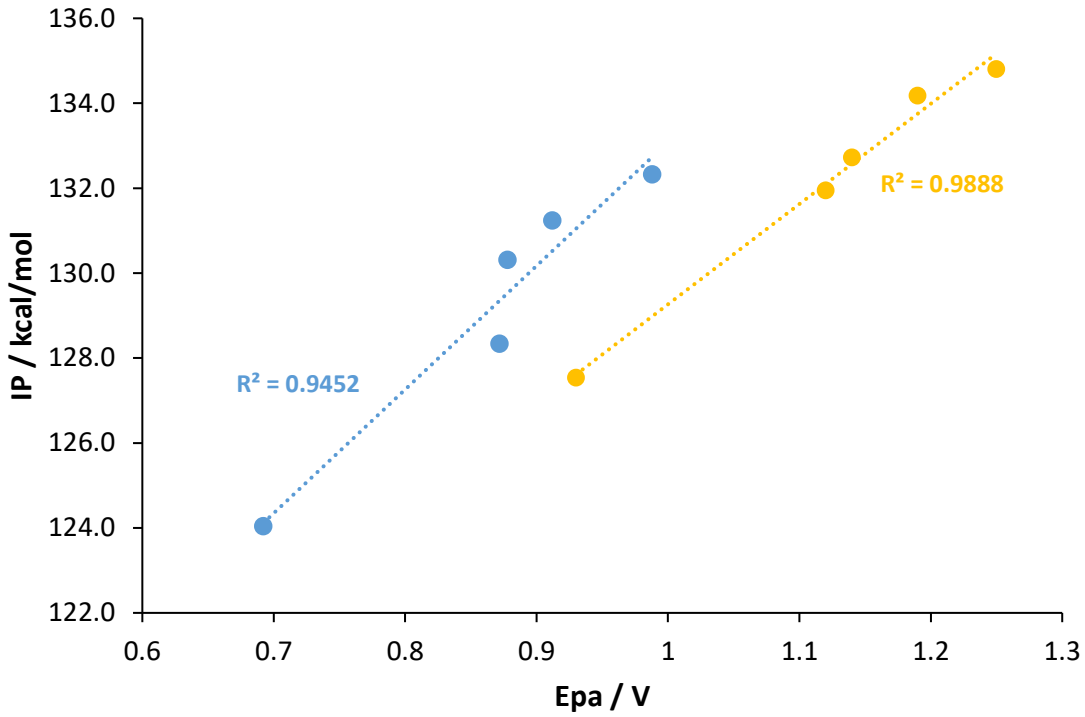

Figure S44: Plot of IP vs $E_{pa}(Ru^{III/II})$ (100 mV s^{-1}) for the $[Fe(\mathbf{L}^{azine})_3]^{2+}$ series of compounds. Blue is the vertical IP, yellow the adiabatic IP.

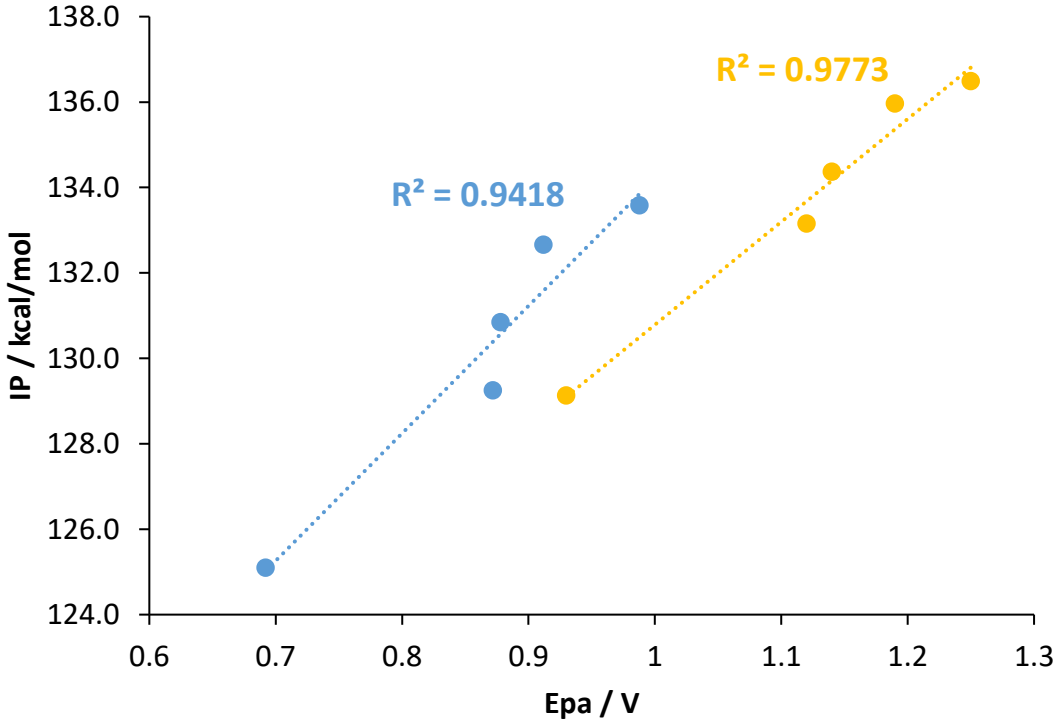

Figure S45: Plot of IP vs $E_{pa}(Ru^{III/II})$ (100 mV s^{-1}) for the $[Ru(\mathbf{L}^{azine})_3]^{2+}$ series of compounds. Blue is the vertical IP, yellow the adiabatic IP.

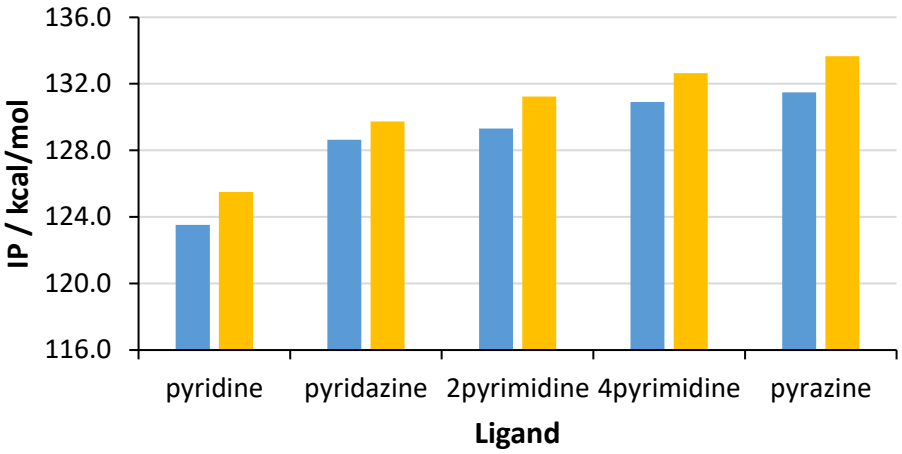

Figure S46: Plot of calculated IP's for the $[Os(\mathbf{L}^{azine})_3]^{2+}$ series of compounds. Blue is the vertical IP, orange the adiabatic IP.

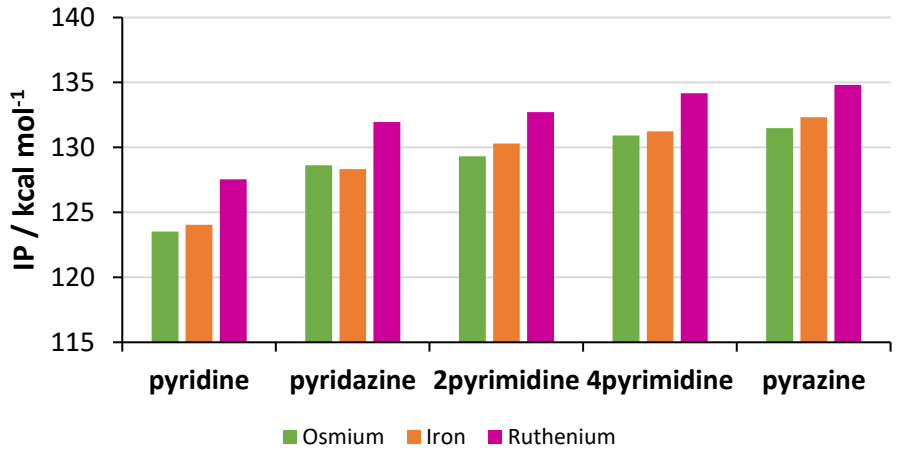

Figure S47: Plot of adiabatic ionisation potentials ($kcalmol^{-1}$) for the 3 families of $[M(\mathbf{L}^{azine})_3]^{2+}$ compounds, M = Fe (orange), Ru (pink) and Os (green).

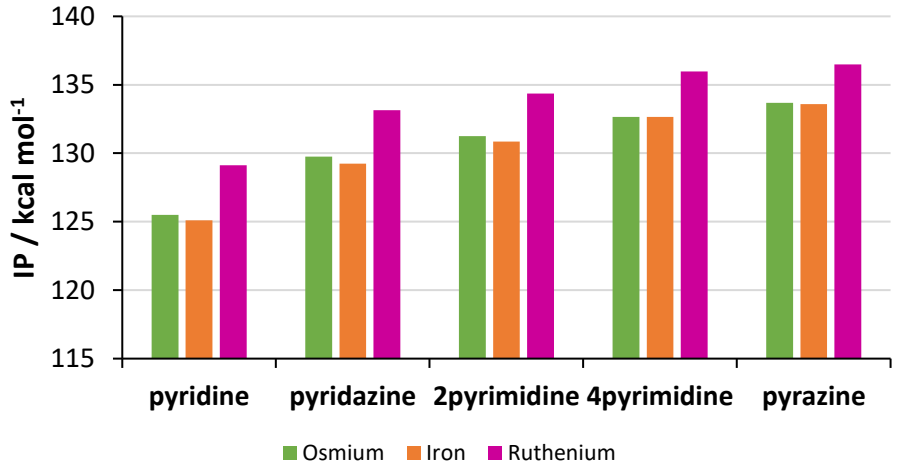

Figure S48: Plot of vertical ionisation potential ($kcal\ mol^{-1}$) for the 3 families of $[M(\mathbf{L}^{azine})_3]^{2+}$ compounds, M = Fe (orange), Ru (pink) and Os (green).

Table S13: Results of calculations on the literature family of tris-ligated 2,2'-bipyridine complexes ([M(2,2'-bipyridine)$_3$]$^{2+}$, M = Fe^{II}, Ru^{II}, Os^{II}) carried out with the computational protocol described above.

	Fe	Ru	Os
HOMO	-5.013000	-5.207800	-5.092200
LUMO	-3.427700	-3.472200	-3.522100
HOMO-LUMO gap	1.585300	1.735600	1.570100
Abs. energy	-1726105	-992618	-989988

DFT Calculations on the Ligands

Initial Calculations on the Heterocycles

Custodio and co-workers have recently shown the direct method of calculating pKa is as efficient as the more commonly used thermodynamic cycle method.[14]

$$pK_a = \frac{1}{RTln10} \times (G_{aq}(H^+) - G_{aq}(HA) + G_{aq}(A^-)$$

Here, $G_{aq}(HA)$ and $G_{aq}(A^-)$ are calculated using standard DFT methods, however the calculation of $G_{aq}(H^+)$ is less straightforward. If a number of experimentally-determined pKa values are known for related species then rearrangement of equation 1 thus allows for the calculation of $G_{aq}(H^+)$ as shown in equation 2.

$$G_{aq}(H^+) = (pK_a(\text{exp}) \times RTln10) + G_{aq}(HA) - G_{aq}(A^-)$$

It has been shown that the calculations have an uncertainty on Gaq(H+) calculated in this is ±1 unit of pKa.

In this work, the value of $G_{aq}(H^+)$ was derived using the unsubstituted parent azine heterocycles (ie. pyridine, pyrimidine, pyridazine and pyrazine) for which the experimental pKa values are known (pyrazine 0.65 < pyrimidine 1.30, pyridazine 2.30 < pyridine 5.20),[15] as the ligands in this study are based on them.

A number of basis sets under different conditions were tested: in the gas phase, with the inclusion of an implicit solvent model (CPCM). We found that the models with the inclusion of CPCM(water) gave more accurate results than those in vacuo (Figure S49 - Figure S52, Table S14). Of the basis sets tested, B3LYP with the inclusion of CPCM(water) was found to have the lowest standard error (Figure S41) giving $G_{aq}(H^+)$ = -269.820 kcal mol^{-1} (see Table S14).

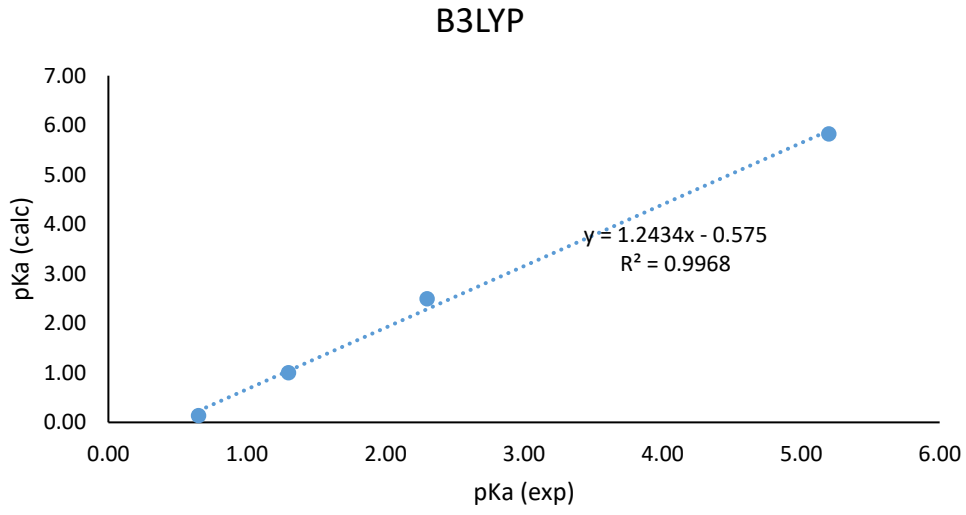

Figure S49: Plot of calculated pKa (B3LYP/D3BJ/TZVPP/CPCM(water)) against the experimental pKa obtained from Joule and Mills,[15] for the four unsubstituted parent azine heterocycles. This has the lowest standard error.

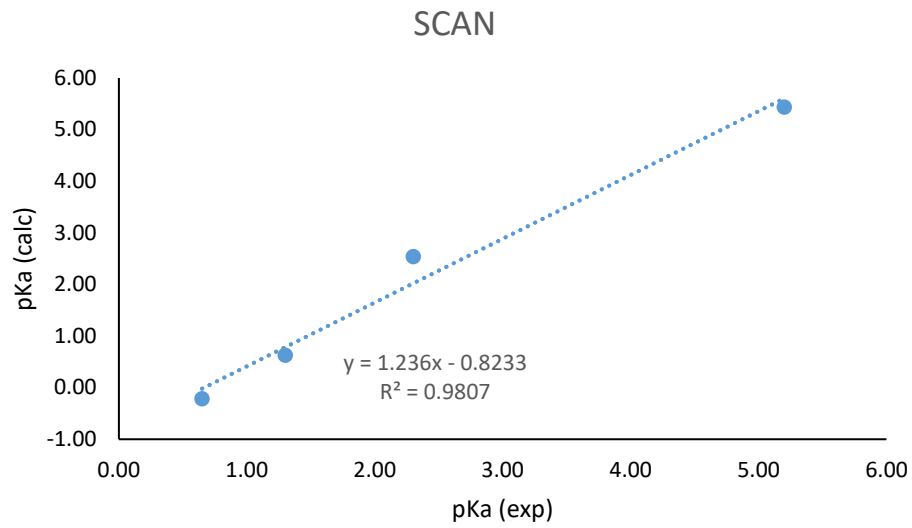

Figure S50: Plot of calculated pKa (SCAN/D3BJ/TZVPP/CPCM(water)) against the experimental pKa obtained from Joule and Mills,[15] for the four unsubstituted parent azine heterocycles.

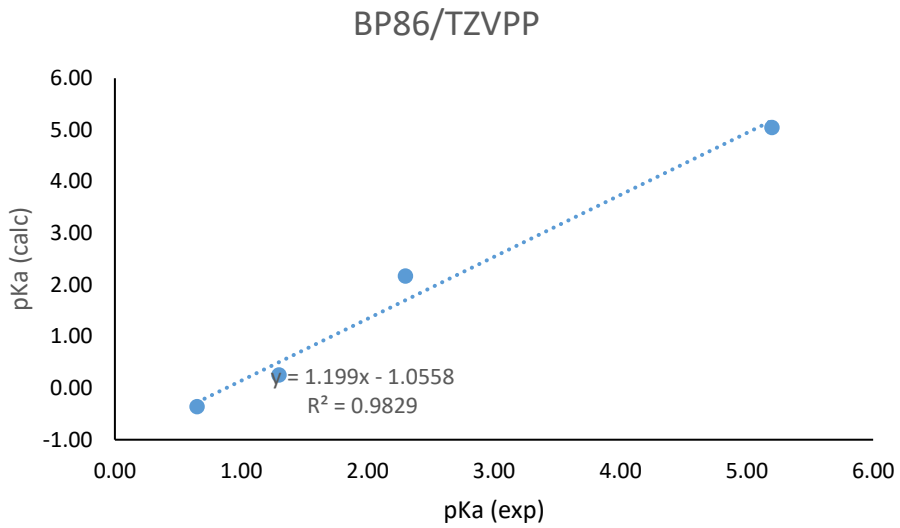

Figure S51: Plot of calculated pKa (BP86/D3BJ/TZVPP/CPCM(water)) against the experimental pKa obtained from Joule and Mills,[15] for the four unsubstituted parent azine heterocycles.

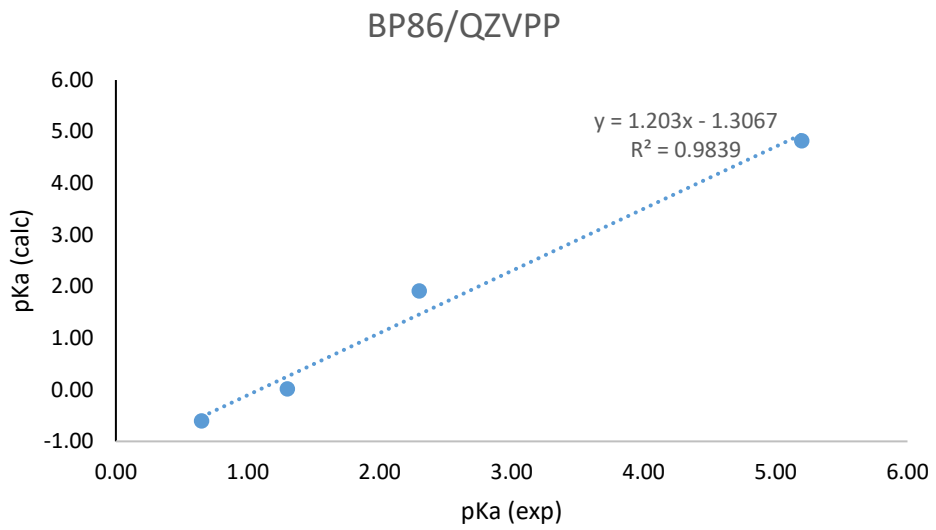

Figure S52: Plot of calculated pKa (BP86/D3BJ/QZVPP/CPCM(water)) against the experimental pKa obtained from Joule and Mills,[15] for the four unsubstituted parent azine heterocycles.

Table S14: Tabulated data obtained from the DFT calculations on the unsubstituted parent azine heterocycles, along with the experimental values observed.[15] B3LYP had the lowest standard error, so the average $G_{aq}(H^+)$ = -269.820 kcal mol^{-1} (blue text below), is used in the subsequent calculations (see below).

		B3LYP			**SCAN**			**BP86**			**BP86 QZVPP**		
	pKa(exp) ref [15]	**G_aq(H+)** kcal mol^{-1}	**pKa(calc)**	**Abs error** pKa units	**G_aq(H+)** kcal mol^{-1}	**pKa(calc)**	**Abs error** pKa units	**G_aq(H+)** kcal mol^{-1}	**pKa(calc)**	**Abs error** pKa units	**G_aq(H+)** kcal mol^{-1}	**pKa(calc)**	**Abs error** pKa units
pyridine	5.20	-270.414	5.64	0.44	-269.891	5.25	0.05	-269.357	4.86	0.34	-269.048	4.63	0.57
pyridazine	2.30	-269.834	2.31	0.01	-269.898	2.36	0.06	-269.387	1.98	0.32	-269.038	1.73	0.57
pyrimidine	1.30	-269.156	0.81	0.49	-268.647	0.44	0.86	-268.142	0.07	1.23	-267.815	-0.17	1.47
pyrazine	0.65	-268.866	-0.05	0.70	-268.384	-0.40	1.05	-268.189	-0.55	1.20	-267.855	-0.79	1.44
			average	**MAE**		**average**	**MAE**		**average**	**MAE**		**average**	**MAE**
			-269.820	0.41		-269.205	0.51		-268.769	0.77		-268.439	1.01

Ligand Calculations using B3LYP

Following the results gathered in the section above the structures of the free $\mathbf{L}^{azine}$ ligands were optimised using the B3LYP functional with the TZVPP basis set with an implicit solvent model (CPCM, water). The structures were optimised for both the ligands ($\mathbf{L}^{azine}$) and the protonated ligands (H$\mathbf{L}^{azine}$, protonated on the donor N of the azine ring) (Figure S53).

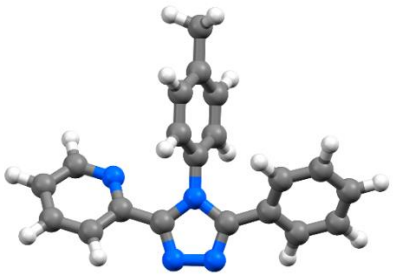

$L^{pyridine}$

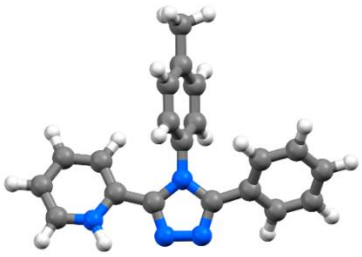

$HL^{pyridine}$

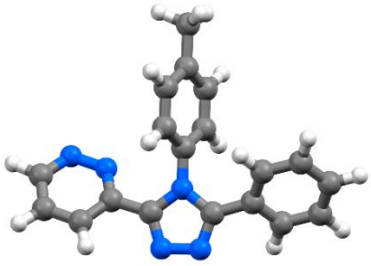

$L^{pyridazine}$

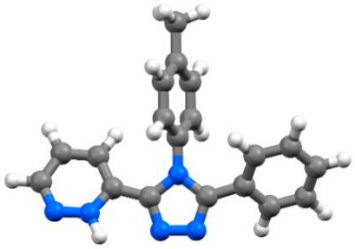

$HL^{pyridazine}$

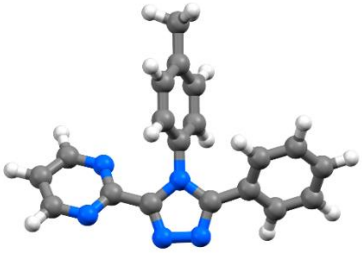

$L^{2\text{-}pyrimidine}$

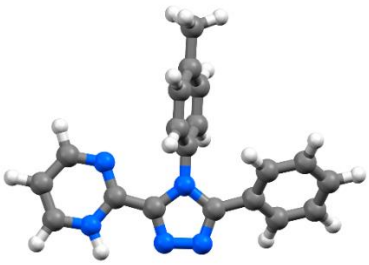

$HL^{2\text{-}pyrimidine}$

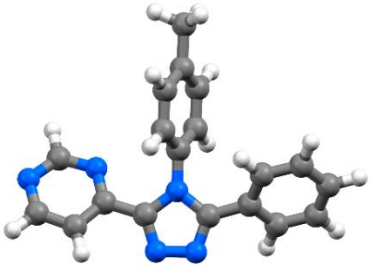

$L^{4\text{-}pyrimidine}$

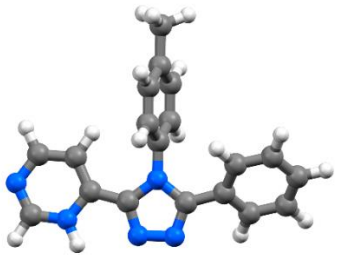

$HL^{4\text{-}pyrimidine}$

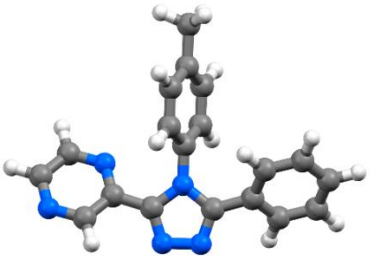

$L^{pyrazine}$

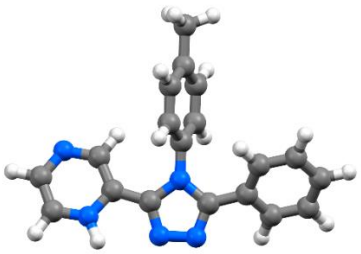

$HL^{pyrazine}$

Figure S53: Optimised structures of the L^{azine} ligands using the B3LYP level of theory.

Using the value obtained for $G_{aq}(H^+)$ above (-269.820 kcal mol^{-1}; see Table S14) and the calculated Gibbs free energy of the solvated **L**^{azine} and H**L**^{azine} (Table S15), we then calculated the pKa values of the **L**^{azine} ligands (Table S15), using the equation below (introduced above, page S34).

$$pK_a = \frac{1}{RTln10} \times (G_{aq}(H^+) - G_{aq}(HA) + G_{aq}(A^-)$$

The plot of calculated pKa of the **L**^{azine} ligand, versus experimentally determined redox potential of the tris- **L**^{azine} complex (Figure S54) shows a strong linear correlation (R^2 = 0.98 for the Ru complexes, R^2 = 0.99 for the Fe complexes).

Table S15: pKa values calculated for the **L**^{azine} ligands with the B3LYP/D3BJ/CPCM(water) level of theory.

	G_aq(AH+)		G_aq(A)		pKa(calc)
azine	a.u.	kcal mol-1	a.u.	kcal mol-1	
pyridine	-990.808	-621741	-990.368	-621466	4.980215
pyridazine	-1006.82	-631790	-1006.39	-631520	1.281749
2pyrimidine	-1006.85	-631810	-1006.42	-631539	1.525504
4pyrimidine	-1006.85	-631810	-1006.42	-631540	0.738327
pyrazine	-1006.84	-631803	-1006.42	-631535	-0.66399

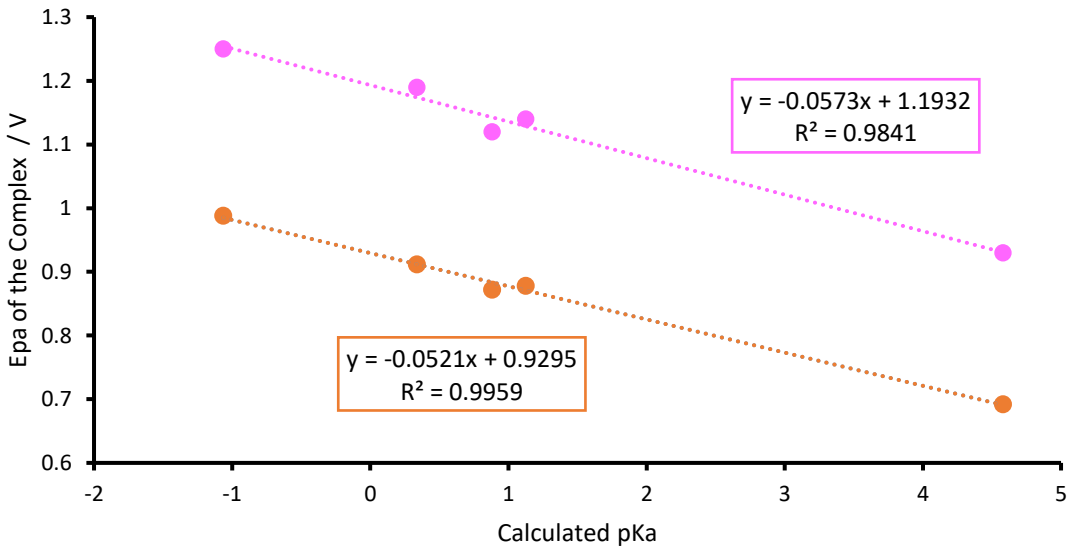

Figure S54: Plot of experimentally determined $E_{pa}(Ru^{III/II})$ for the tris-**L**^{azine} complex versus the calculated **L**^{azine} ligand pKa using the B3LYP/D3BJ/CPCM(water) level of theory.

NMR Spectra of the Complexes

Note that all ^{1}H NMR integrations shown in these spectra are based on the tolyl CH_3 signal being set to 9H (as one complex has 3 ligands each of which has one tolyl CH_3 = 9H).

$[Ru(L^{pyridine})_3](PF_6)_2$ (1)

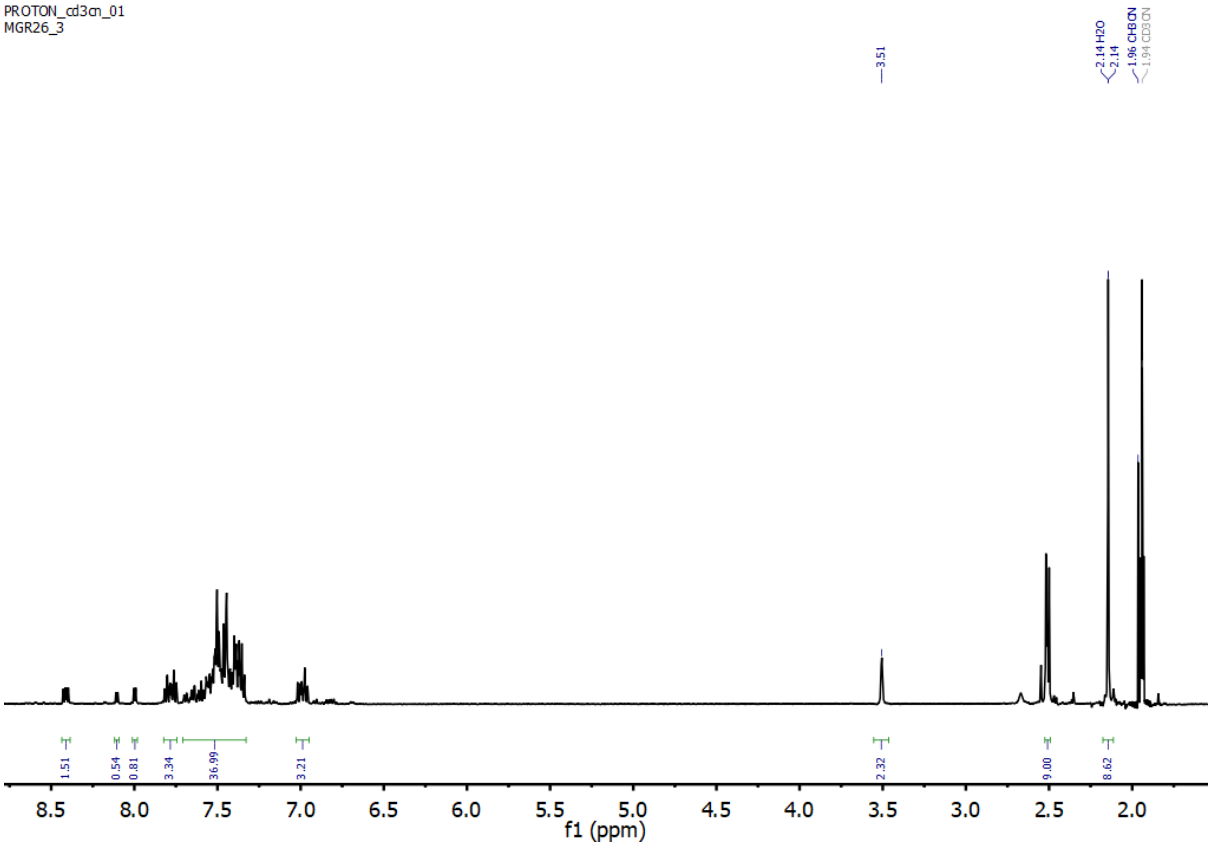

Figure S55: ^{1}H NMR (500 MHz, 298 K, CD_3CN) of complex **1.**

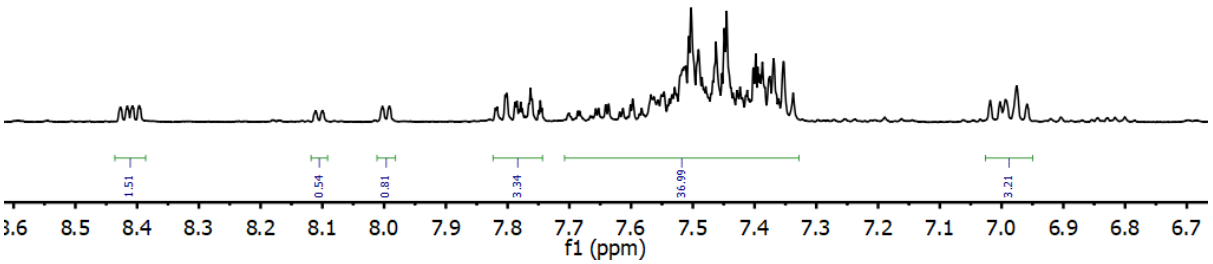

Figure S56: Partial ^{1}H NMR (500 MHz, 298 K, CD_3CN) of complex **1**, focussing on aromatic signals.

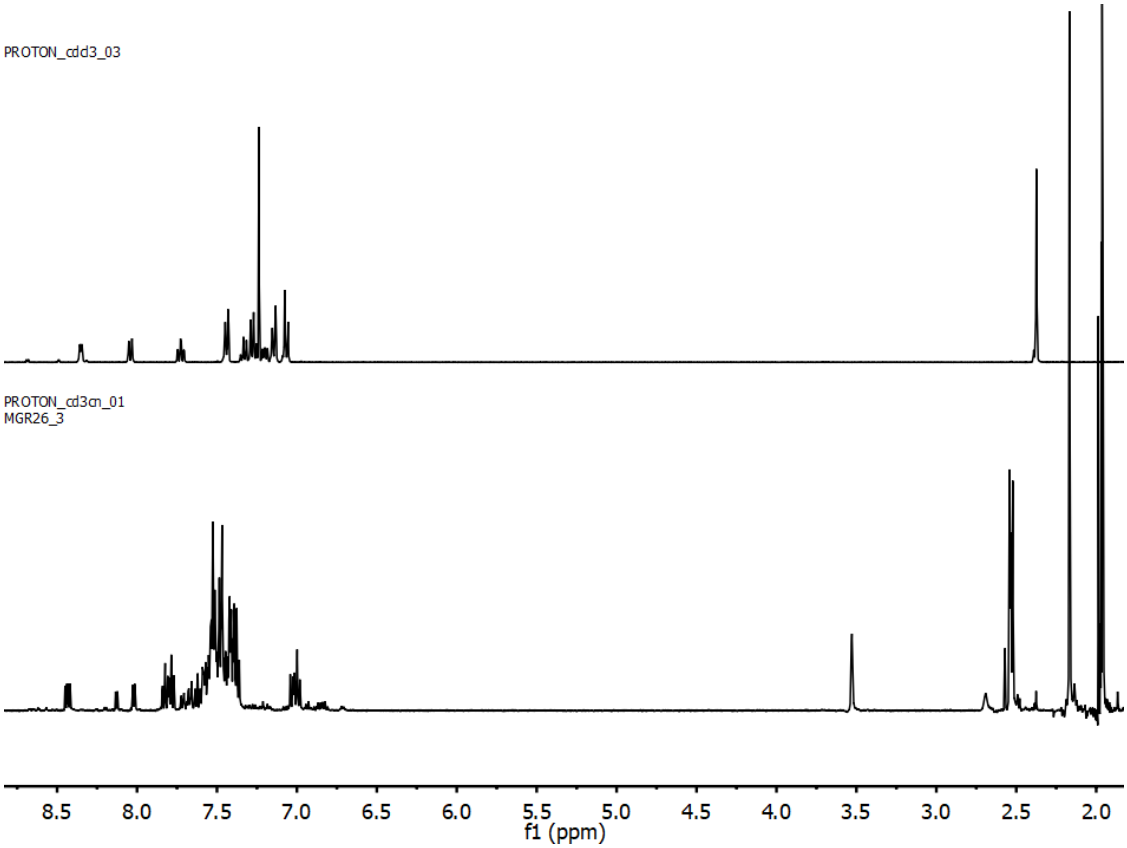

Figure S57: Stacked ^{1}H NMR of (top) $\mathbf{L^{pyridine}}$ (500 MHz, 298 K, $CDCl_3$) and (bottom) complex **1** (500 MHz, 298 K, CD_3CN).

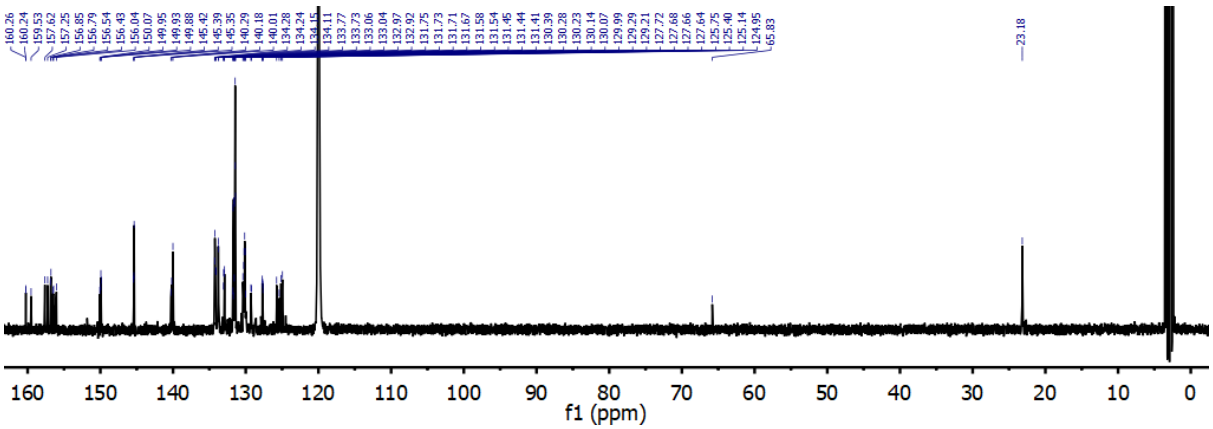

Figure S58: ^{13}C NMR (125 MHz, 298 K, CD_3CN) of complex **1**.

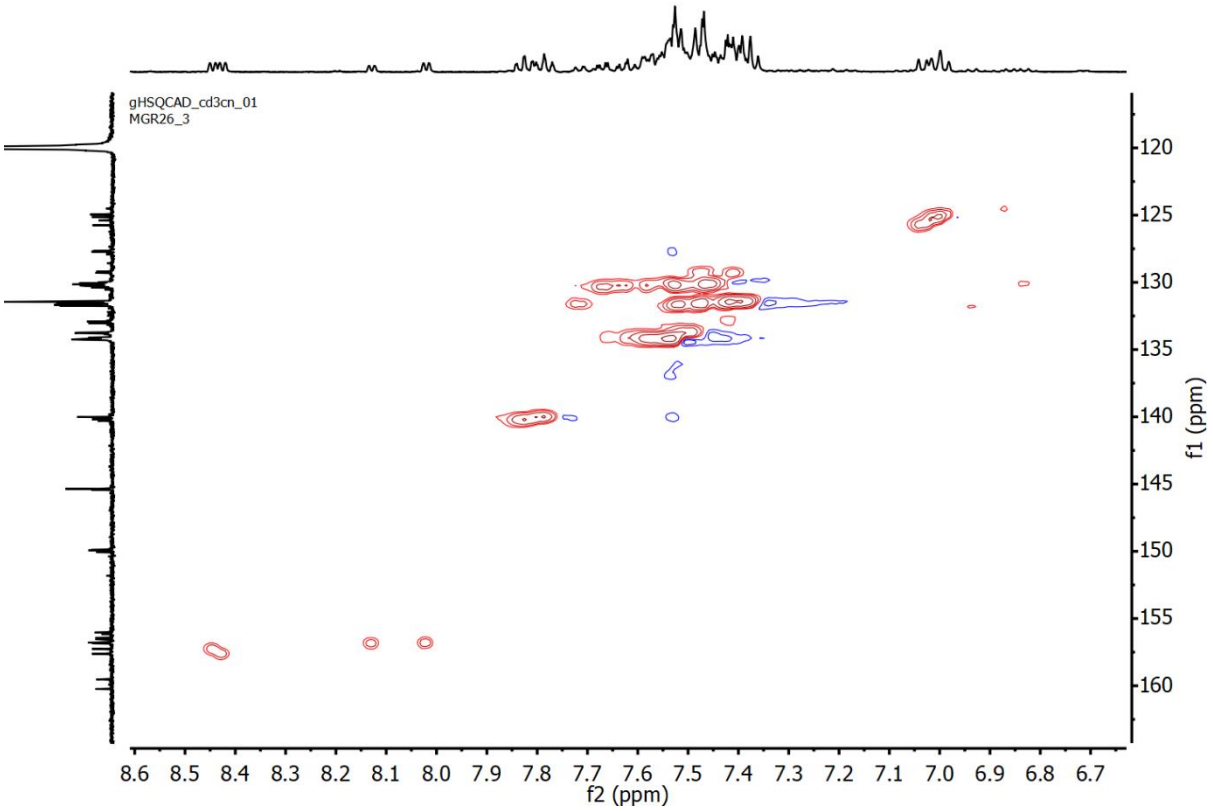

Figure S59: HSQC of complex **1** (298 K, CD_3CN).

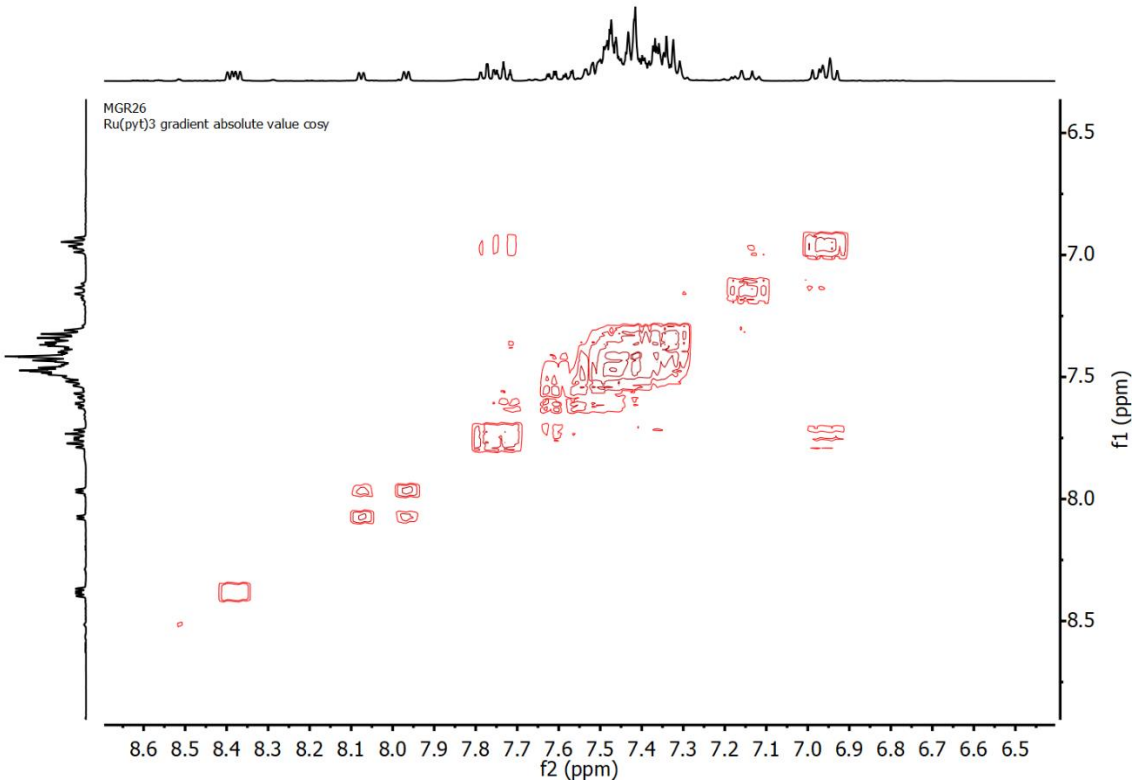

Figure S60: COSY spectrum of complex **1** (298 K, CD_3CN).

$[Ru(L^{pyridazine})_3](PF_6)_2$ (2)

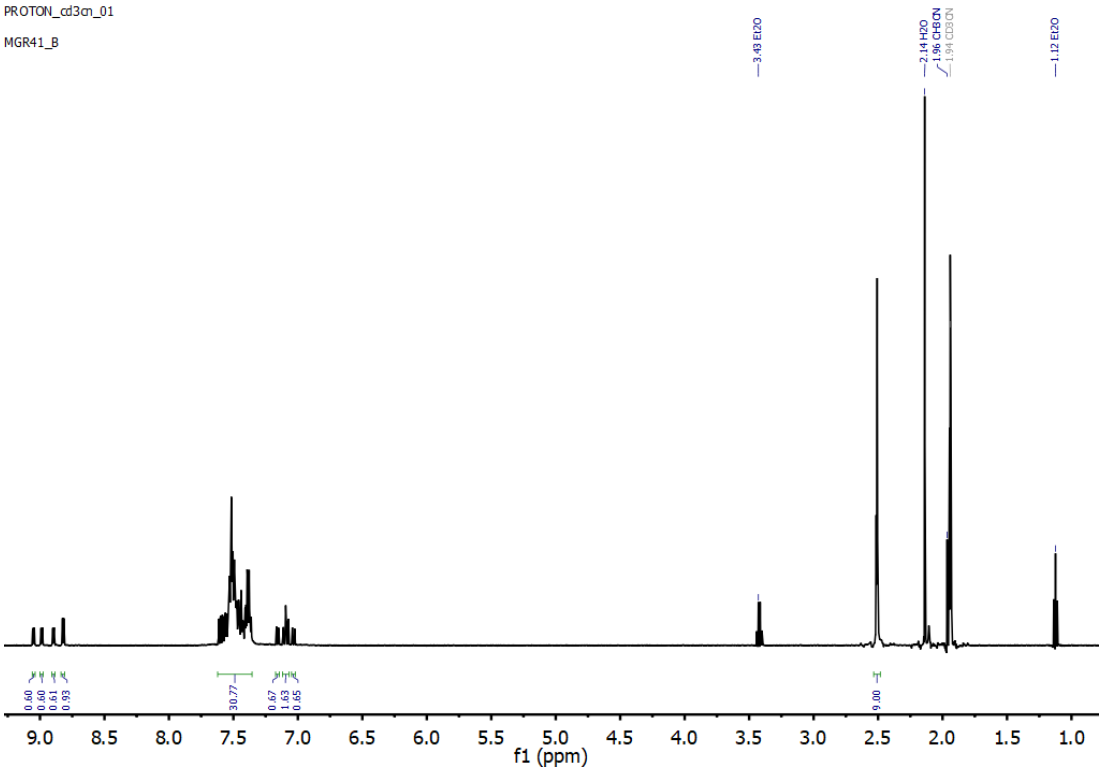

Figure S61: ^1H NMR (500 MHz, 298 K, CD_3CN) of complex **2**.

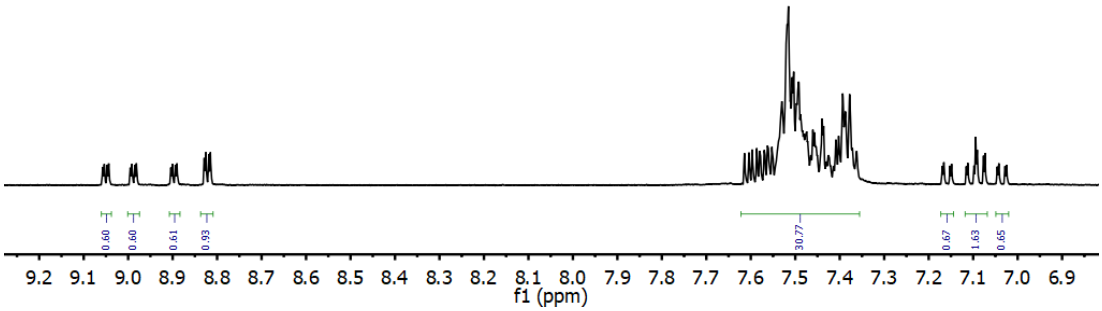

Figure S62: Partial ^{1}H NMR (500 MHz, 298 K, CD_3CN) of complex **2**, focussing on aromatic signals.

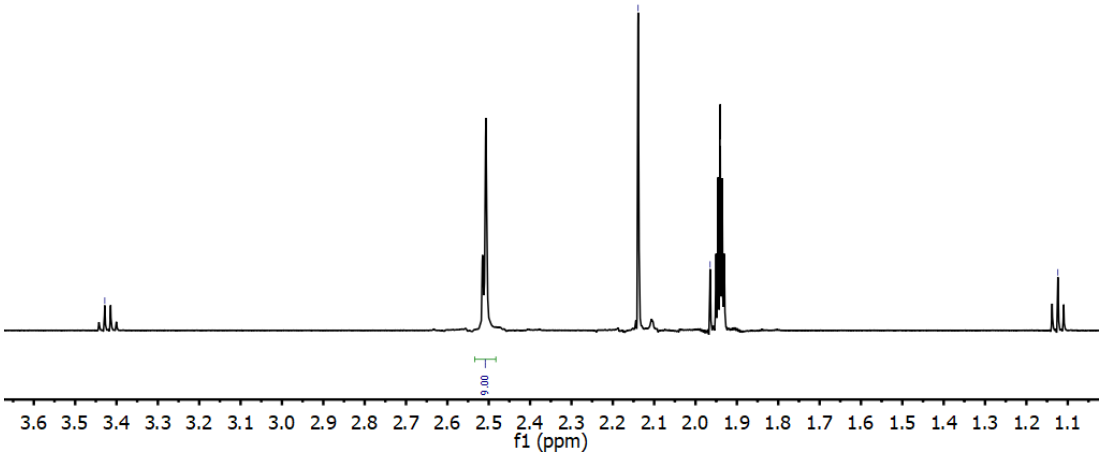

Figure S63: Partial ^{1}H NMR (500 MHz, 298 K, CD_3CN) of complex **2**.

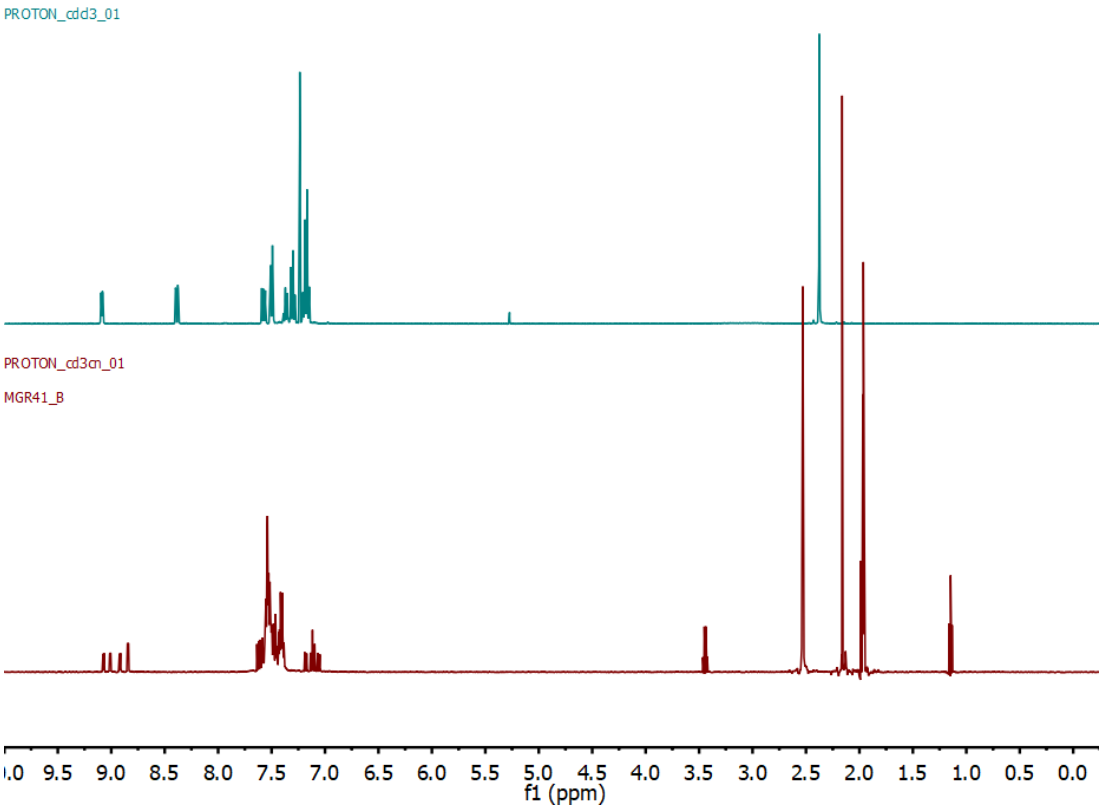

Figure S64: Stacked ^{1}H NMR of (top) $\mathbf{L}^{\mathbf{pyridazine}}$ (500 MHz, 298 K, $CDCl_3$) and (bottom) complex **2** (500 MHz, 298 K, CD_3CN).

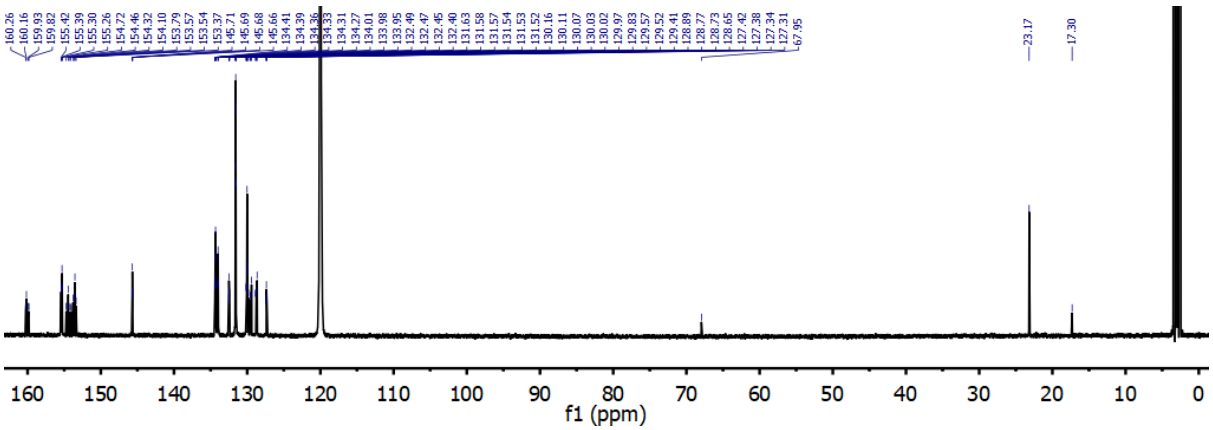

Figure S65: ^{13}C NMR (125 MHz, 298 K, CD_3CN) of complex **2**.

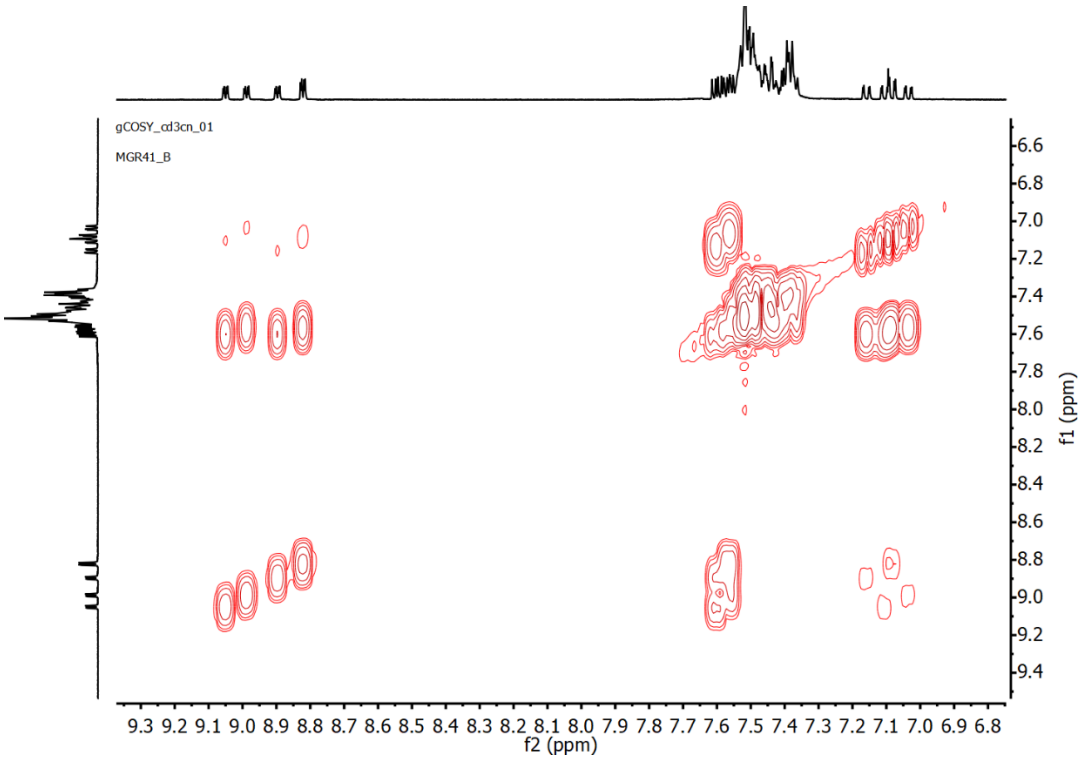

Figure S66: COSY spectrum of **2** (298 K, CD_3CN).

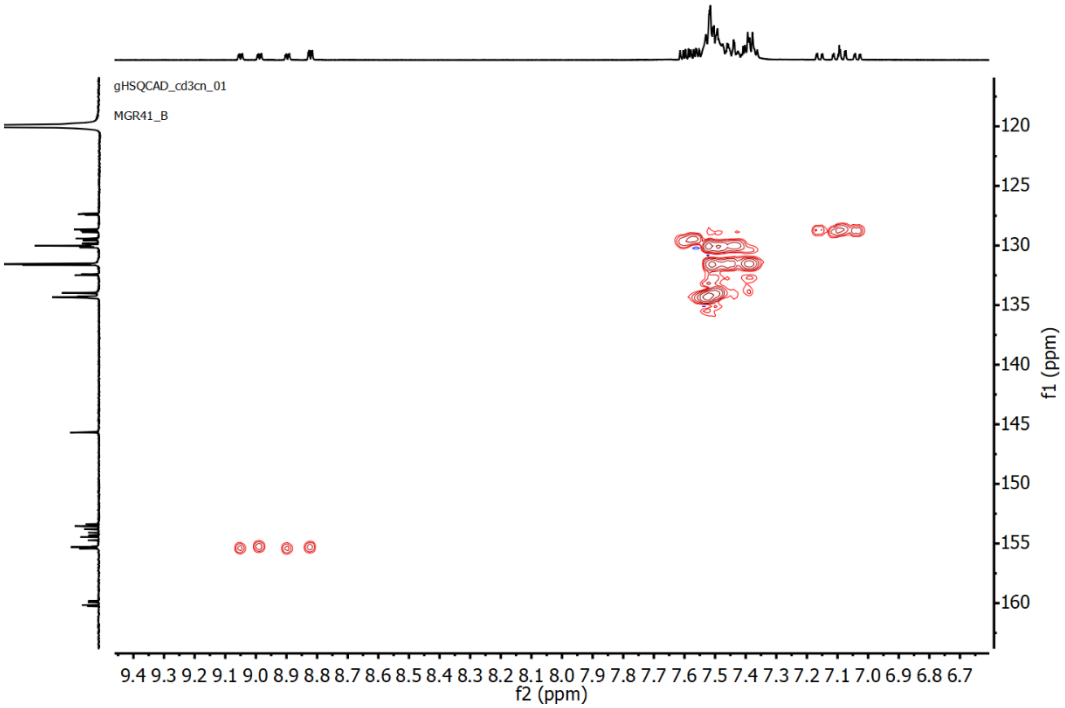

Figure S67: HSQC spectrum of **2** (298 K, CD_3CN).

$[Ru(L^{4\text{-pyrimidine}})_3](PF_6)_2$ (3)

PROTON_cd3cn_01

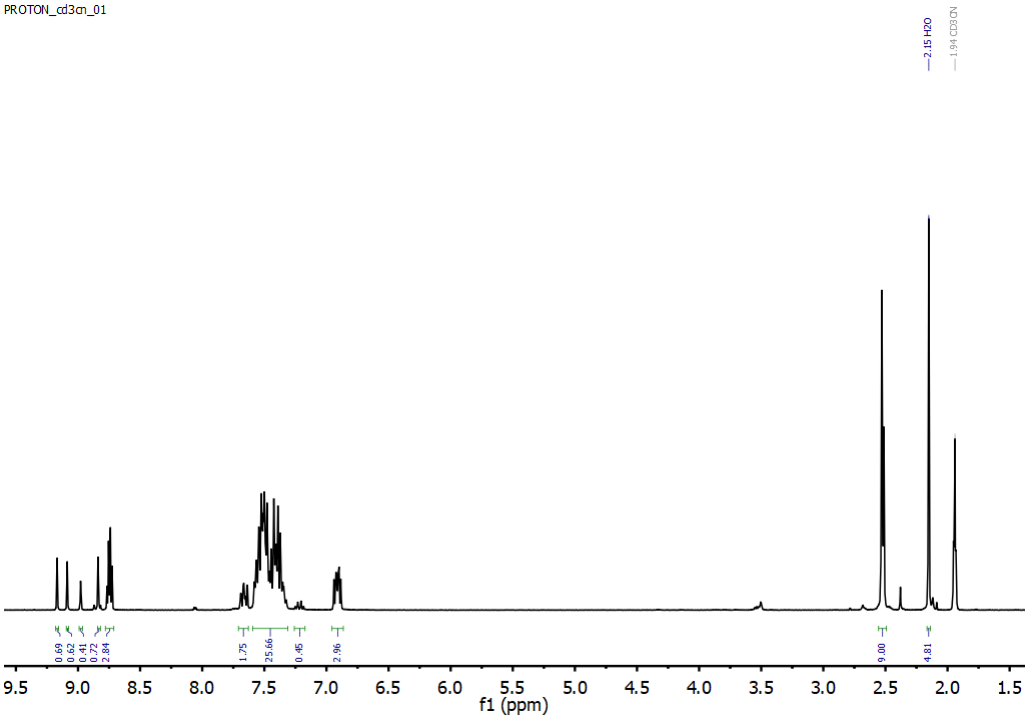

Figure S68: ^{1}H NMR (500 MHz, 298 K, CD_3CN) of complex **3.**

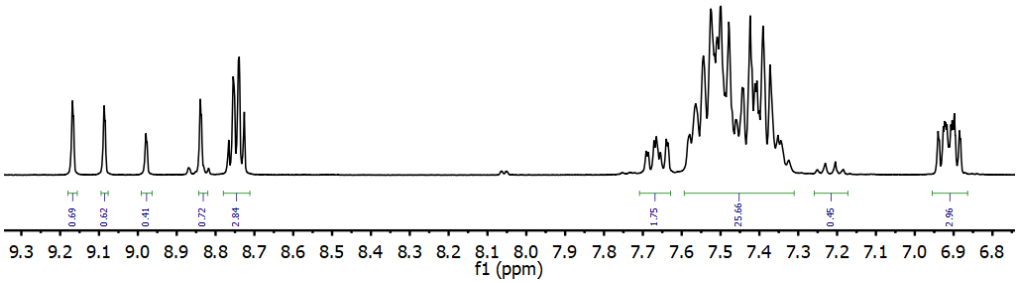

Figure S69: Partial ^{1}H NMR (500 MHz, 298 K, CD_3CN) of complex **3**, focussing on aromatic signals.

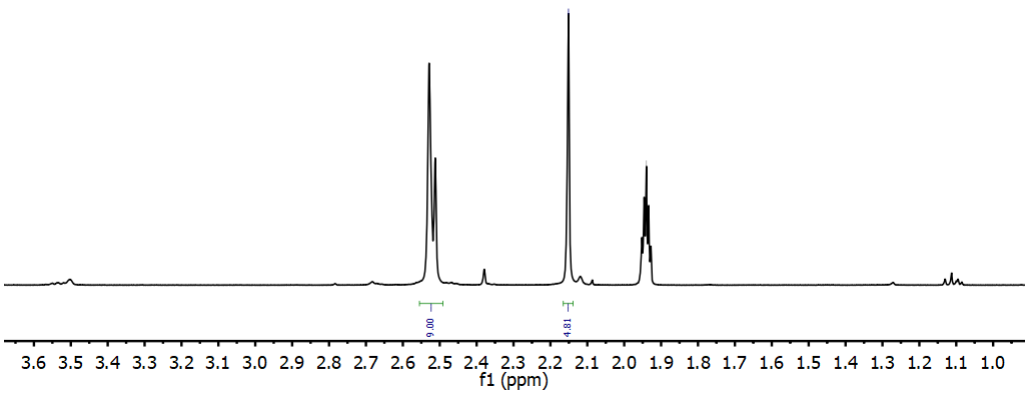

Figure S70: Partial ^{1}H NMR (500 MHz, 298 K, CD_3CN) of complex **3**.

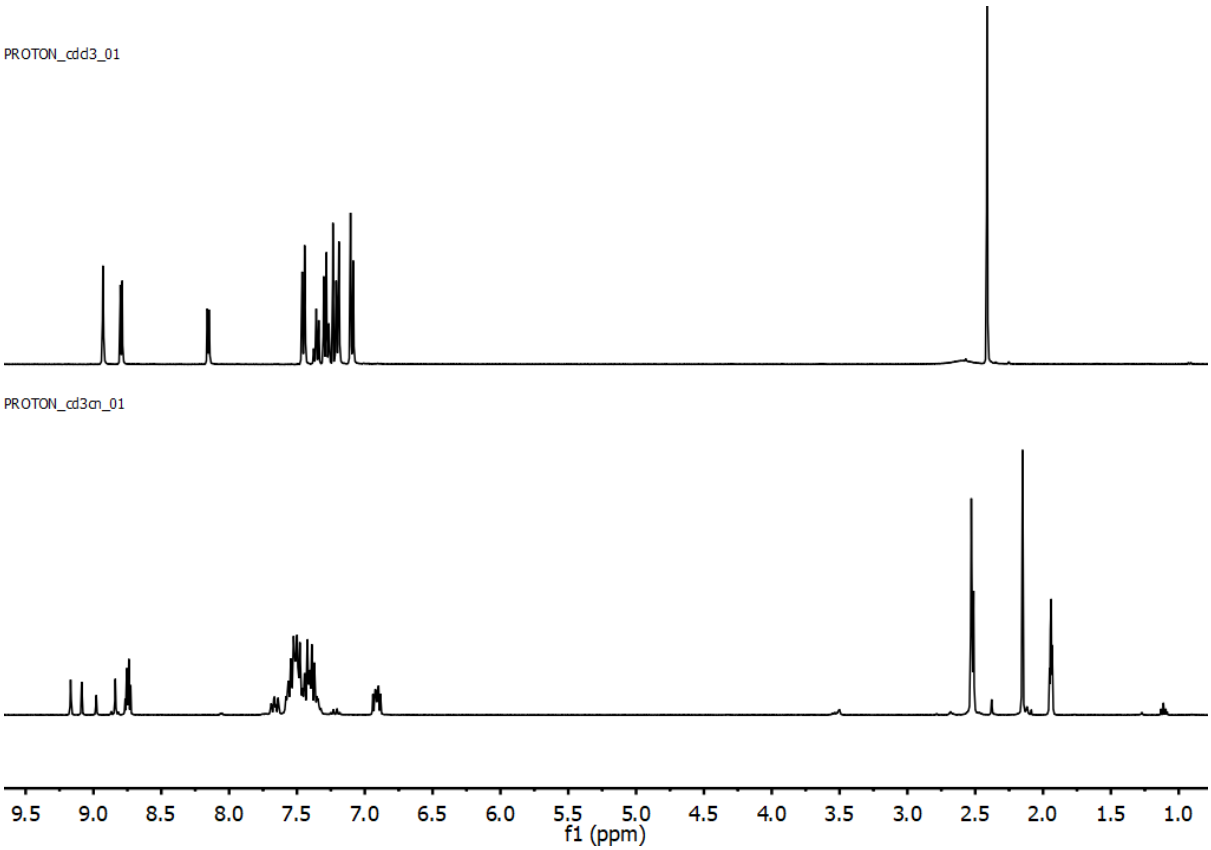

Figure S71: Stacked ^{1}H NMR of (top) **L$^{4\text{-pyrimidine}}$** (500 MHz, 298 K, $CDCl_3$) and (bottom) complex **3** (500 MHz, 298 K, CD_3CN).

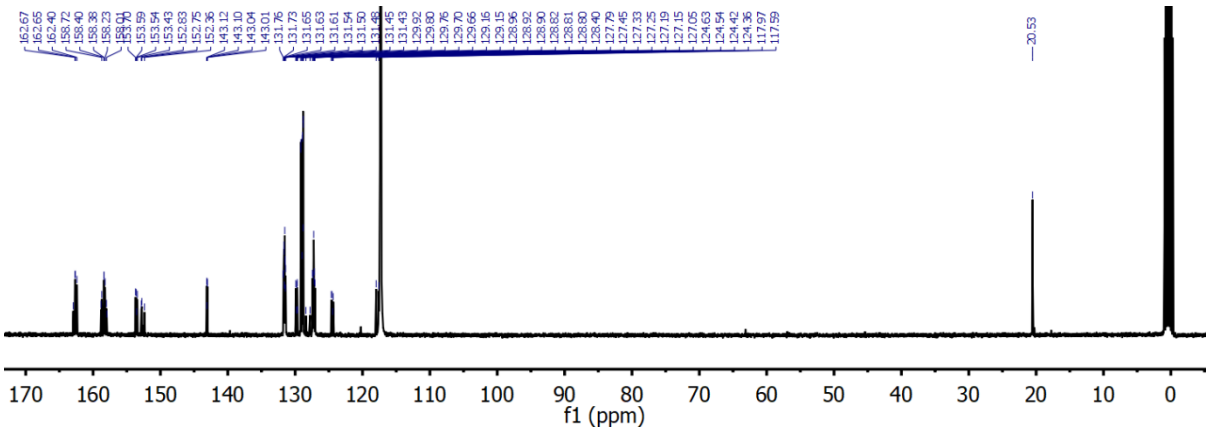

Figure S72: ^{13}C NMR (125 MHz, 298 K, CD_3CN) of complex **3**.

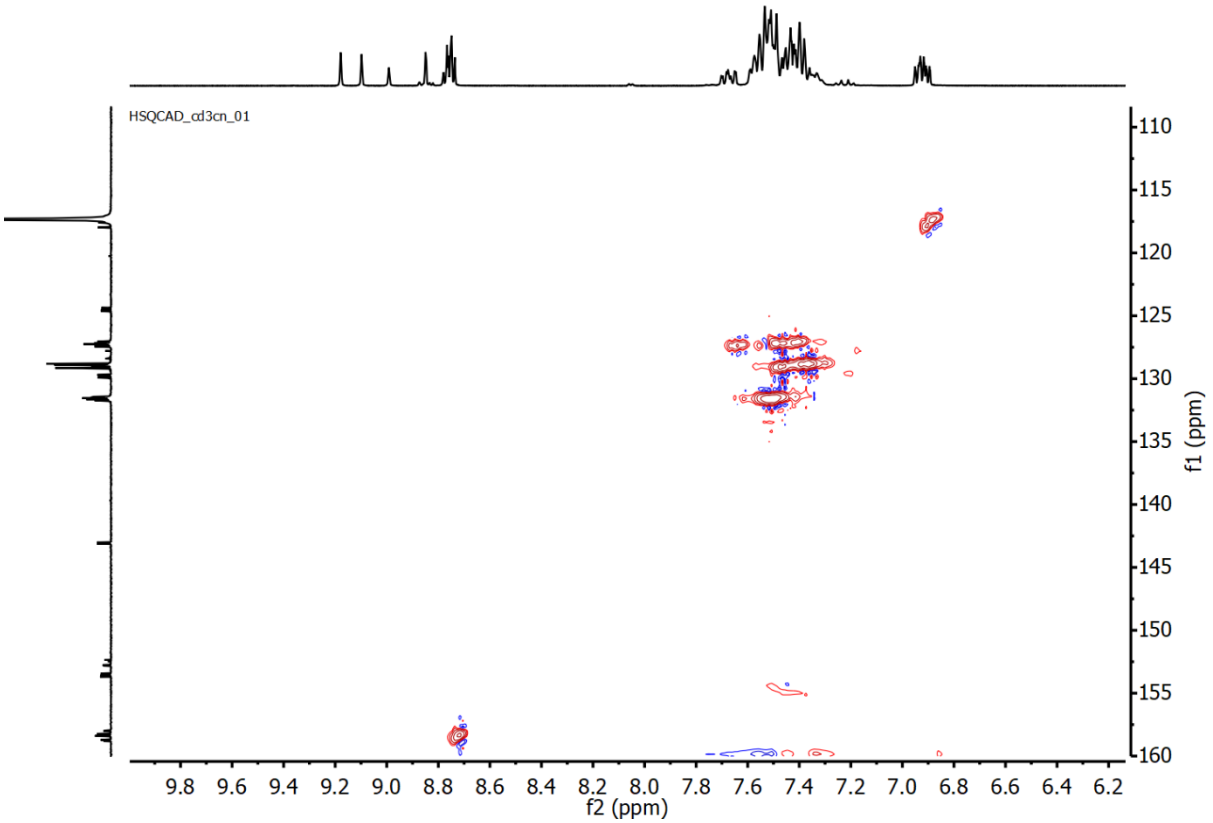

Figure S73: HSQC spectrum of complex **3** (298 K, CD_3CN).

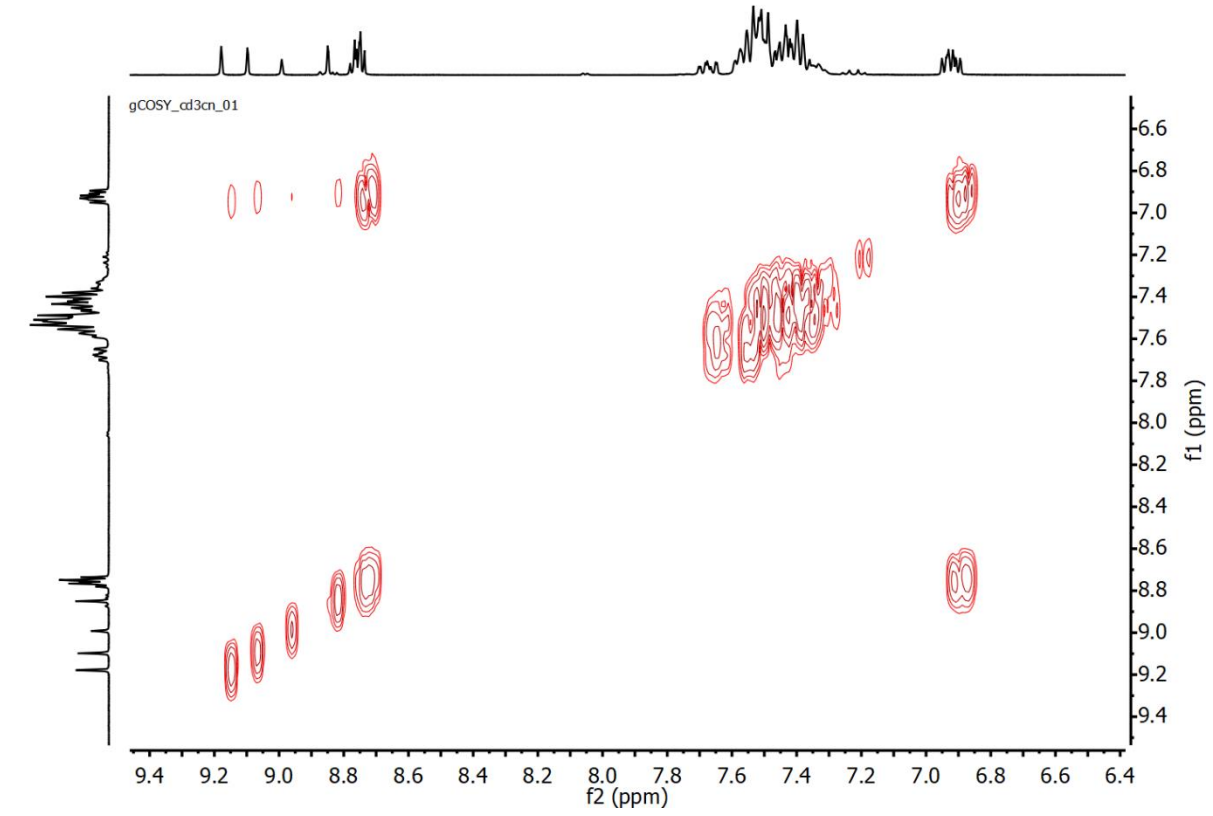

Figure S74: COSY spectrum of complex **3** (298 K, CD_3CN).

$[Ru(L^{pyrazine})_3](PF_6)_2$ (4)

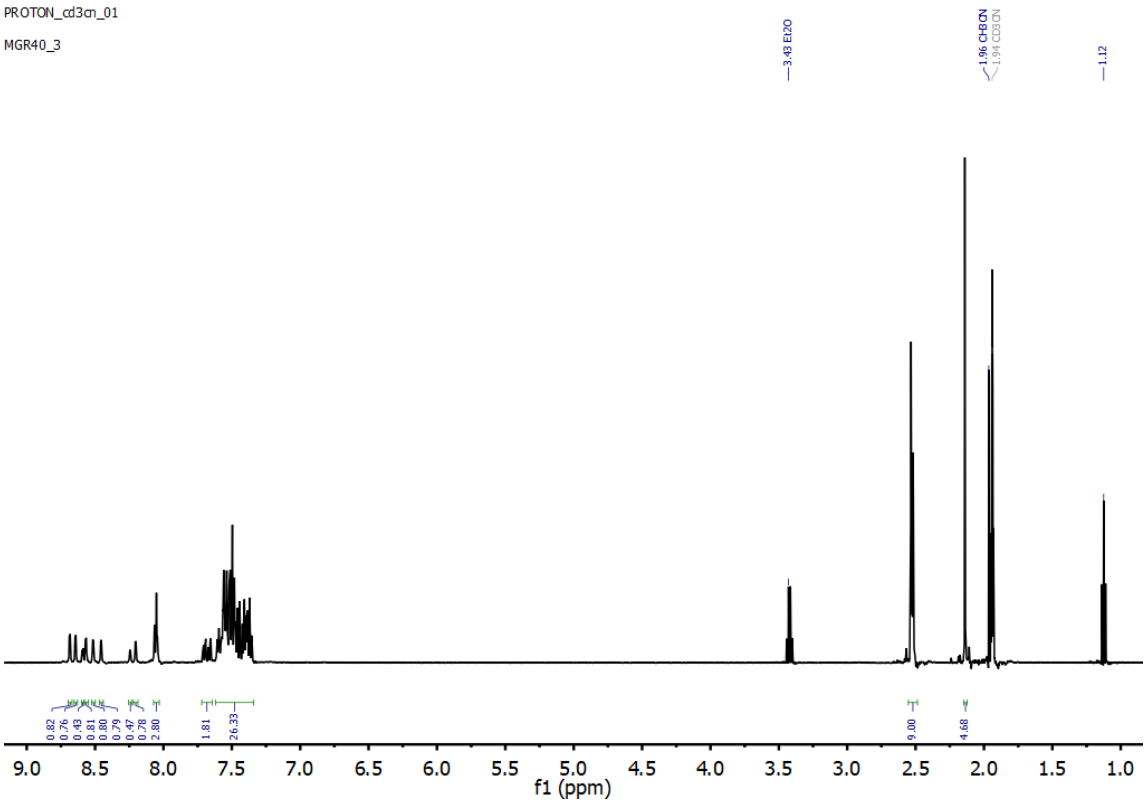

Figure S75: ^{1}H NMR (500 MHz, 298 K, CD_3CN) of complex **4.**

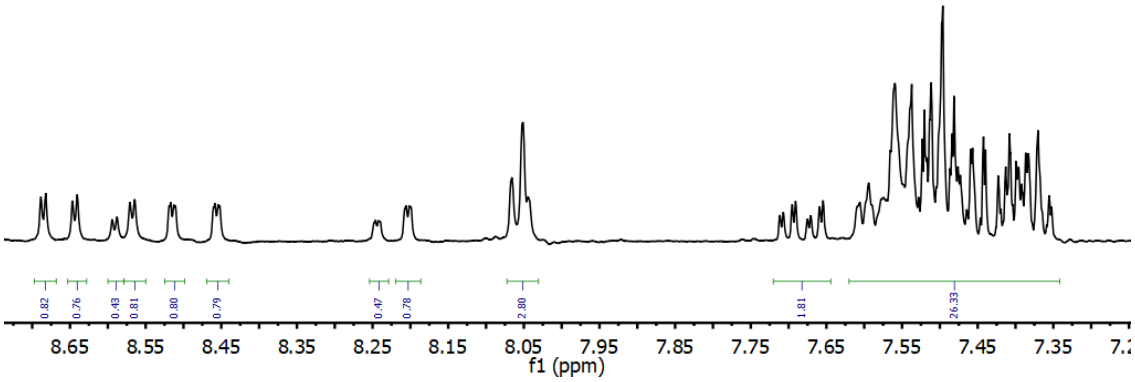

Figure S76: Partial ^{1}H NMR (500 MHz, 298 K, CD_3CN) of complex **4**, focussing on aromatic signals.

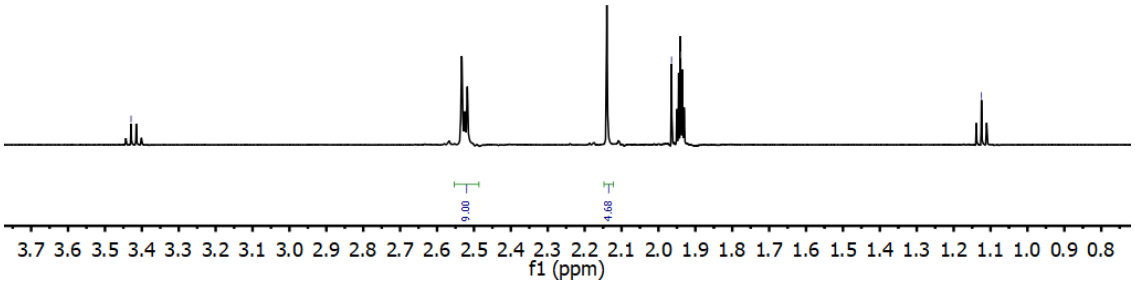

Figure S77: Partial ^{1}H NMR (500 MHz, 298 K, CD_3CN) of complex **4**.

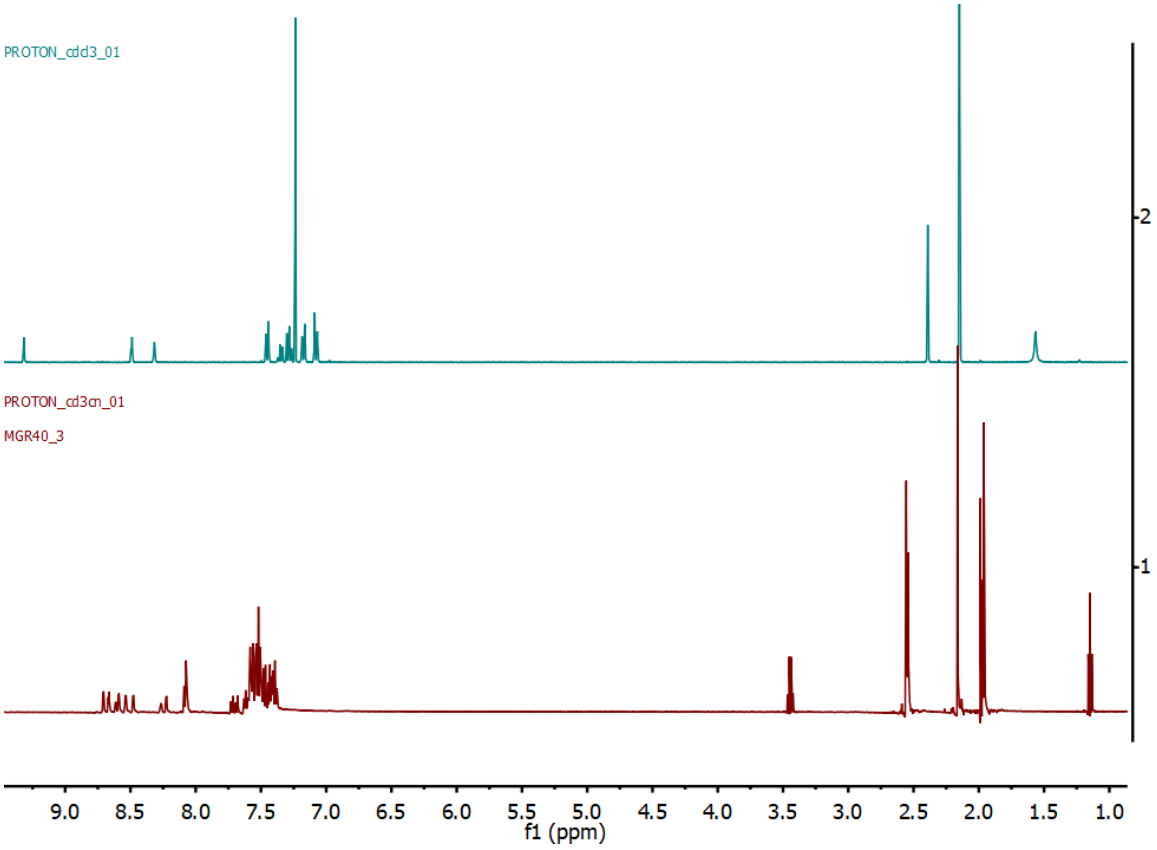

Figure S78: Stacked ^{1}H NMR of (top) $\mathbf{L}^{\mathbf{pyrazine}}$ (500 MHz, 298 K, $CDCl_3$) and (bottom) complex **4** (500 MHz, 298 K, CD_3CN).

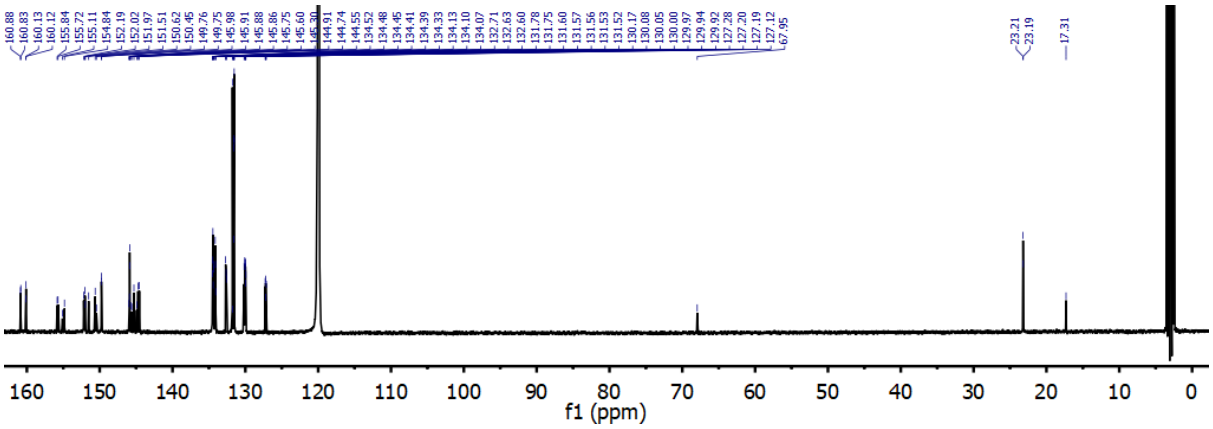

Figure S79: ^{13}C NMR (125 MHz, 298 K, CD_3CN) of complex **4**.

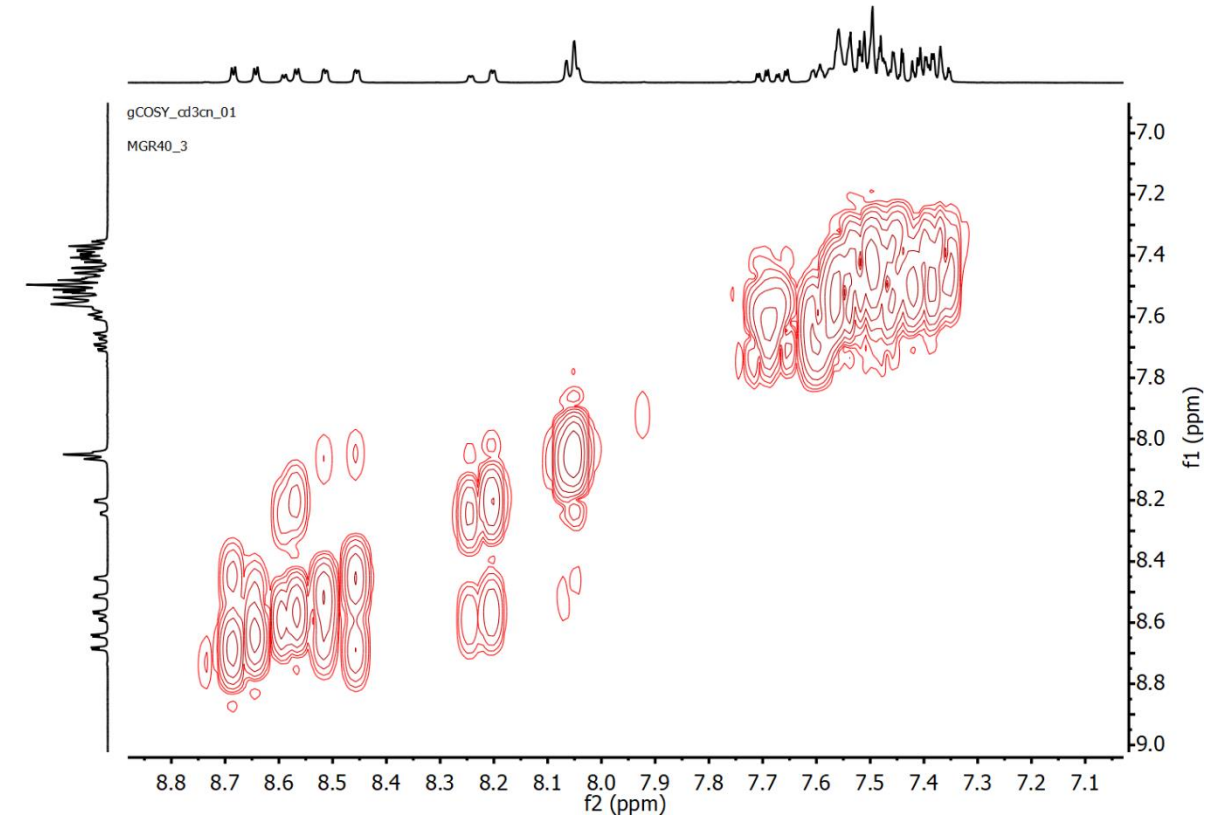

Figure S80: COSY spectrum of complex **4** (298 K, CD_3CN).

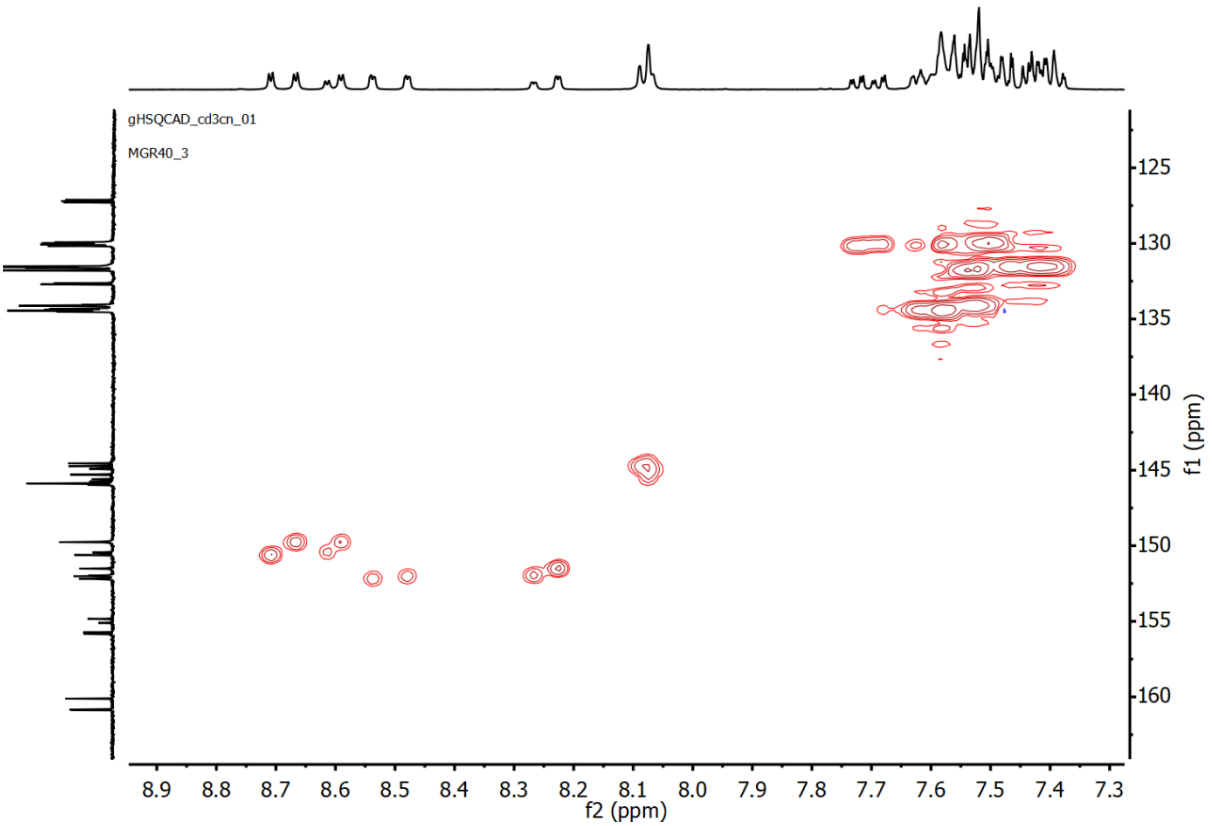

Figure S81: HSQC spectrum of complex **4** (298 K, CD_3CN).

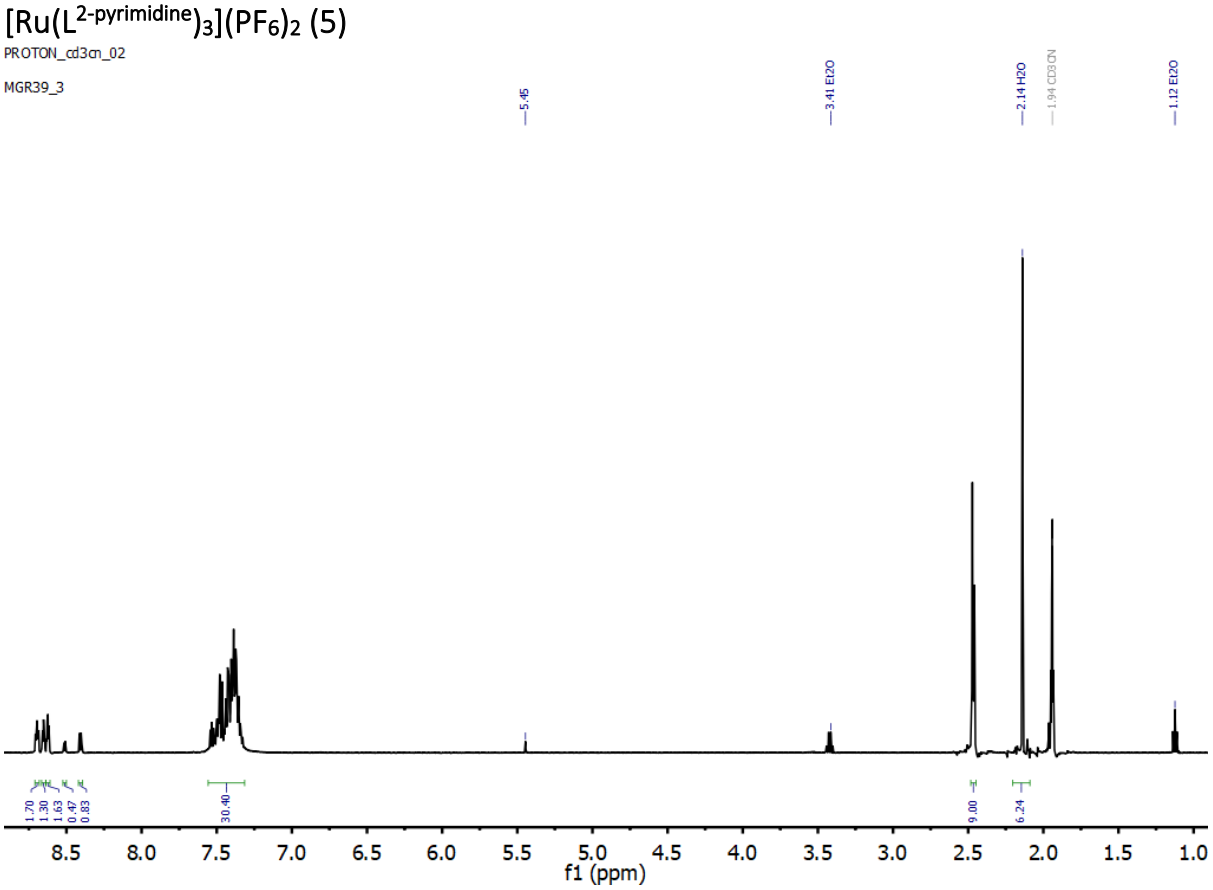

Figure S82: ^{1}H NMR (500 MHz, 298 K, CD_3CN) of complex **5.**

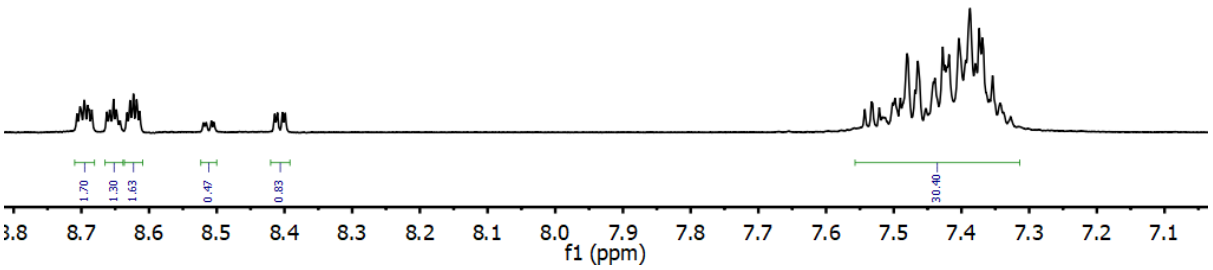

Figure S83: Partial ^{1}H NMR (500 MHz, 298 K, CD_3CN) of complex **5**, focussing on aromatic signals.

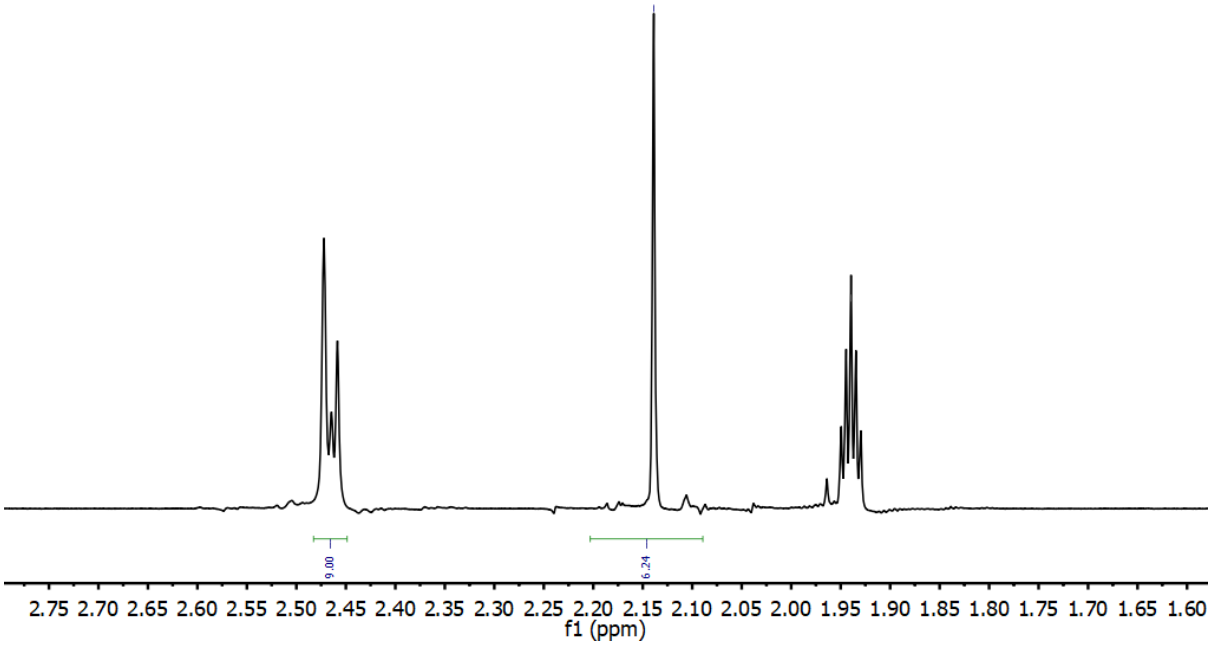

Figure S84: Partial ^{1}H NMR (500 MHz, 298 K, CD_3CN) of complex **5**.

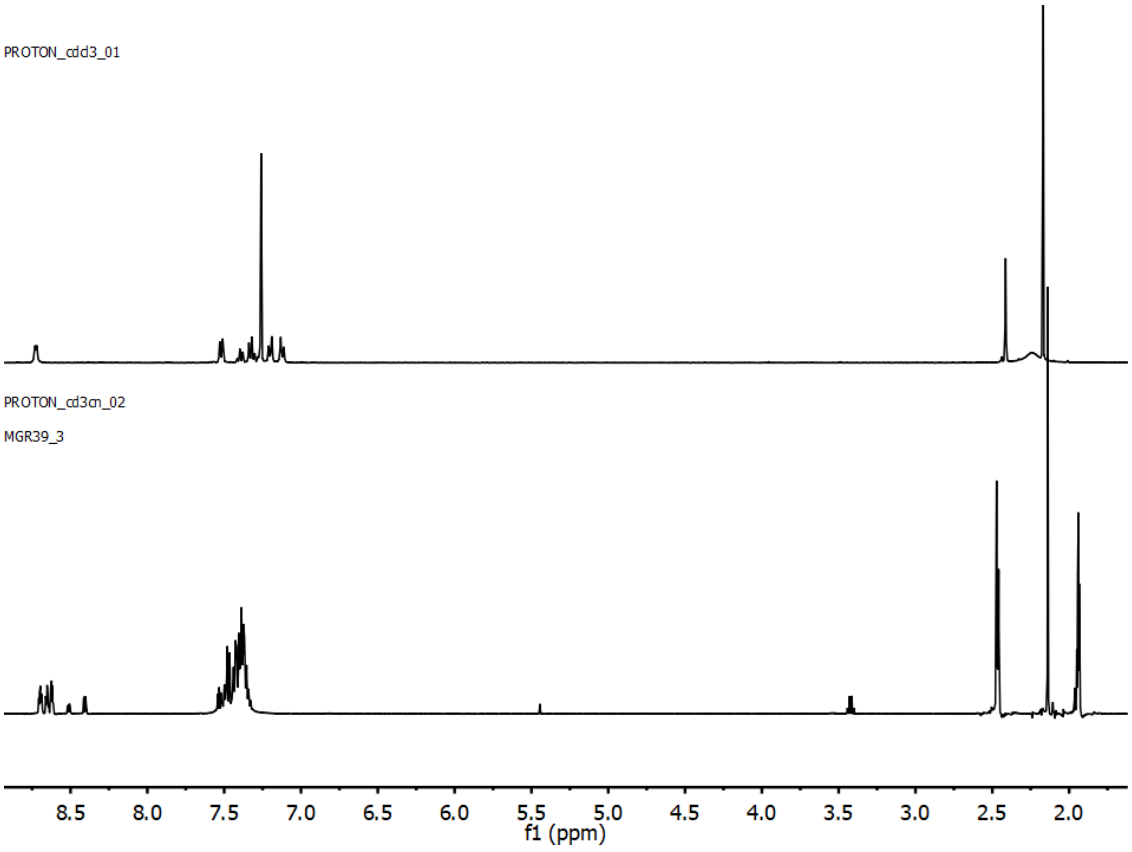

Figure S85: Stacked ^{1}H NMR of (top) $\mathbf{L}^{\text{2-pyrimidine}}$ (500 MHz, 298 K, $CDCl_3$) and (bottom) complex **5** (500 MHz, 298 K, CD_3CN).

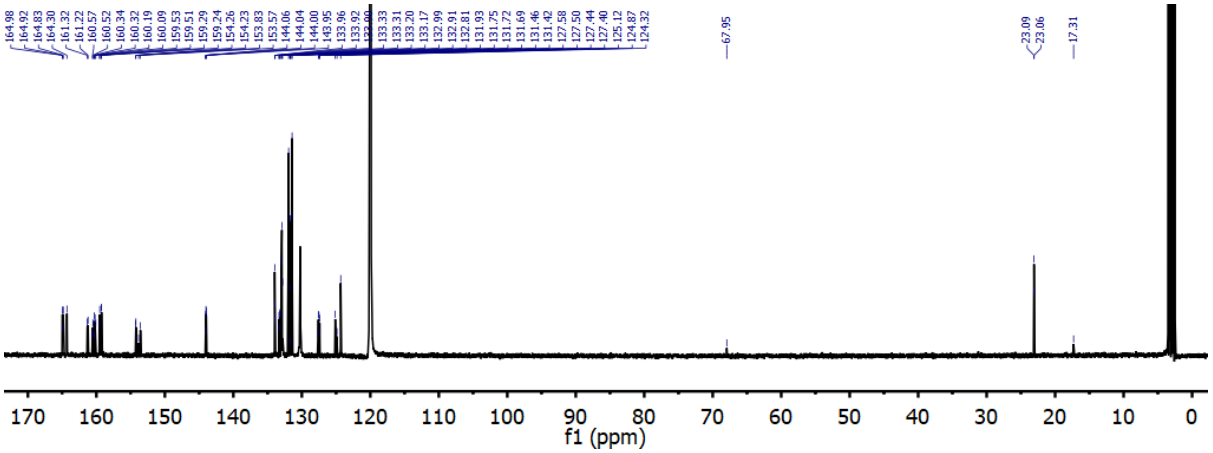

Figure S86: ^{13}C NMR (125 MHz, 298 K, CD_3CN) of complex **5**.

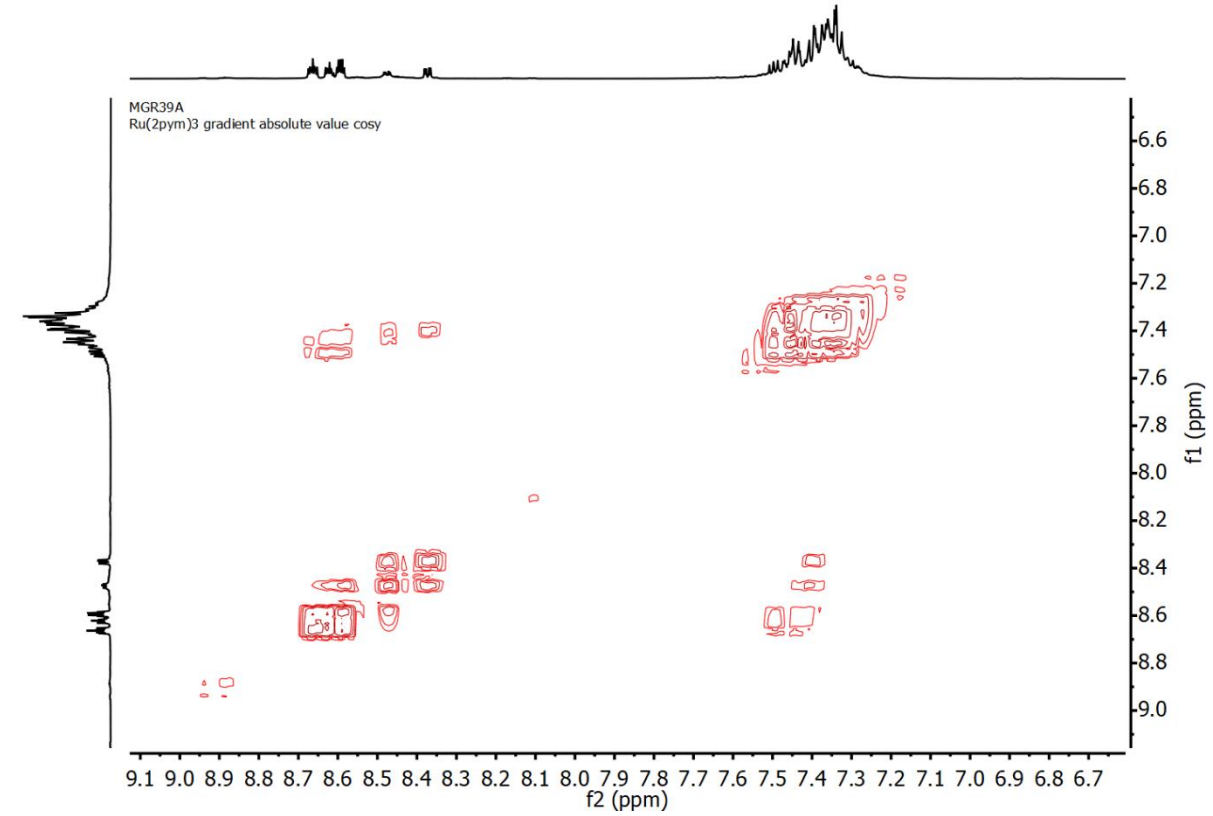

Figure S87: COSY spectrum of complex **5** (298 K, CD_3CN).

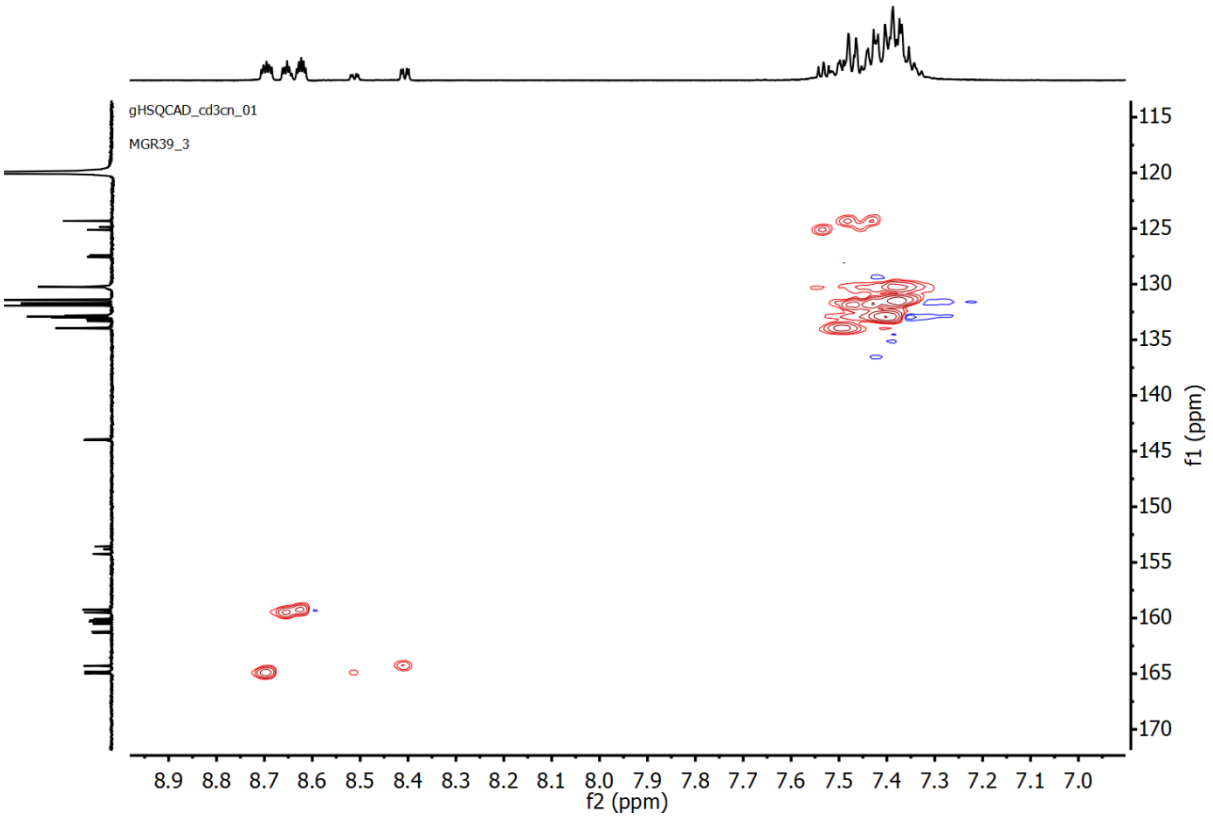

Figure S88: HSQC spectrum of complex **5** (298 K, CD_3CN).

References

1. A. Spek, *Acta Cryst. C*, 2015, **71**, 9-18.
2. P. van der Sluis and A. L. Spek, *Acta Crystallogr., Sect. A*, 1990, **46**, 194-201.
3. C. F. Macrae, I. J. Bruno, J. A. Chisolm, P. R. Edgington, P. McCabe, E. Pidcock, L. Rodriguez-Monge, R. Taylor, J. van de Streek and P. A. Wood, *J. Appl. Cryst.*, 2008, **41**, 466-470.
4. S. D. Ernst and W. Kaim, *Inorg. Chem.*, 1989, **28**, 1520-1528.
5. Y. Kawanishi, N. Kitamura and S. Tazuke, *Inorg. Chem.*, 1989, **28**, 2968-2975.
6. K. C. Zheng, J. P. Wang, W. L. Peng, X. W. Liu and F. C. Yun, *J. Mol. Struct.-Theochem.*, 2002, **582**, 1-9.
7. A. D. Becke, *Phys. Rev. A*, 1988, **38**, 3098-3100.
8. J. P. Perdew and W. Yue, *Phys. Rev. B*, 1986, **33**, 8800-8802.
9. S. Grimme, S. Ehrlich and L. Goerigk, *J. Comput. Chem.*, 2011, **32**, 1456-1465.
10. D. Andrae, U. Häußermann, M. Dolg, H. Stoll and H. Preuß, *Theoretica chimica acta*, 1990, **77**, 123-141.
11. F. Weigend and R. Ahlrichs, *Phys. Chem. Chem. Phys.*, 2005, **7**, 3297-3305.
12. Y. Takano and K. N. Houk, *J. Chem. Theory Comput.*, 2005, **1**, 70-77.
13. F. Neese, F. Wennmohs, U. Becker and C. Riplinger, *J. Chem. Phys.*, 2020, **152**, 224108.
14. F. R. Dutra, C. d. S. Silva and R. Custodio, *J. Phys. Chem. A*, 2021, **125**, 65-73.
15. J. A. Joule and K. Mills, *Heterocyclic Chemistry*, Blackwell Publishing, Padstow, Cornwall, UK, Fourth Edition edn., 2000.